NOTE TO USERS

A Study of Lead Softening

by

Daryl Geoffrey Vineberg

Department of Mining, Metals and Materials Engineering
McGill University
Montreal, Canada

August 2003

A thesis submitted to the Faculty of Graduate Studies and
Research in partial fulfillment of the requirements
For the degree of Master of Engineering

Your file Votre référence
ISBN: 0-612-98572-5
Our file Notre référence
ISBN: 0-612-98572-5

ABSTRACT

Softening represents one of the stages in the pyrometallurgical refining of lead, in which oxygen is top-blown into a bath of impure bullion through a group of lances in order to preferentially oxidize arsenic, antimony and tin dissolved in the melt. The oxides of these species float to the melt surface, where they are removed as dross.

It has been observed at Teck Cominco Lead Operations in Trail, BC that there is an "ignition temperature" in the range of 600 °C, below which the softening reactions are reported to occur very slowly, if at all. Currently, disproportionately large efforts are made to initiate and sustain the softening process. This research was motivated by Teck Cominco's wish to have a clearer understanding of the ignition temperature phenomena, and a more robust and reliable process control.

Experimental trials were performed using a homemade thermogravimetric analyzer with a data acquisition system. The unit was constructed in such a way as to allow for simultaneous video recording of the sample surface, for future examination and reference. Lead or alloyed lead samples, weighing 6.25 g, were brought to temperature (500, 550, or 600 °C) under an argon atmosphere. The sample surface was exposed to oxygen at 100 cm^3/min for a period of sixty (60) minutes, during which time the mass gain was recorded.

The results of twenty-four trials are discussed. The framework for investigation was a complete factorial design, to determine which of the following parameters were significant in lead softening reactions:

A = initial nominal wt% As

B = initial nominal wt% Sb

C = initial nominal wt% Sn

D = melt temperature (°C)

It was determined by linear regression analysis that temperature had the most significant effect on mass transfer and chemical reaction kinetics. Arsenic (wt%) was also significant in increasing mass gain over the sixty (60) minute test. The effect of tin on the rates of mass gain was significant, even when present in only very small amounts. The observed decrease in mass gain was attributed to the rapid formation of a passive layer of tin oxide which thereafter acted as a barrier to mass transfer.

Observed behaviours in some of the alloy systems tested were unexpected, specifically the presence of (i) complex liquid oxides (ii) "elastic" oxide films, and (iii) unskimmable films. In some of the Pb-As and Pb-Sb alloy systems, a "self-cleaning" complex liquid oxide was observed and the oxide initially present at the melt surface was "consumed," thereby exposing a clean surface for oxygen introduction. This behaviour was found to increase the kinetics of mass transfer across the gas-melt interface upon oxygen introduction, as compared to trials where coherent oxide phases present at the surface could not be removed.

RÉSUMÉ

Le ramollissement représente l'une des étapes dans le raffinement pyro-métallurgique du plomb, lorsque l'oxygène est soufflé de la surface dans un bain de lingots a travers un groupe de lances afin d'oxyder l'arsenic, l'antimoine et l'étain dissous dans la fusion de façon préférentielle. Les oxydes de ces espèces flottent à la surface de la fusion d'où ils sont enlevés en forme de scories.

Dans les installations de Teck Cominco Lead Operations à Trail en Colombie Britannique, l'on a noté qu'il existe une "température d'ignition" aux environs de 600 °C, au-dessous de laquelle les réactions de ramollissement, s'il y en a, ont lieu très lentement. Actuellement, des efforts tout à fait disproportionnés sont entrepris pour initier et soutenir le processus de ramollissement. Ces recherches résultent du désir de Teck Cominco de mieux comprendre le phénomène de la température d'ignition tout en obtenant un contrôle plus sûr et sérieux sur le processus.

Des essais expérimentaux ont été entrepris avec un appareil d'analyse thermogravimétrique fait à la main, muni d'un système d'acquisition de données. L'appareil fut construit de façon à permettre l'enregistrement vidéo simultané de la surface échantillon pour pouvoir l'examiner et s'y référer par la suite. Des échantillons de plomb ou d'alliages de plomb, pesant 6.25 g, furent chauffés à 500, 550, ou 600 °C dans une atmosphère d'argon. La surface échantillon fut exposée à l'oxygène à 100 cm^3/min. pendant soixante (60) minutes durant lesquelles le gain de masse fut enregistré.

Les résultats de vingt-quatre essais sont examinés. La structure de l'investigation était un design entièrement factoriel, pour déterminer lequel des paramètres suivants était important dans les réactions de ramollissement du plomb:

A = % Poids initial nominal de As

B = % Poids initial nominal de Sb

C = % Poids initial nominal de Sn

D = température de la fusion (°C)

A l'aide d'une analyse de régression linéaire, l'on a pu établir que la température avait l'effet le plus important sur le transfert de la masse et la cinétique de réactions chimiques. Le % de poids d'arsenic joue aussi un rôle important dans l'augmentation du gain de la masse au cours de l'essai de soixante (60) minutes. L' effet de l'étain sur le taux du gain de la masse est considérable, même lorsqu'il n'y avait que de minimes pourcentages. La diminution notée dans le gain de la masse fut attribuée à la formation rapide d'une couche passive d'oxyde d'étain qui agit comme une barrière contre le transfert de masse par la suite.

Les comportements notés dans certains des systèmes d'alliages employés dans les essais furent entièrement inattendus, particulièrement la présence des : (i) oxydes liquides complexes, (ii) films d'oxyde "élastiques", et (iii) films impossibles d'"écumer". Dans quelques-uns des systèmes d'alliages Pb-As et Pb-Sb, un oxyde liquide complexe "auto-nettoyant" fut noté et l'oxyde présent au début sur la surface de la fusion fut "consommé," exposant ainsi une surface propre pour l'introduction de l'oxygène. Il a été déterminé que ce comportement augmente la cinétique du transfert de masse à travers l'interface de la fusion-gaz lors de l'introduction de l'oxygène, en comparaison avec les essais où des phases d'oxyde cohérentes présentes à la surface ne pouvaient être enlevées.

ACKNOWLEDGEMENTS

This research was made possible through the financial support of NSERC and Teck Cominco. Thanks are given to Greg Richards, Steven Barclay and Yemi Oyediran at Teck Cominco for their technical support.

I am grateful to the staff of the Department of Mining, Metals and Materials Engineering at McGill University, specifically Ka Wing Ng for being a great resource and a critical mind, and Professor A. Laplante for his help with statistical analysis. Most especially, I am indebted to my supervisor Ralph Harris for his continued support, direction, patience, technical expertise, sense of humour, and for cultivating my interest in metallurgy from my very first undergraduate semester at McGill.

I wish to also recognize the technical staff in the Department: Monique Riendeau, Slavek Poplawski, and Helen Campbell whose helpfulness was very much appreciated. John Bartczak deserves special thanks for his creative ideas, and for helping this concept to be materialized. I wish also to sincerely thank Faramarz Zarandi for his generosity in sharing his SEM expertise, and Magali Maccario for her help with the statistical design.

Heartfelt gratitude is given to Sina Kashani-Nejad for being a true friend and a critical colleague, and to Rebekah Blok for her beautiful heart, mind and body. I would also like to thank my immediate family, David, Allyna, Lisa, Howard, Mike, and Peggy for their support and encouragement.

TABLE OF CONTENTS

LIST OF FIGURES

List of Figures

LIST OF TABLES

NOMENCLATURE

Abbreviations

AA	atomic absorption
atm	atmospheres (multiply by 101325 to obtain value in Pa)
at%	weight in atomic %
BP	boiling point
°C	degrees Celcius
cal	calories (multiply by 4.18 to obtain joules)
CDF	Continuous Drossing Furnace
CSD	Continuous Sulfur Drossing
cm	centimetres
cm^2	square centimetres
cm^3	cubic centimetres
cm^2/sec	square centimetres per second
cm^3/min	cubic centimetres per minute (divide by 6 x 10^7 to obtain value in m^3/s
(d)	diameter
DVTGA	naming scheme for TGA tests
EDX	Energy-Dispersive X-Ray Analysis
F	overall fit of linear regression analysis
g	grams
g/l	grams per litre
(h)	height
hr	hour
ICP	Induction-Coupled Plasma
ID	inner diameter
J/mol	joules per mole
K	degrees Kelvin
kcal	kilocalories (multiply by 4.18 to obtain kilojoules)
keV	kiloelectron volts
kJ	kilojoules
l	litre
l	liquid
(l)	length
liq	liquid
ln	natural logarithm
lpm	litres per minute
m	meters
$M_{b+n}O$	metal rich metal oxide
mg	milligrams

$mgcm^{-2}hr^{-1}$	milligrams per square centimetre per hour
mm	millimetres
mm Hg	millimetres mercury (multiply by 133.3 to obtain Pa)
mm/min	millimetres per minute
MO_{a-x}	oxygen deficient metal oxide
mol	mole
mol%	composition in molar %
MP	melting point
mt	million tonnes
N	mole fraction
Nm^3	normal cubic metres
Nm^3/hr	normal cubic metres per hour
OD	outer diameter
P	probability of t-score value
p_{O_2}	equilibrium oxygen partial pressure
ppm	parts per million
PVC	polyvinyl chloride
s	seconds
S2	second solid phase
t	time
t-	student t-score value
TGA	thermogravimetric analysis
tph	metric tonnes per hour
VAC	voltage, alternating current
(w)	width
wt%	composition in wt%
X	mole fraction
XRD	X-Ray Diffraction
$US	United States dollars
%	percent
”	inches (multiply by 2.54 to obtain cm)

Chemical Symbols

Ag	silver
Ar	argon
Au	gold
As	arsenic
As_4	tetratomic arsenic gas
As_2O_3	arsenic (III) oxide
As_2O_5	arsenic (V) oxide
As_4O_6	arsenic (III) oxide gas
Bi	bismuth

Co	cobalt
Cu	copper
Cu_2S	copper sulfide (matte)
Fe	iron
H_2O	water
Hg	mercury
In	indium
Na_3AsO_4	sodium arsenate
$NaNO_3$	nitre (sodium nitrate)
NaOH	caustic soda (sodium hydroxide)
N_2	diatomic nitrogen
Ni	nickel
O, O_2, O_3	monatomic oxygen, diatomic oxygen and triatomic oxygen (ozone), respectively
Pb	lead
Pb_2	diatomic lead gas
$Pb(AsO_3)O_2$	complex lead-arsenic compound
$Pb(AsO_4)_2$	complex lead-arsenic compound
$Pb_2As_2O_7$	complex lead-arsenic compound
$Pb_3As_2O_8$	complex lead-arsenic compound
$Pb_3(AsO_4)_2$	complex lead-arsenic compound
$Pb_4As_2O_9$	complex lead-arsenic compound
$Pb_8As_2O_{13}$	complex lead-arsenic compound
$PbCO_3$	cerussite
PbO	litharge
$PbO{\bullet}Sb_2O_3$	lead antimonite
$PbO{\bullet}Sb_2O_5$	lead antimonate
Pb_4SbO_6	complex lead-antimony oxide
PbS	lead sulfide (matte)
$PbSO_4$	anglesite
Pb0.26Sn	lead alloyed with 0.26 wt% tin
Pb0.90As	lead alloyed with 0.90 wt% arsenic
Pb2.00Sb	lead alloyed with 2.00 wt% antimony
PbSb	lead antimony gas
$PbSb_2O_6$	lead antimony complex oxide
$Pb_{3+x}Sb_2O_{8+x}$	lead antimony complex oxide
$Pb_4Sb_2O_9$	lead antimony complex oxide
$Pb_6Sb_6O_{11}$	lead antimony complex oxide
$PbSnO_3$	lead metastannate
Pb_2SnO_4	lead orthostannate
S	sulfur
Sb	antimony
Sb_2	diatomic antimony gas
Sb_4	tetratomic antimony gas

Sb_2O_3	valentinite (antimony (III) oxide)
Sb_2O_4	cervantite
Sb_2O_5	antimony (V) oxide
Sb_4O_6	antimony (III) oxide gas
Se	selenium
SO_2	sulfur dioxide
Sn	tin
SnO_2	tin (IV) oxide
Te	tellurium
Zn	zinc

Subscripts

g	gas phase
l	liquid phase
s	solid
t	time

Symbol		**S.I. Units**	**Typical Units**
a	activity of solute or species	unitless	
A	constant in Arrhenius equation	s^{-1}	
c	concentration of the diffusing species at the plane	kg-mole/m^3	
C_p	specific heat capacity	J/kgK	
D	diffusivity of solute	m^2/s	
$\delta\gamma$	difference in surface tension along L_s	kg s^{-2}	
E_a	activation energy	J	kJ
η	viscosity	kg/ms	
f°	activity coefficient, equivalent to γ	unitless	
γ	activity coefficient	unitless	
ΔG	change in Gibbs Energy	J/kg-mole	kJ/g-mole, kJ/mol kJ
ΔG°	standard free energy of formation	J/kg-mole	kJ/g-mole, kJ/mol, J kJ
J	instantaneous flow rate per unit area of the diffusing species across a plane	atoms $m^{-2}s^{-1}$	
k	rate coefficient	s^{-1}	
K	equilibrium product of activities of products over activities of reactants	unitless	
L_s	characteristic length	m	
λ	thermal conductivity	W/mK	

Nomenclature

Symbol		S.I. Units	Typical Units
Ma	Marangoni number	unitless	
P	pressure	Pa	atm, kPa, mm Hg
R	universal gas constant (8.314 J/mol/K)	J/kg-mole/K	J/g-mole/K
ρ	density	kg m^{-3}	g cm^{-3}
T	temperature	K	°C
X	mole fraction	unitless	
X'	molar ratio	unitless	
$\underline{X}$	dissolved species	kg-mole/m^3	
$\underline{X}_{Pb}$	dissolved species in lead	kg-mole/m^3	
$\partial c/\partial x$	concentration gradient normal to the plane	atoms m^{-4}	

CHAPTER 1: INTRODUCTION

1.1 Lead History, Properties, Production & Economics

1.1.1 History

Lead is a very corrosion-resistant, dense, ductile and malleable blue-grey metal that has been in use for at least 5000 years. Although it has probably been known to humanity for more than 6000 years, its softness made it of little value for weapons, tools or ornaments[1]. The ease of working with lead, specifically its ductility and its corrosion resistance likely lead to its first applications in building materials, and pipes for transporting water. The bright yellow colour of litharge (PbO) found use as pigment for glazing ceramics.

With the dawn of the age of electricity and communications, and later the demands of World War I, lead found greater applications as for example, in bearing metals, solder and cable covering. The invention and production of public and private motorized vehicles found lead as the ideal material for starting-lighting-ignition (SLI) lead-acid storage batteries[2]. Lead was also used in the form of tetraethyl lead (TEL) as a performance-enhancing, anti-knock agent in gasoline, in concentrations of roughly 3.0 grams per gallon of fuel[3].

By the mid-1980's, there was a shift in use of lead, influenced primarily by the identification of lead as a neuro-toxin[1] and some lead compounds as being carcinogenic[4]. This resulted in reducing or eliminating the use of lead in nonbattery products, including gasoline, paints, solders, and water systems[2]. However, lead had found further applications in SLI-type battery and non-SLI battery applications such as traction batteries as sources of power for industrial forklifts, mining equipment, as well as stationary sources of power in uninterruptible electric power systems for hospitals, and telecommunications networks[1, 2]. A breakdown of lead's commercial applications in the U.S. is shown in Figure 1. In the U.S. (2001), lead-acid batteries, including starting-lighting-ignition (SLI) and industrial

types continued to be the dominant use of lead, accounting for roughly 90% of reported lead consumption[5].

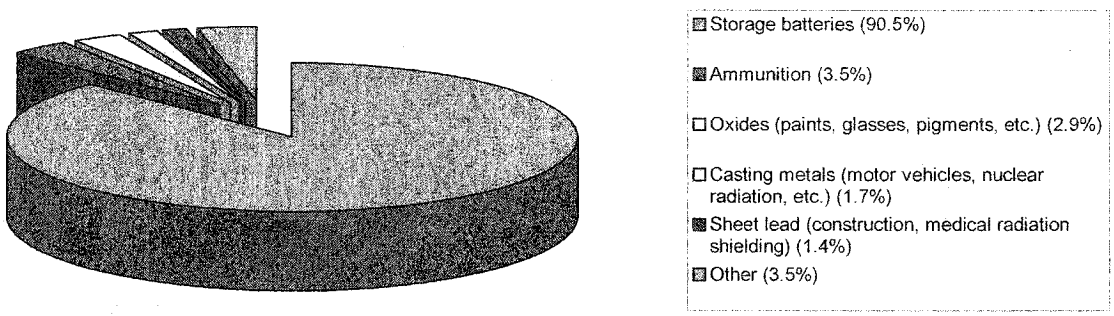

Figure 1. U.S. Consumption of Lead in 2001, by Product (after Smith, 1991, ref.6).

1.1.2 Properties

When freshly cast, lead has a bright appearance, but exposure to air soon causes the surface of the lead to oxidize, and become grey or grey-white. In a similar manner, exposure of lead to aqueous solutions of sulfates or carbonates will cause the formation of protective sulfate or carbonate layers, which have low solubilities in aqueous solutions with a wide range of pH values (with the exception of acetate, chlorate and nitrate solutions). This property makes lead an ideal construction material for the manufacturing and storage of sulfuric, phosphoric and chromic acids[1].

1.1.3 Production

1.1.3.1 Primary Lead

The most commonly mined lead-bearing ores are galena (PbS), cerussite ($PbCO_3$), and anglesite ($PbSO_4$)[1]. World production of refined lead, roughly 1% of world iron production[6], decreased to 6.47 million tonnes (mt) in 2001 from 6.55 mt in 2000[5]. Year 2001 mine production figures for the highest lead-producing countries are presented in Figure 2. Of the 43 countries in which lead was mined, the top five were responsible for 71% of the world's production. Those countries were Australia (23%), China (19%), the United States (15%), Peru (9%) and Canada (5%)[5].

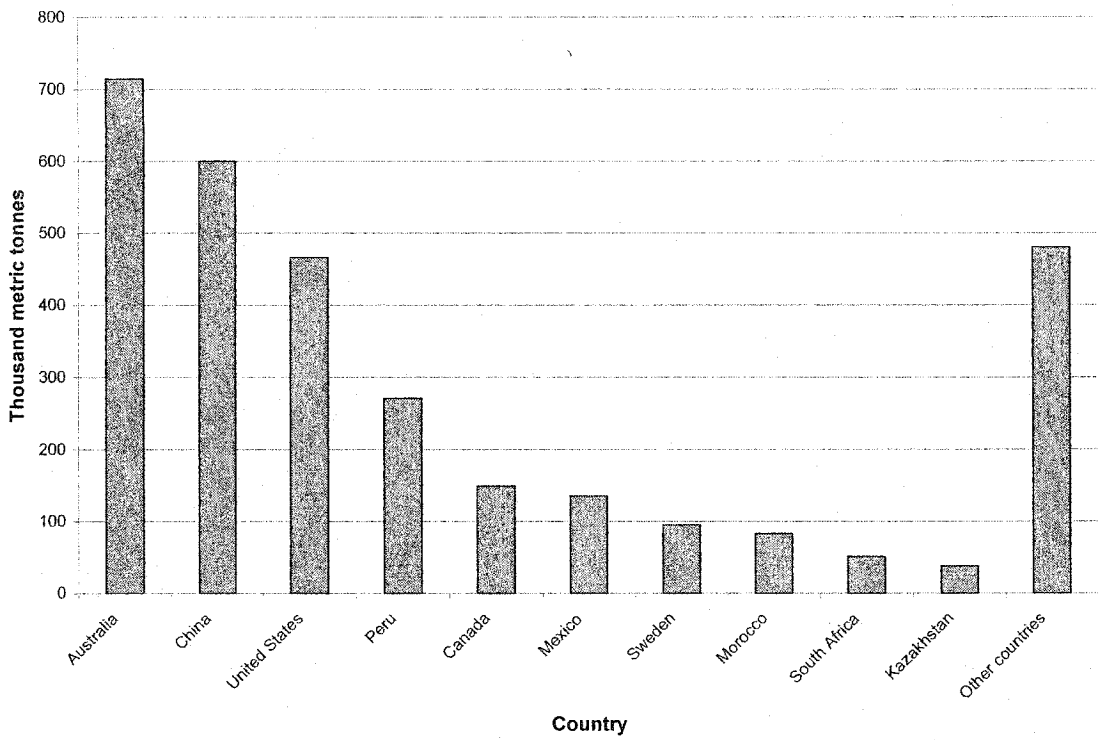

Figure 2. Leading countries in world mine production of lead in concentrates 2001 (after Smith, 2002, ref. 7)

1.1.3.2 Secondary lead

Secondary lead is derived mainly from scrapped lead-acid batteries and accounted for 79% of refined lead production in the United States[5]. Laws are now in place in 42 states that prohibit the disposal of spent lead-acid batteries and mandate the collection of these batteries through a "customer return policy" when a replacement battery is purchased[5].

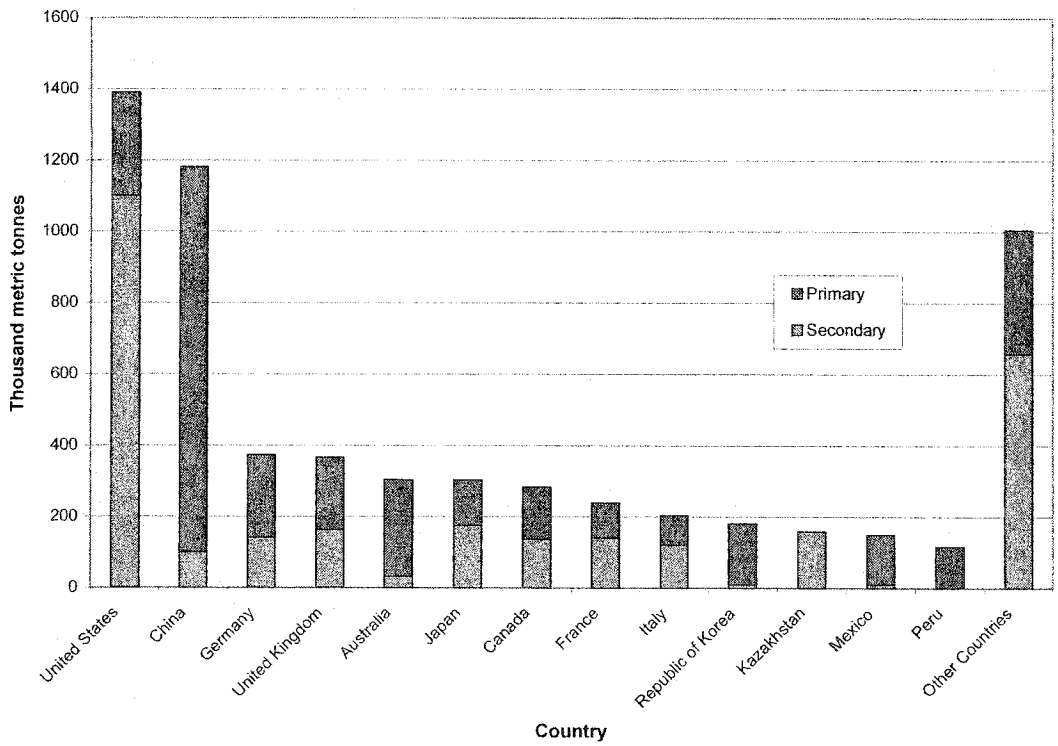

Figure 3. Leading countries in world lead refinery production 2001 (after Smith, 2001, ref.5.)

1.1.3.3 Refining

Of the total world production of 6.47 mt of lead refined in 2001, roughly 43% came from secondary sources. Year 2001 production figures for the highest producing countries are presented in Figure 3.

The average 2001 London Metal Exchange (LME) price was 0.446 $US per pound, up 0.010 $US per pound from the 2000 average price.

1.1.4 Economics

1.1.4.1 Reasons for decline 2002

The U.S. Government agencies issued certain rules which had a direct impact on the lead industry: These rules included lower threshold requirements for reporting lead and lead compounds released to the environment; new definitions for classification of solid waste

disposal facilities; and the approval of new, non-toxic forms of ammunition for hunting water fowl[5]. The new rules identify lead and lead compounds as persistent bioaccumulative toxic (PBT) chemicals.

1.1.4.2 Substitutes

Substitution of plastics has reduced the use of lead in building construction, electrical cable covering, cans, and containers. Other metals such as aluminum, tin, iron as well as plastics are in competition with lead in the domains of packaging and protective coatings. Tin-antimony and tin-silver alloys have all but replaced lead in solder for new or replacement potable water systems in the United States[7].

1.1.4.3 Current Research

New research is centred on valve-regulated lead-acid (VRLA) battery performance in hybrid-electric vehicles (HEV). Although these battery systems have been successfully used in larger HEV's, such as hybrid-electric buses, they have yet to be tested in smaller commercially available HEV's, such as the Honda Insight or the Toyota Prius[5]. Other work involves development of the first 36/42 (36-volt battery, 42-volt alternator) lead-acid systems for automotive use.

It is the opinion of the U.S. Geological Survey Minerals Yearbook (2001) that lead-acid batteries will continue to dominate the demand for lead for the foreseeable future[5].

1.2 Lead Refining

Primary lead is produced by one of two pyrometallurgical routes: (i) conventional roasting/sintering followed by reduction in smelting furnace (e.g. a blast furnace) (Figure 4), or (ii) by direct-to-lead smelting technologies such as the Kivcet flash smelter. In the latter, concentrate, coke and reductant are fed to the flash smelter, and an impure lead bullion is produced directly.

Lead produced by these processes exits the smelting vessel in the range of 900°C – 1180°C[1,8], temperatures at which molten lead acts as a solvent for many impurity elements,

such as Cu, Fe, Ni, Co, Zn, In, As, Sb, Sn, Ag, Au, Bi, S, Se, Te and O[9]. The refining of lead involves the stepwise removal of these impurities, and proceeds by pyrometallurgical or electrolytic processing, or a combination of these two routes. Most smelters worldwide employ the pyrometallurgical refining route[10], the general flowsheet for which is found in Figure 5. In each successive step, one or more impurity is removed to trace levels.

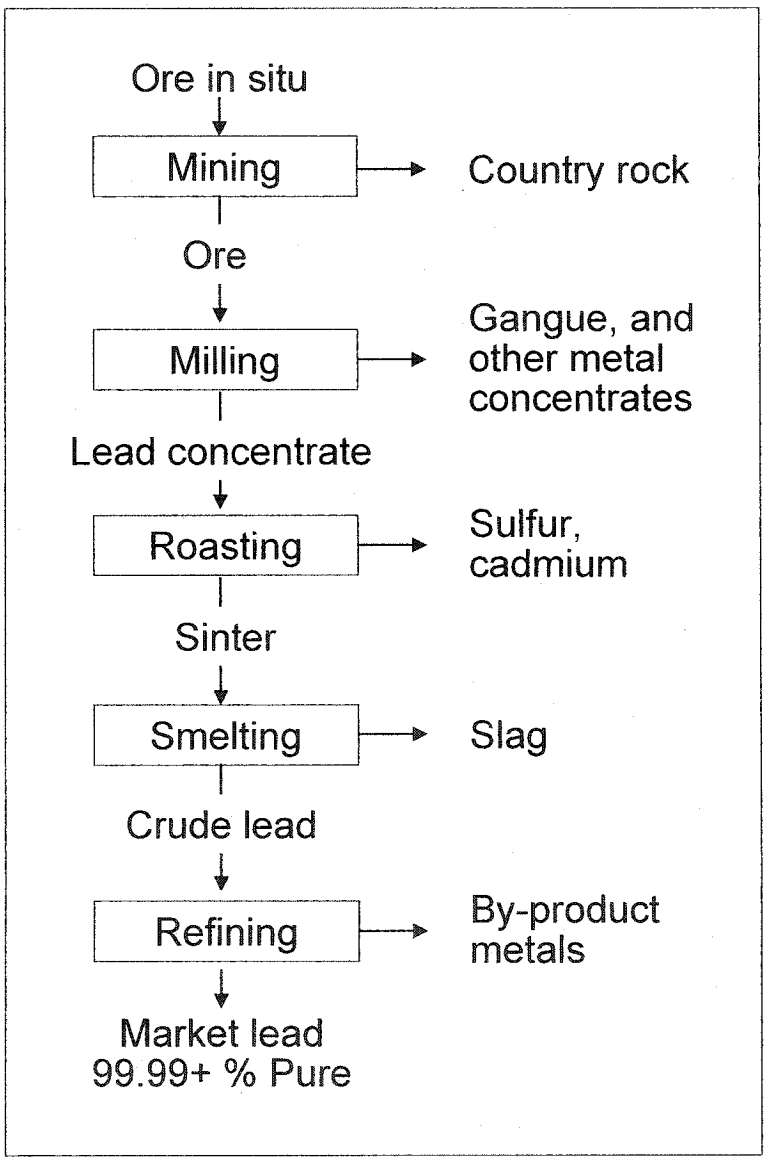

Figure 4. Lead production flowsheet (after Davey, 1980, ref. 9)

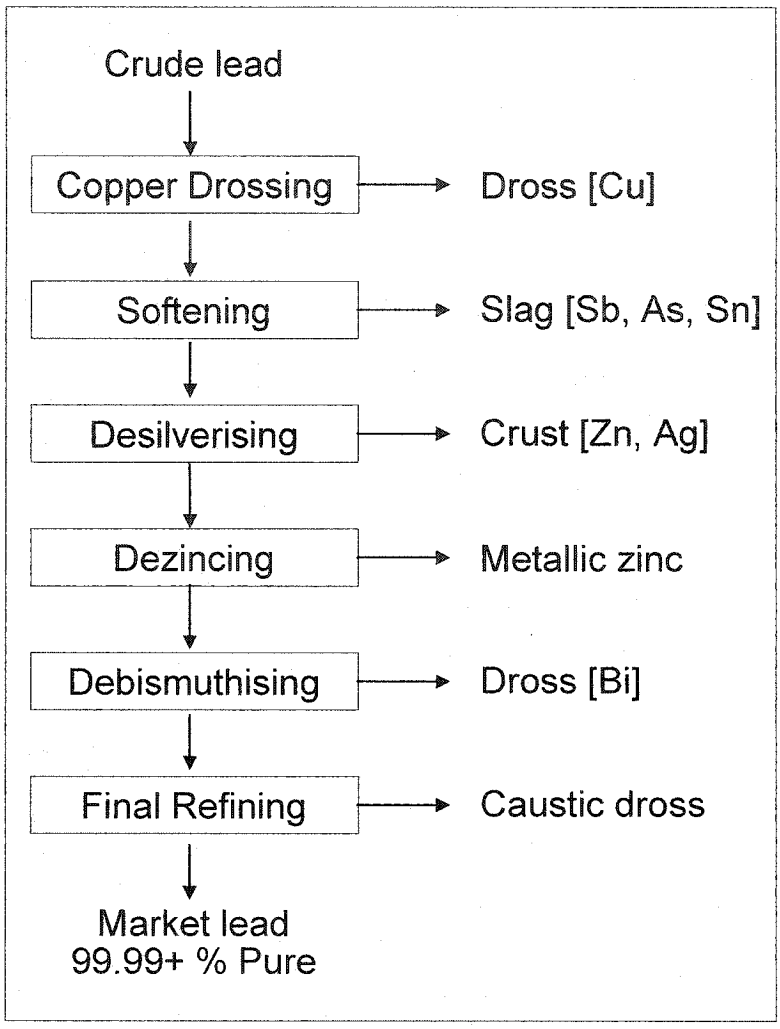

Figure 5. Lead refining flowsheet (after Davey, 1980, ref. 9).

The first refining step involves cooling of the lead bullion to about 400°C, as this has the effect of precipitating the copper since copper solubility in lead decreases with decreasing temperature. Apart from a small amount of oxides, the copper dross is composed mainly of sulfides, arsenides or antimonides, hence the term "copper drossing"[11]. The lead is further cooled to just above its freezing point (310-327°C, depending on impurity content[9]), and coupled with the addition of sulfur, the copper level can be reduced to 0.02 – 0.002 wt% Cu[1]. The decopperized lead is then flowed to the softening vessel, wherein the less noble dissolved species (i.e., As, Sb, and Sn) are preferentially oxidized and removed from the

melt surface as dross. This stage is of particular interest to the current research, and will be discussed in greater detail below.

As the remaining impurities at this stage are all more noble than lead, they are removed by precipitation as intermetallic compounds after special reagent additions[9]. Zinc is added to remove silver as a silver-zinc crust (after which residual zinc must be removed.) Calcium and magnesium are added through the Kroll-Betterton process to remove bismuth. A final refining of the lead is achieved by addition of caustic dross and an oxidizing element, followed by skimming of the resultant caustic dross[9].

In plants that employ a combination pyrometallurgical-electrolytic route, the lead is generally decopperized, softened, and cast into ingots. These ingots (following re-melting and re-casting into anodes if necessary) are then refined electrolytically, leaving behind a complex "impurity" slime on the anode. "Impurities" include gold, silver, and bismuth.

Electrolytic refining employs the Betts Process[1] and is particularly beneficial if a low bismuth content final product is required. Electrical cost is usually a significant factor in such a plant design when considering this added benefit. As of 1991, electrolytic refining of commercial lead accounted for 20% of total lead-refining capacity[12]; plants are operated at Teck Cominco in Trail, B.C., La Oroya in Peru, Shenyang Smelter in China and Kamioka in Japan[1, 10, 13].

1.3 Lead Softening

"Softening" refers to the refining operation which removes those elements which "harden" lead in its solid state, namely As, Sb and Sn. These elements can be preferentially oxidized to lead, since their standard change in Gibbs free energy are more negative for the oxidation reactions than is the case for lead.

In practice, several variants of softening are employed, the selection of which is plant-specific. These are discussed in detail in the following sections.

1.3.1 Harris Process

The kettle process of softening is a low-temperature (~450°C) operation in which NaOH is added to the melt to remove As, Sb and Sn as sodium plumbate, arsenate, antimonate and stannate. An oxidizing agent such as nitre may be added to speed up the operation[1]. The oxidation reaction for arsenic, for example, would be the following:

$$2\,\underline{As}_{(bullion)} + 2\,NaNO_3 + 4\,NaOH \leftrightarrow 2\,Na_3AsO_4 + N_2 + 2\,H_2O \qquad (1)$$

NaOH serves a double purpose in this operation, in that it not only chemically reacts with the oxides, but it also acts as a suspension medium for the latter, facilitating their separation from the lead. NaOH can hold about 20% of either As or Sb in suspension, or 30% of Sb, before becoming too thick to flow[9]. Once the products are separated, the caustic soda is regenerated.

The Harris Process may involve a specially designed reaction vessel, which offers more intensive mixing of the lead with reagents[1], and a molten salt column for suspension of the products. Although this process oxidizes very little lead and can be operated selectively for arsenic and tin with respect to antimony[10], its main disadvantage is its high capital cost and operating cost[14].

1.3.2 Modified Harris Process

This variation of the Harris process is carried out at 450-500°C in open kettles, using the same oxidants, NaOH and $NaNO_3$. In this operation, there is no molten salt column, and thus the product of reaction is a dry dross with high lead entrapment. Since the drosses are generally recycled in the smelter circuit, significant costs are associated with high levels of As, Sb, or Sn, from the point of view of recirculating loads and reagent consumption[14].

1.3.3 Furnace Softening

Conventional softening is operated in the range of 600-760°C, depending on the initial impurity level in the lead (i.e., a function of typical smelter feed), requisite levels to be met,

and the discretion of the particular refining operation. The operation may be run batchwise or continuously; a batch operation offers the advantage of more easily handling lead with irregular impurity content, but has the inherent disadvantage of needing to be maintained at elevated temperatures for long periods of time. The softening vessel may be a reverberatory furnace or a kettle (or series of kettles.) In all cases, air or oxygen is injected into the melt to produce a liquid slag composed mainly of lead oxide but also containing arsenic and antimony oxides[1]. The basic reactions are generally presumed to be the following, which imply that all reactions occur between dissolved species in the melt:

$$\tfrac{1}{2}\, O_{2\,(g)} \leftrightarrow \underline{O}_{(bullion)} \tag{2}$$

$$Pb_{(l)} + \underline{O}_{(bullion)} \leftrightarrow PbO_{(slag)} \tag{3}$$

$$2\,\underline{Sb}_{(bullion)} + 3\,\underline{O}_{(bullion)} \leftrightarrow Sb_2O_{3\,(slag)} \tag{4}$$

$$2\,\underline{As}_{(bullion)} + 3\,\underline{O}_{(bullion)} \leftrightarrow As_2O_{3\,(slag)} \tag{5}$$

$$\underline{Sn} + 2\,\underline{O}_{(bullion)} \leftrightarrow SnO_{2\,(slag)} \tag{6}$$

Where operated in a furnace, this process' disadvantages include high refractory wear and the necessity to maintain two furnaces for continuous operations[14].

1.4 Lead Softening at Teck Cominco

In practice, Teck Cominco currently carries out only partial softening, since it is known that the presence of arsenic and antimony help to stabilize the anode slimes in the subsequent electrolytic refining stages[15]; when the impurity level is too low the slimes may fall away and contaminate the electrolyte and the cathode deposit. In other commercial lead refining operations (where impurity elements are lacking), up to 0.5 wt% antimony may be added to the bullion to give better slime coherence[1].

1.4.1 Flowsheet 1 (1986)

Until 1986, arsenic and antimony from the silver recycle stream were used to supplement the bullion feed, to achieve the As and Sb levels necessary for anode slime stability. Since that time, higher impurity contents in the Sullivan concentrates and other smelter feed materials necessitated construction of a partial softening process to maintain impurities at levels which could be handled by Teck Cominco's Betts process downstream[15].

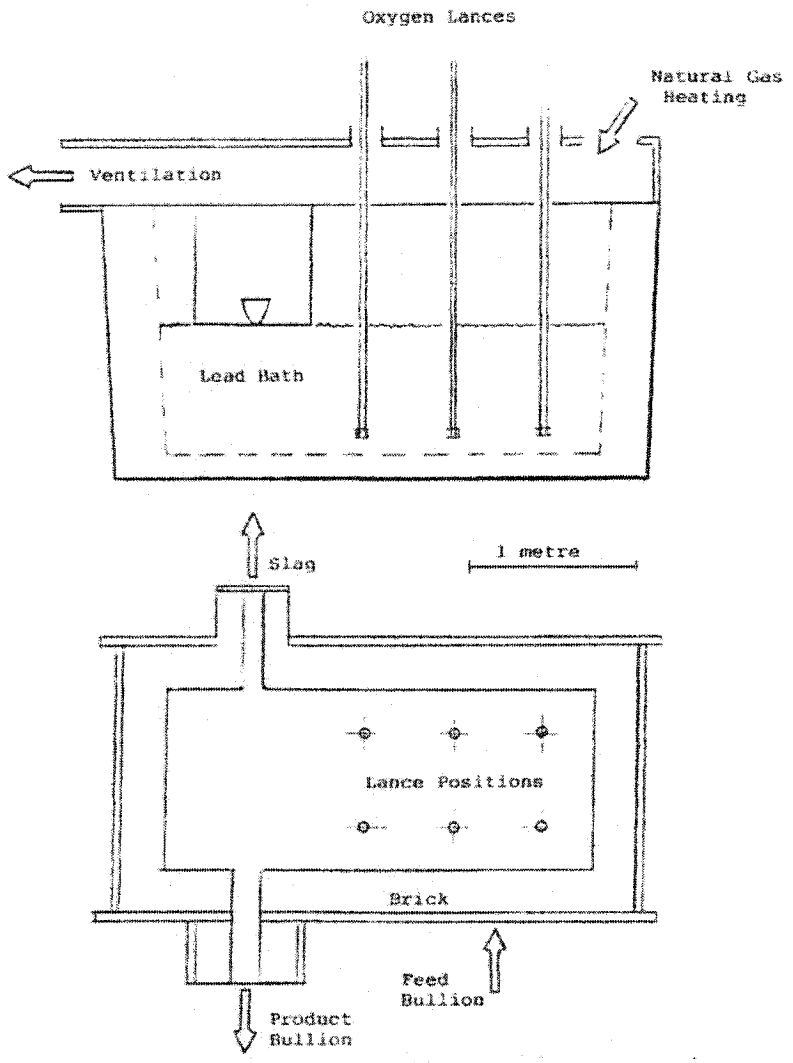

Figure 6. Original Cominco softening vessel (After deGroot, 1989, ref.15)

The original process used a blast furnace settler as a container. It was lined with chrome magnesite brick, could hold 20 tonnes of lead at a depth of 0.8 m, used four to six lances to inject 98 % oxygen into the melt, and it had natural gas burners to keep the slag fluid at 700 °C[15]. This vessel is shown in Figure 6. Oxygen efficiency was claimed to be 90 %; this was confirmed visually by virtue of seeing a few bubbles breaking the surface[15].

The softening circuit, Figure 7, consisted of the softening vessel and two holding pots, which were arranged in such a way as to allow mixing of crude bullion from the Copper Drossing Furnace (CDF) with partially softened lead from the softener[10].

The softener was kept in a temperature cycle between 617 and 628 °C by interlocking the feed pump with melt temperature. Since metal oxidation was exothermic, the melt temperature in the softener increased when oxygen was injected. When the temperature was high, unsoftened, cooler, 450 °C, lead was introduced into the vessel, thus lowering the temperature, and raising the impurity level. At this point, the cycle would then begin again. This same pumping action cycles (4-6 times/hr) had the effect of displacing softened lead as an underflow to the original holding pot, and displacing slag as an overflow to a slag pot[15]. The slag was kept fluid at about 700 °C by a natural gas burner.

The advantage of the setup consisted in the following: diverting a small portion of a charge of lead bullion to a small softening furnace meant that the major portion of the lead bullion did not have to be heated to the high temperature required for softening[16]. The small portion was softened and then an equally small portion was returned to the main charge or fed to a separate vessel.

1.4.2 Flowsheet 2 (1991)

In the summer of 1991, modifications were made to increase the softening capacity and increase control of the product softened lead composition[10]. The modified layout is shown in Figure 8.

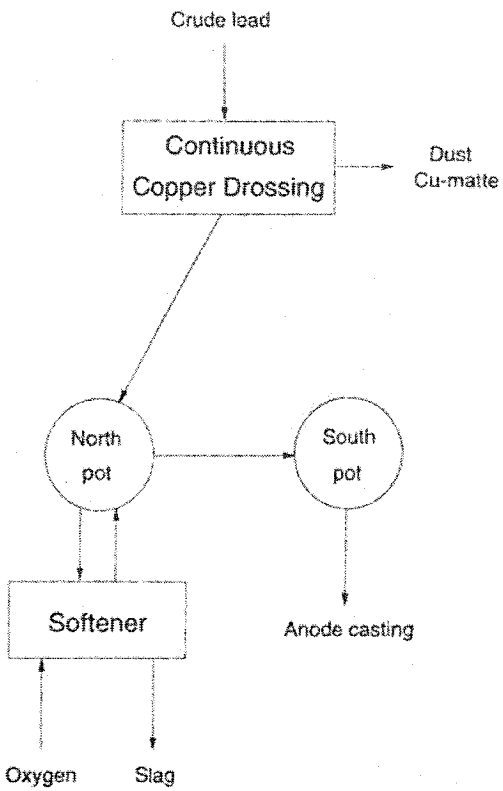

Figure 7. Softener circuit (after Kapusta, 1995, ref. 10)

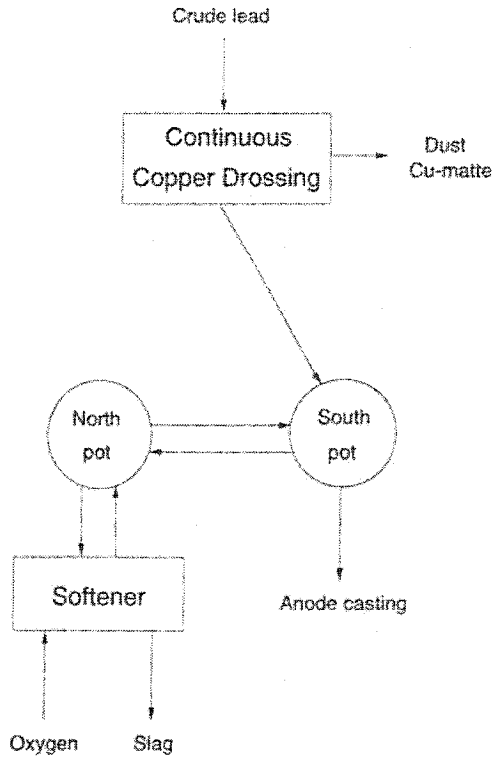

Figure 8. Modified softener circuit (after Kapusta, 1995, ref. 10)

In 1992, the softening vessel was replaced with a larger, 100-tonne hemispherical vessel with eight vertical lances in a circular arrangement centred over the pot. In operation, the lances were submerged about one metre into the lead bath. Bath temperature was maintained between 615 °C and 630 °C, and a cycling mode was preserved similar to that described above [10, 17].

1.4.3 Flowsheet: (current)

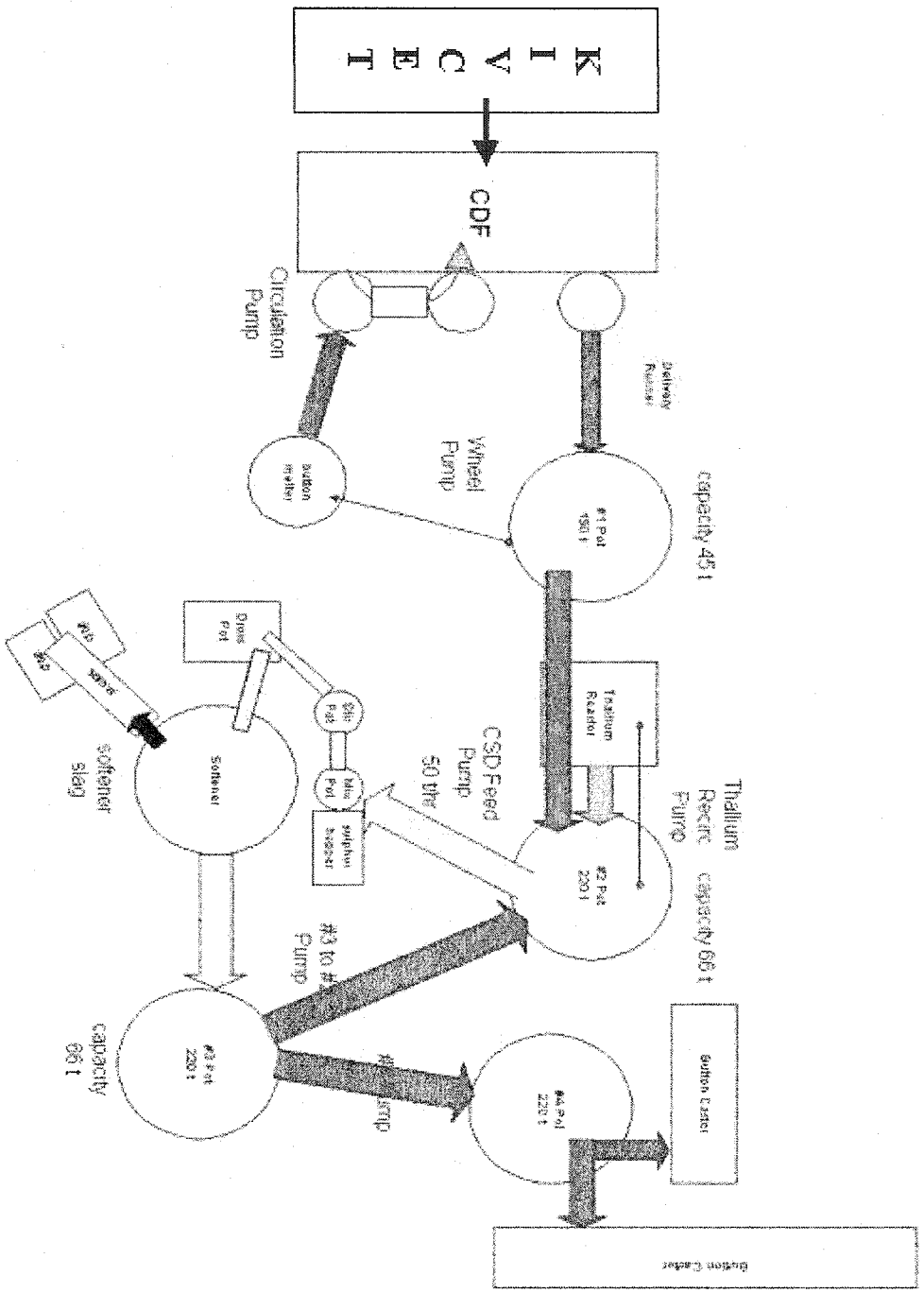

Figure 9. Current Teck Cominco lead refining flowsheet (courtesy of Teck Cominco, Trail, BC)

The current softening circuit was originally modified in the late 1990's as part of the modernization of Teck Cominco's lead circuit and start up of the Kivcet direct-to-lead process[18]. The current pyrorefining refining flowsheet is shown in Figure 9.

In the current set-up, the Kivcet Furnace is operated batch-wise. Freshly smelted lead bullion is then flowed to the Continuous Drossing Furnace (CDF), where the lead is cooled to just over 400 °C, and liquid sulfur is added, to reduce the copper content to roughly 0.05 - 0.06 wt % Cu. Lead is then directed to the #1 Pot and from there to the #2 Pot. Depending on the thallium content in the feed, the #2 Pot may be in circuit with the Thallium Reactor, wherein zinc chloride is added to produce thallium chloride salt, and from which the lead is flowed back to the #2 Pot. Lead from the #2 Pot flows to the Continuous Sulfur Drossing (CSD), wherein the lead is cooled to just above its melting point (~ 330 °C) for the purpose of lowering the copper content down to < 0.005 wt% Cu. The CSD consists of the following components: CSD Feed Pump, Mix Pot, Stir Pot, and Dross Pot. In the Mix Pot, solid sulphur prills are screw-fed into the pot (where the rate of rotation controlled, depending on copper level). There is a mixer in this vessel which creates a vortex (when the impellers are clean), into which the sulphur prills are added for optimal mixing. From the Mix Pot, the lead flows to the Stir Pot, and then to the Dross Pot. The Dross Pot is equipped with automatic drossing, which comprises a rake of sorts which skims the surface.

Lead from the Dross Pot flows to the Softener, which may or may not be operating (explained below), and from there to the #3 Pot. From the #3 Pot, lead flows to the #4 Pot, and then onto the Button Casters.

When all the pots have been freshly filled by flow of lead from the Kivcet furnace, the Kivcet tap is shut. At this point, two almost independent recycle circuits operate. The first consists of the CDF, #1 Pot and Button Melter, and the second consists of the #2 Pot, CSD, Softener, and #3 Pot.

In addition to the circuits mentioned above, there is a piece of equipment called the Button Melter, which is a vessel in which addition from lead refining may be made, depending on the required final lead composition. For example, bismuth may be added if a bismuth-lead alloy is required.

1.4.3.1 Softener Operation

The softener is operated semi-continuously as required. The 3-m high, 200-tonne vessel (Figure 10) contains an inner cylinder open at the bottom, into which oxygen is injected into the melt at a depth of 1 m. In this way, the reaction zone is maintained within the inner "ring", and the outer "ring" of lead remains unsoftened and serves as an "insulator". As the oxidation of Sb, As, Sn and Pb are exothermic, more than enough heat is generated from these reactions – such that cooling is a more important issue. Oxygen flow is controlled between 50 and 130 Nm^3/hr (total for the 3-4 lances) to control the temperature to roughly 620 °C[19]. The temperature is monitored by a thermocouple encased in a steel rod, positioned in the centre of the inner ring.

The outer vessel is water-cooled in the upper section and a series of natural gas burners maintain the slag fluid at the melt surface and along the tapping launders.

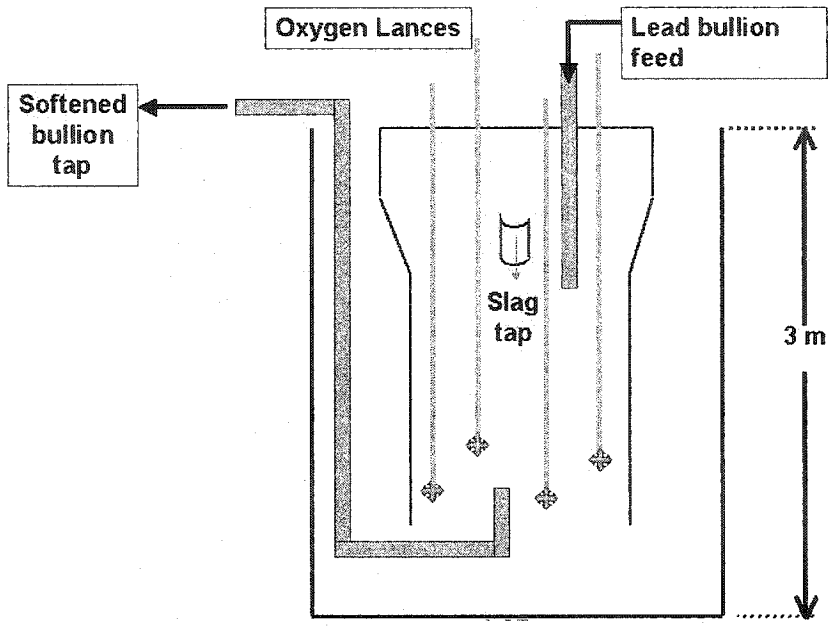

Figure 10. Current softening vessel (after Barclay, Omediran, 2003, refs. 19,20)

Feed bullion from the Continuous Sulfur Drossing (CSD) is introduced intermittently at a rate of 40 tph into the inner ring of the softener from the top of the vessel through a tube extending below the layer of slag. Sixty (60) tonnes of new lead are introduced every three (3) hours on average, and the lead is recirculated in the second circuit (#2 Pot, CSD, Softener, and #3 Pot, as described above) until all the lead is at the lower end of the 1.0 – 1.4 wt % Sb specification[19]. It is at the same time desirable to keep the arsenic concentration below <0.6 wt%. Only when the softener output levels reach the upper limit of the antimony specification is softening initiated. The end point of the softener operation is determined by 3 hourly lead assays of the product assay, input assay and Kivcet bullion assay. In practice, when the Sb content in the Kivcet is very high, the softener would be kept running for a longer period, so that the bullion coming off the Kivcet could be diluted by the hyper-softened lead.

The lances used in the softener are composed of two sections: the lower part, roughly 1 m long is made of 316 stainless steel, while the upper part, also roughly 1 m long, is made of

black iron. Softening consists of lowering the lances only partly into the melt, and injecting oxygen until the uppermost "layer" of lead is reacting. Only then are the lances lowered slightly deeper, and the underlying level is "ignited". This proceeds stepwise to a depth of ~1 m, until the entire inner cylinder is "ignited". As the process initiation is difficult and unpredictable, softener staff try to keep the softener running for as long as possible, in order to avoid the need to 're-initiate' the softening reaction process. Softened lead is tapped from the bottom of the furnace, and is flowed up a riser and exits at the top. Slag flows off continuously from the top of the vessel (~10 tonnes/24 hours operation), and flows down launders to a slag granulator[20]. When the input bullion Sb levels are low enough that softening is not required, the lances remain idle, and lead is flowed through the vessel in the same manner. On average, the softener is operated for 20-40% of the week[19].

Typical assays for the input bullion, softened bullion, and softener slag are presented in Table 1.

Table 1. Typical assays of input bullion, softened bullion and softener slag (year 2002 averages). Rem* indicates that the balance represents lead together with small amounts of other minor elements.

Stream	Sb (wt%)	As (wt%)	Sn (wt%)	Pb (wt%)
Input bullion	1.42	0.47	0.026	rem*
Softened bullion	1.125	0.263	0.0054	rem*
Softener slag	13.27	7.98	1.54	60.86

1.5 Research Objectives

The softening operation continues to be a challenge to the staff at Teck Cominco. This research was motivated by Teck Cominco's wish to have a clearer understanding of the ignition temperature phenomena, and a more robust and reliable process control.

A well-known expert in the field of lead extractive metallurgy, Davey[9] stated in 1980 that:

> "The physical chemistry of softening has not been fully examined, largely because there is small possibility of significant improvement by optimizing operations. The thermodynamic data on the metal oxides are uncertain, and sound activity data on the oxide systems do not exist."

Despite this evaluation, the research group at Teck Cominco believed it worthwhile to further investigate the nature of oxygen-injection high-temperature lead softening.

A series of thermogravimetric oxidation trials was designed to study the effect of temperature and the presence of impurity elements on lead softening. The goal was to determine the significance of the following parameters:

A = initial nominal wt% As

B = initial nominal wt% Sb

C = initial nominal wt% Sn

D = melt temperature (°C)

During experimental trials, temperature-time history was to be recorded. Mass gains were also to be recorded using data acquisition software and trials were to be simultaneously filmed in order to correlate observable sample surface phenomena with thermogravimetric data.

CHAPTER 2: LITERATURE REVIEW

In an effort to predict the products of reaction when molten lead containing impurity elements is exposed to oxygen, the system under study will first be considered from the perspective of thermodynamics, then from the point of view of kinetics, and finally on the basis of industrial observations.

2.1 Thermodynamic Considerations

In the operation of the continuous lead softening process, a two-phase system of a bullion, low in arsenic and antimony, and an oxide slag relatively high in those components exists in equilibrium[21]. Unlike some of the other refining stages which are governed by kinetics, Davey[9] considers lead softening to be governed by equilibrium considerations.

The Pb-O, Pb-As-O, Pb-Sb-O and Pb-Sn-O systems are discussed below. Note: Appendix I contains additional activity and interaction coefficient data on the lead system compiled by the present researcher, which may be of use to future students.

2.1.1 Pb-O System

QUICK FACTS:

Pb: MP 327.5 °C, BP 1749 °C.

PbO: MP 888° C

Vapour pressure of liquid **Pb**: 6.96×10^{-7} atm at 600 °C (Maier[22])

Vapour pressure of solid **PbO**: 1.10×10^{-9} atm at 600 °C (Maier[22])

The simplest system to consider is the lead-oxygen system. According to phase diagrams[23] in the literature (Figure 11 - Figure 13), the only expected equilibrium phases are $Pb_{(l)}$, $PbO_{(solid)}$ and oxygen, when oxygen is introduced into a bath of pure lead at softening temperatures (e.g., 600 °C).

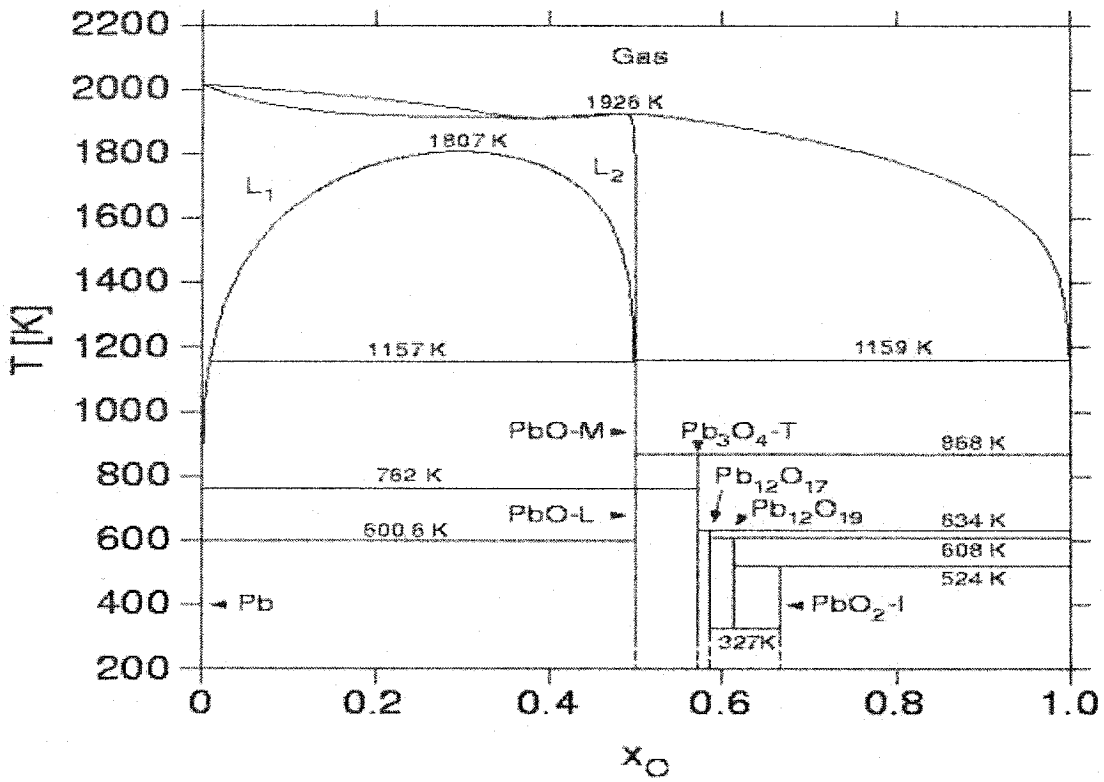

Figure 11. Pb-O Phase Diagram (after Levin et al., 1964, ref 23)

For the PbO oxidation product, the chemical reaction at 600°C would be written as follows:

$$2\ Pb_{(liquid)} + O_{2\,(gas)} = PbO_{(solid)} \qquad \Delta G°_{600C} = -263.54\ kJ/mol \qquad (7)$$

Assuming a_{Pb} and a_{PbO} to both be unity, the equilibrium O_2 partial pressure for this reaction is 1.71×10^{-16} atm. The implication is that lead will oxidize readily in the presence of oxygen.

(Note: unless otherwise stated, thermodynamic values are taken from FACT*Sage*™ [24])

There is good agreement in the literature for the oxygen dissolution reaction into molten lead, as well as the lead oxidation reaction, Table 2.

Table 2. Gibbs Free Energy values for lead-oxygen reactions

Reaction	Gibbs Free Energy Equation	Reaction Number
$\frac{1}{2} O_{2\ (1\ atm)} = \underline{O}_{(1\ at.pct)}$	$\Delta G°_{600C} = -105.9\ kJ\ mol^{-1}$ From Otsuka et al.[25]: $\Delta G°\ (in\ Pb) = -117170 + 12.90T\ (\pm 500)\ J \cdot mol^{-1}$	(8)
$\frac{1}{2} O_2 = \underline{O}_{Pb\ (1\ at.\ pct)}$	$\Delta G°_{600C} = -107.6\ kJ\ mol^{-1}$ From Jacobs and Jeffes[29]: $\Delta G° = -28\ 283 + 2.902\ T$, cal, valid from 500 to 1100°C	(9)
$Pb_{(l)} + \frac{1}{2} O_{2(g)} = PbO_{(yellow)}$	$\Delta G°_{600C} = -131.1\ kJ\ mol^{-1}$ From Alcock & Belford[28]: $\Delta G°\ (720\text{-}1070°K) = -52.43 + 0.02412T\ (\pm 0.31kcal)$	(10)
$Pb_{(l)} + \frac{1}{2} O_{2(g)} = PbO_{(yellow,\ s)}$	$\Delta G°_{600C} = -132.0\ kJ\ mol^{-1}$ From Jacobs & Jeffes[29]: $\Delta G° = -52\ 217 + 23.635\ T\ (\pm 50)$, cal, 475-857°C	(11)
$Pb_{(l)} + \frac{1}{2} O_{2(g)} = PbO_{(s)}$	$\Delta G°_{600C} = -131.8\ kJ\ mol^{-1}$	(12)

The activity of Pb in the lead-oxygen solutions may be assumed to obey Raoult's law since the solubility of oxygen in lead is very small. Since the mole fraction of lead, N_{Pb}, is unlikely to be much less than 0.999, the Raoultian activity of lead, a_{Pb}, equals N_{Pb}, and, it may be regarded as unity within the limits of experimental error[28].

Kharif et al.[26] found that at experimental temperatures up to 1143 K, the solubility of PbO in liquid lead is less than 3 mol%, while the solubility of lead in PbO was less than 0.01

at% but no there was no mention in the article of the solubility of $O_{dissolved}$. These workers stated that it could therefore be assumed that the activities of liquid lead and solid PbO in the coexisting phases are close to unity.

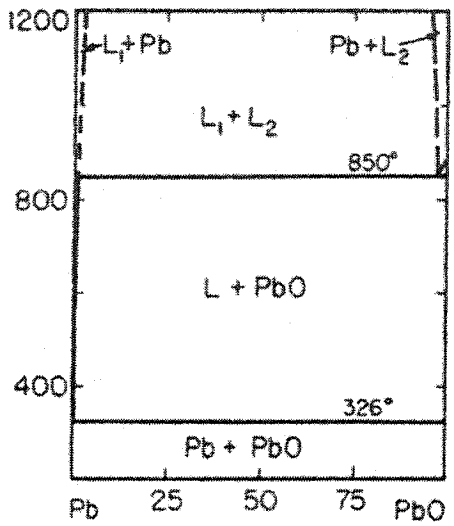

Figure 12. Pb-PbO Phase Diagram (after Massalski, 1990, ref 31)

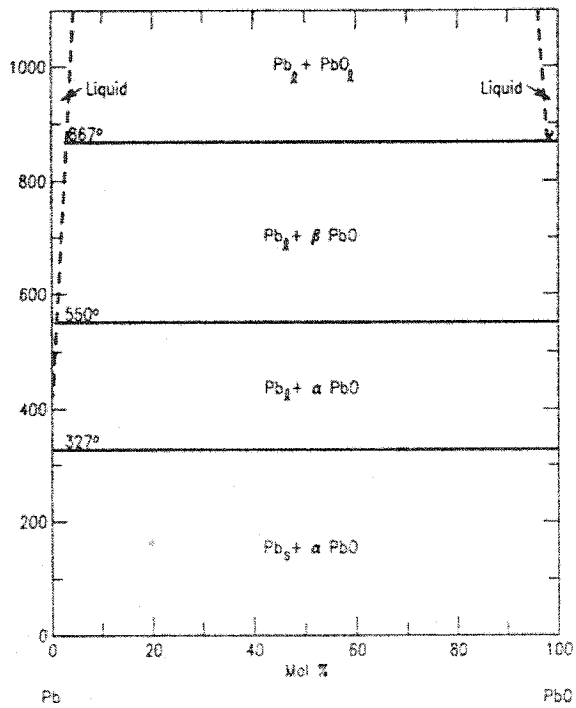

Figure 13. Pb-PbO system (after Roth et al., 1996, ref. 39)

According to the experimentally-determined solubility diagram[27] presented below (Figure 14), the solubility of O in Pb at 600°C is approximately 0.001 mol%. Alcock and Belford[28] report that, at 595 °C, the dissolved oxygen content is equal to 0.0318 at% O (0.00246 wt% O). At 700 °C, results indicate that Sievert's law is obeyed to the saturation limit, which is 0.143 at% O (from Jacobs & Jeffes[29]). Taken together, these results indicate that a very small amount of oxygen will dissolve into the lead.

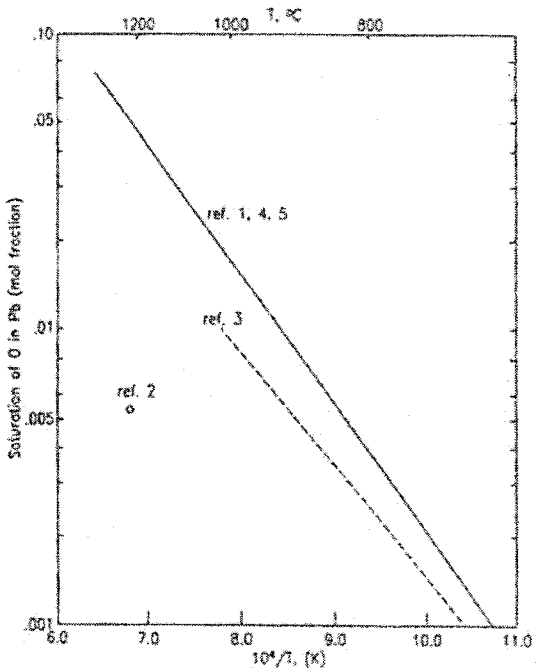

Figure 14. Pb-PbO-O System(after McHale, 1991, ref 27)

2.1.2 Pb-As-O System

QUICK FACTS:

As: Sublimation Point 614 °C at 1 atm, MP 817 °C at 35.8 atm

As_2O_3: MP 313 °C, BP 460 °C

As_2O_5: MP 740°C

$As_{(gas\ phase)}$ contains As_x (x =1, 2, 3, 4) with **As_4** as the predominant species up to approximately 1127 °C [30].

Examining the As-Pb binary phase diagram (Figure 15 and Figure 16), it can be seen to be a eutectic type[31, 32] with no stable intermetallic compounds and exhibiting complete mutual miscibility in the liquid state.

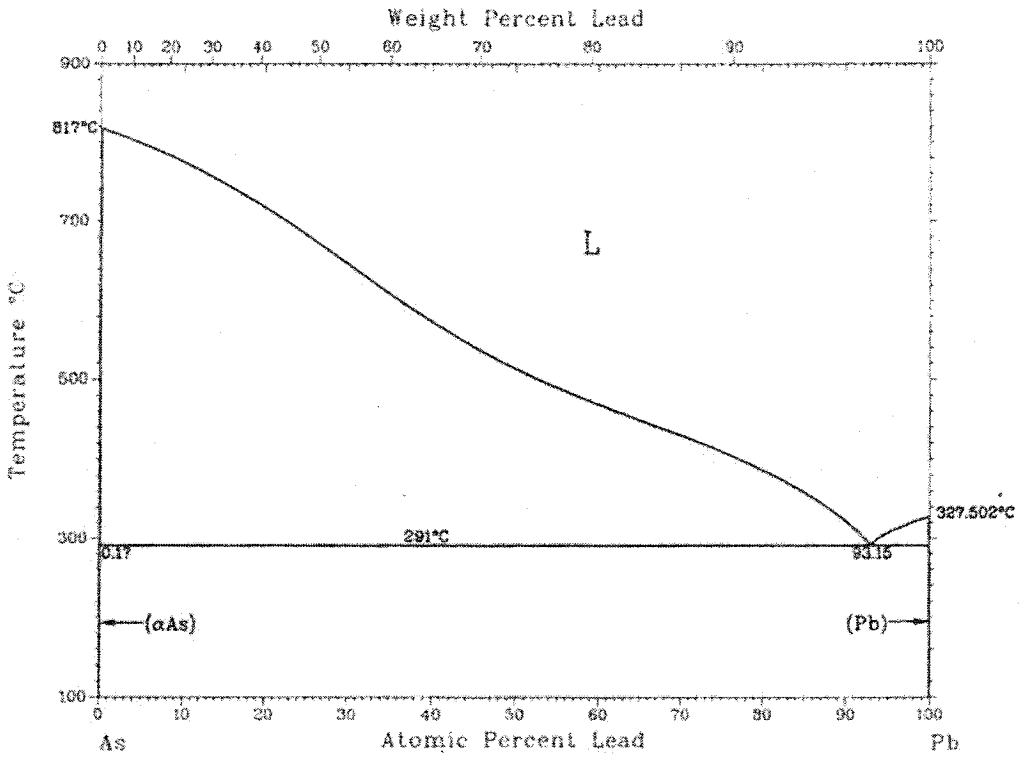

Figure 15. As-Pb Phase Diagram (after Massalski, 1990, ref. 31)

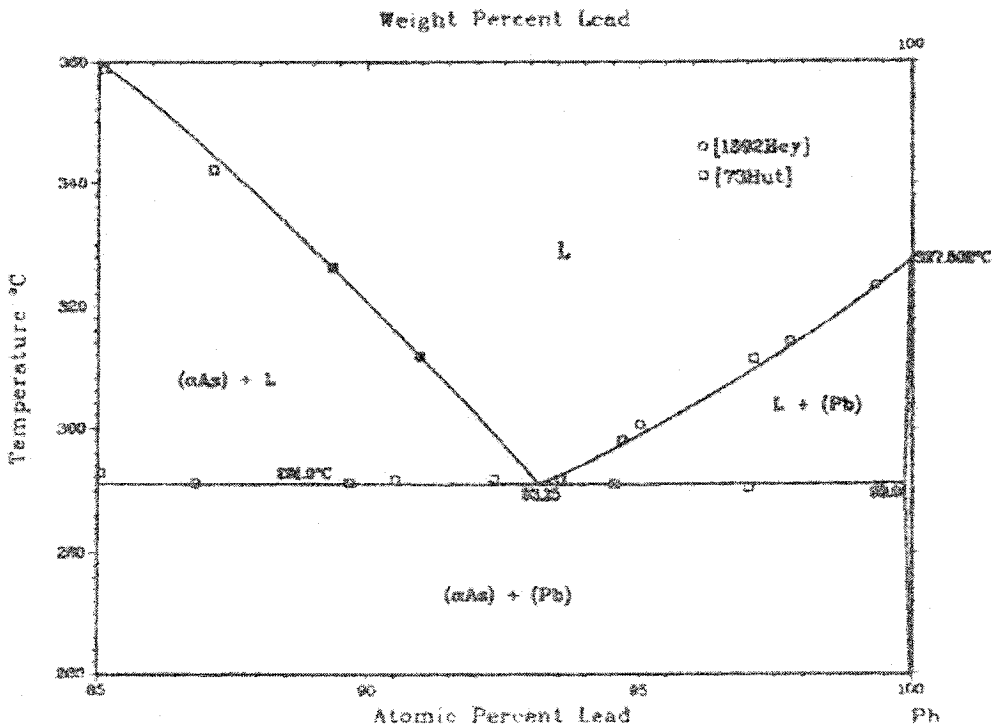

Figure 16. As-Pb Phase Diagram from 85 to 100 at% Pb (after Gokcen, 1990, ref 32)

Much research has been done to determine the activity of the components of the Pb-As system, at different temperatures. Results from these studies are presented briefly below.

Itagaki et al[33] found that the activity of arsenic exhibited a slight positive deviation from Raoultian behaviour when N_{As} was less than 0.15 (Figure 17 and Figure 18). Onderka's work[34] also indicated a positive deviation (Figure 19).

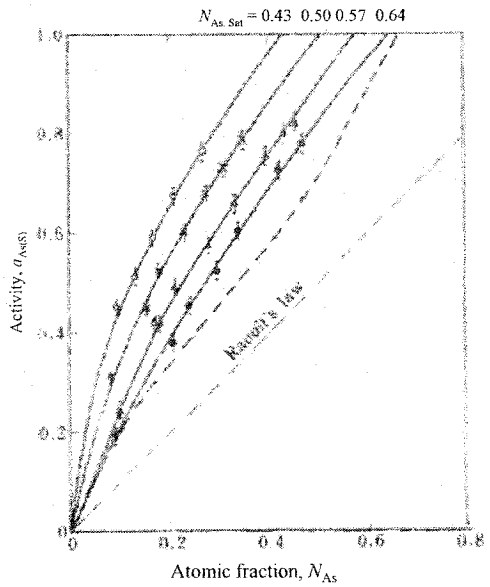

Figure 17. Raoultian activity of arsenic in the liquid Pb-As alloy

--O-- 737 K --x--776.5 K --Δ-- 816 K --●-- 855K (after Itagaki, 1978, ref 33)

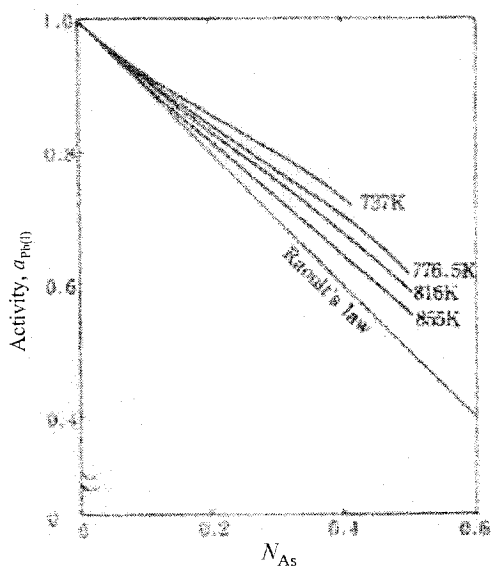

Figure 18. Raoultian activity of lead in the liquid Pb-As alloy (after Itagaki, 1978, ref 33)

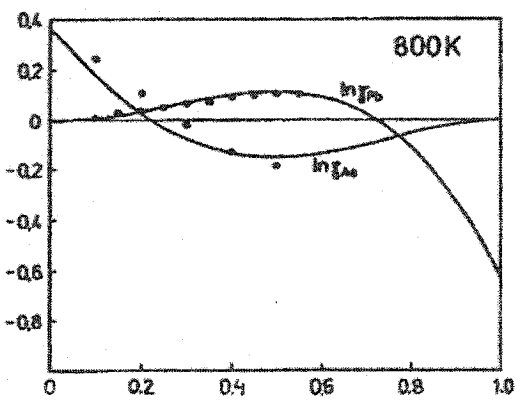

Figure 19. Raoultian activity coefficients for Pb, As in Pb-As system at 800K. Axes are ln γ vs. at % As/Pb (after Onderka, 1990, ref. 34)

From optimized parameters, Sundström and Taskinen[35] calculated temperature dependent functions of the activity coefficients of the components in infinite dilution in liquid lead, Figure 20:

$$\ln \gamma^{\circ}_{As} = -0.577 + 966.5/T \qquad (13)$$

At 600 °C, $\ln \gamma^{\circ}_{[As]} = 1.70$

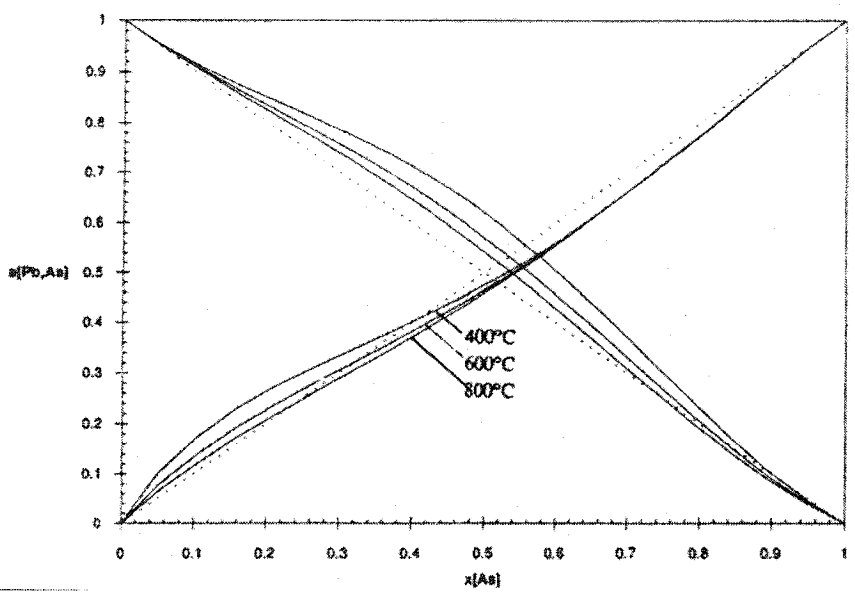

Figure 20. Activities for arsenic and lead at 400 °C, 600 °C, and 800 °C, standard states $As_{(l)}$ and $Pb_{(l)}$. (after Sundström and Taskinen, 1989, ref. 35)

Rannikko et al.[36] found that at infinite dilutions of lead,

$$\ln \gamma^{\circ}_{As} = -0.325 + 444.17/T \text{ (K)} \qquad (14)$$

$$\ln \gamma^{\circ}_{Pb} = -1.168 - 2.65/T \text{ (K)} \qquad (15)$$

At 600°C, $\ln \gamma^{\circ}_{As} = 1.20$.

They found that arsenic showed a negative deviation from the Raoultian solution at concentrations above 10 at% As, Figure 21.

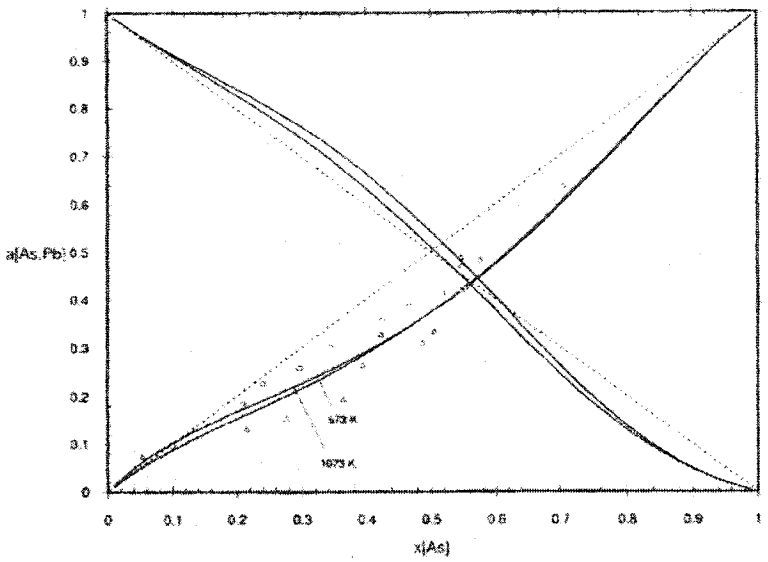

Figure 21. Assessed arsenic and lead activities in As-Pb at 673 and 1073K (after Rannikko et al., 1993, ref. 36)

For the general arsenic oxidation reaction,

$$\tfrac{4}{3}\,As_{(l)} + O_{2(g)} = \tfrac{2}{3}\,As_2O_{3(s)} \qquad \Delta G°_{600} = -296.56\ kJ\ mol^{-1}\ O_2 \qquad (16)$$

Taking the arsenic and arsenic oxide activities both as unity, the equilibrium O_2 partial pressure for this reaction would be 1.81×10^{-18} atm.

The reaction can also be written as:

$$2\,As_{(l)} + 3\,PbO_{(s)} = As_2O_{3\,(l)} + 3\,Pb_{(l)} \qquad \Delta G°_{600} = -99.06\ kJ\ mol^{-1} \qquad (17)$$

Using $X_{As} = 0.027$ (0.9 wt%), $\gamma_{As} = 1.5$ (average of values from Sundström[35] and Rannikko[36]), $\gamma_{As_2O_3} = 2.24$ (average of values from Itagaki[33] and FACT*Sage*™), and $X_{As_2O_3} = 0.25$ (Zunkel[37] distribution),

$\Delta G_{600} = \Delta G°_{600} + RT\ lnQ = -56.8\ kJ\ mol^{-1}$, i.e., the reaction is spontaneous.

Zunkel's[37] results at 650 °C support the above conclusion with the following reaction expression and corresponding $\Delta G°$ value:

$$2\ As_{(1\ wt\%\ in\ Pb\ (l))} + 3\ PbO_{(l)} = As_2O_{3\ (l)} + 3\ Pb_{(l)} \qquad \Delta G^\circ_{650} = -40.99\ kJ\ mol^{-1} \qquad (18)$$

The thermodynamic software consulted (FACT*Sage*™) makes no mention of specific complex As-Pb-O phases which may form, with the exception of a liquid slag (Liq-slag) solution phase. The following are the results for a lead bullion containing arsenic contacting oxygen:

0.01 As	+	0.99 Pb	+	0.5 O_2	=
(600,1,liq,#1)		(600,1,liq,#1)		(600,1,g,#1)	

0.50064E-02 mol	(0.99936	Pb	*where* $\gamma_{Pb} = 1.0$	
	+ 0.29807E-07	As	*where* $\gamma_{As} = 1.332$	
	+ 0.64397E-03	O	*where* $\gamma_{O} = 4.705E\text{-}5$	)
	(600.00 C, 1 atm, Pb-liq)			
+ 0.99000 mol	(0.99495	PbO	*where* $\gamma_{PbO} = 1.0$	
	+ 0.50505E-02	As_2O_3	*where* $\gamma_{As_2O_3} = 0.133$	T)
	(600.00 C, 1 atm, Slag-liquid)			

DELTA G = -1.269E+02 KJ

Data on 1 product species identified with "T" have been extrapolated

This FACT*Sage*™ output indicates that the bullion containing 0.01 at% As would come to be in equilibrium with a PbO-As_2O_3 slag with a 200:1 molar ratio.

Consultation of the various available pseudobinary phase diagrams based on the Pb-As-O ternary system indicates that a number of complex phases may exist, specifically in the temperature range below the melting point of PbO (880 °C), the arsenic oxide phase may act as a fluxing agent towards the PbO, and produce a complex oxide phase.

Kasenov et al.[38] constructed a phase equilibrium diagram for the PbO-As_2O_5 systems (Figure 22), which has been redrawn in Figure 23.

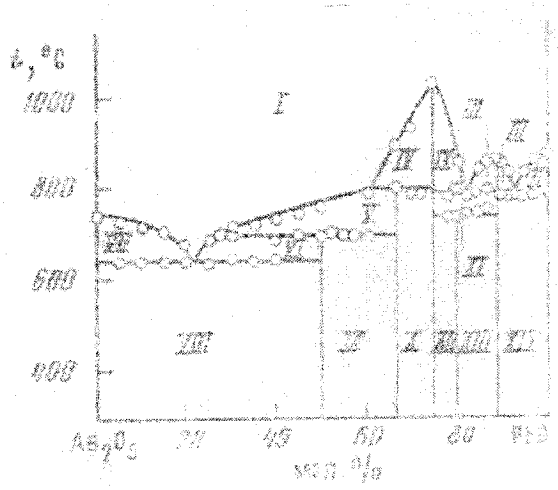

Figure 22. As_2O_5-PbO pseudobinary phase diagram (after Kasenov et al, 1991, ref 38).

Liquid (I), *l* + PbO (II), *l* + $Pb_8As_2O_{13}$ (III), *l* + $Pb_3(AsO_4)_2$ (IV), *l* + $Pb_2As_2O_7$ (V), *l* + $Pb(AsO_3)O_2$ (VI), *l* + As_2O_5 (VII), As_2O_5 + $Pb(AsO_3)_2$ (VIII), $Pb(AsO_3)_2$ + $Pb_2As_2O_7$ (IX), $Pb_2As_2O_7$ + $Pb(AsO_4)_2$ (X), $Pb_3(AsO_4)_2$ + $Pb_8As_2O_{13}$ (XI), $Pb_3(AsO_4)_2$ + $Pb_4As_2O_9$ (XII), $Pb_4As_2O_9$ + $Pb_8As_2O_{13}$ (XIII), $Pb_8As_2O_{13}$ + As_2O_5 (XIV)

Figure 24 appears to be based on the same diagram, but the phase notation suggests[39] that the complex phases are composed of bound PbO-As_2O_5 molecules, an assertion rejected by the original researchers who insist that $Pb_8As_2O_{13}$, $Pb_4As_2O_9$ and $Pb_2As_2O_7$, $Pb_3(AsO_4)_2$ are "individual compounds, not bound complexes consisting of lead and arsenic oxides"[40].

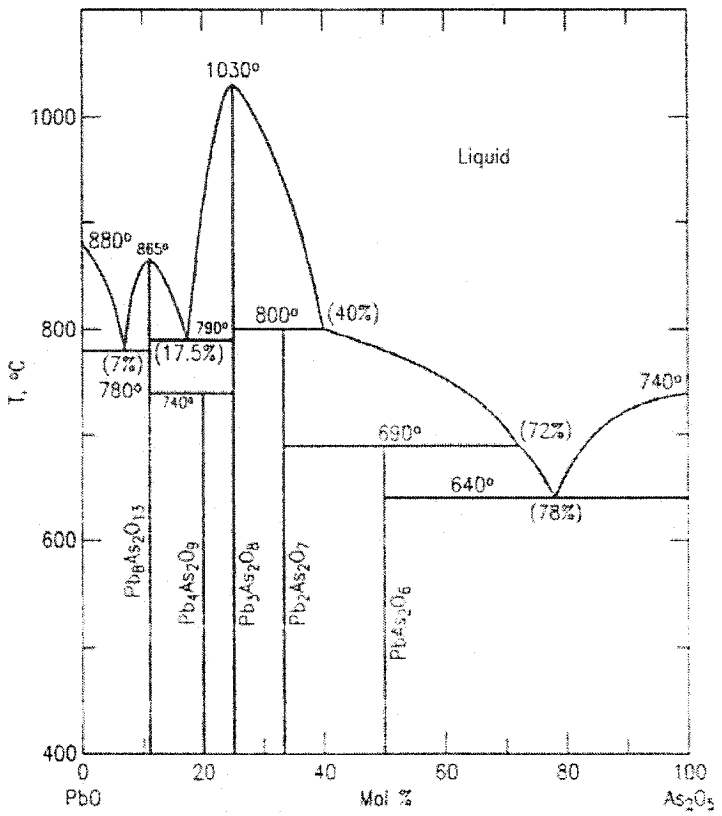

Figure 23. PbO-As_2O_5 pseudobinary phase diagram (after Roth et al., 1996, ref. 39)

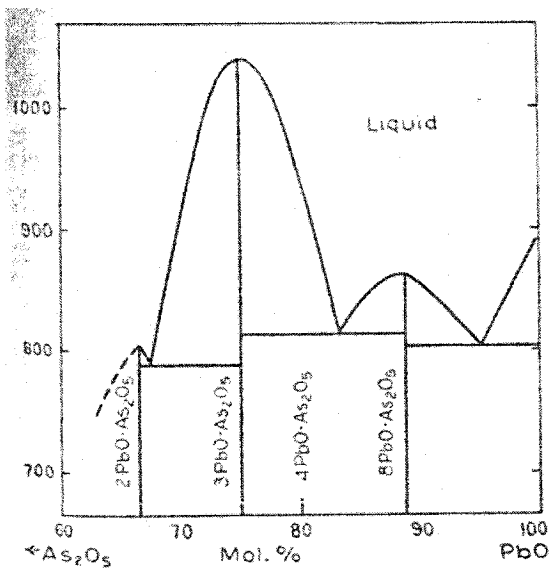

Figure 24. System PbO-2PbO•As_2O_5 (after Roth et al., 1996, ref. 39)

Zunkel and Larson[37] studied the PbO-As_2O_3 system extensively. Their findings (Figure 25) are interpreted in the following manner: (i) at low As_2O_3 contents of the slag, the equilibrium As content of the metal phase increases with increasing As_2O_3 content in the slag indicating a single-phase solid-solution slag, (ii) for As_2O_3 contents greater than the solid-solution slag region, the As equilibrium content in the metal phase remains constant indicating a two-phase slag region; and (iii) for As_2O_3 contents grater than the two-phase slag region, the As equilibrium content in the metal phase continues to increase with increasing As_2O_3 concentration in the slag indicating a single-phase liquid slag region.

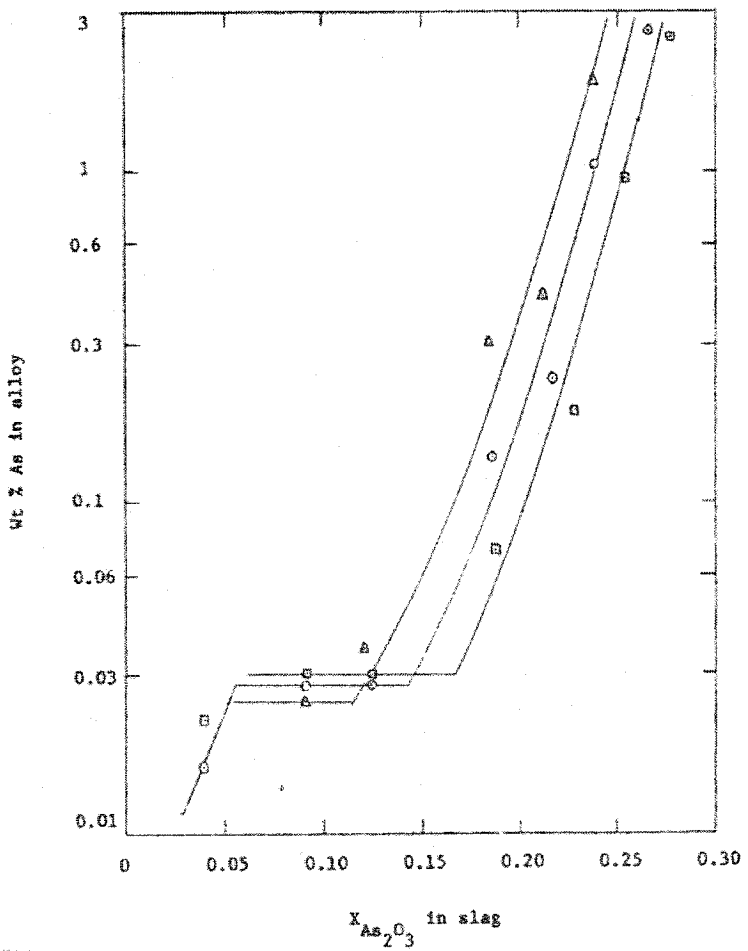

Figure 25. Equilibrium arsenic contents of Pb-As alloys in contact with PbO-As_2O_3 slags (after Zunkel et al., 1967, ref. 37)

The overall equilibrium can be described by the following equation:

$$2\,\underline{As}_{(1\ wt\%\ in\ Pb,\ l)} + 3\,PbO_{(l)} \leftrightarrow As_2O_{3\,(l)} + 3\,Pb_{(l)} \qquad \Delta G°_{650C} = -40.99\ kJ\ mol^{-1} \qquad (19)$$

From their data, a partial PbO-As_2O_3 pseudobinary phase diagram was generated (Figure 26), and is redrawn with the fields labelled in Figure 27. It indicates that a liquid oxide phase exists under the following conditions:

- at 500°C where $X'_{As} > 0.36$ (where X'_{As} is the molar ratio of As/(As+Pb) in the oxide phase)
- at 600°C where $X'_{As} > 0.33$ (where X'_{As} is the molar ratio of As/(As+Pb) in the oxide phase)

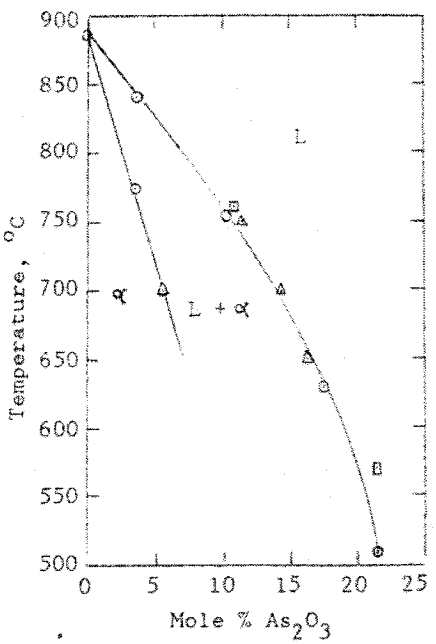

Figure 26. Phase diagram for the Pb-rich end of the PbO-As_2O_3 system (after Zunkel et al., 1967, ref. 37)

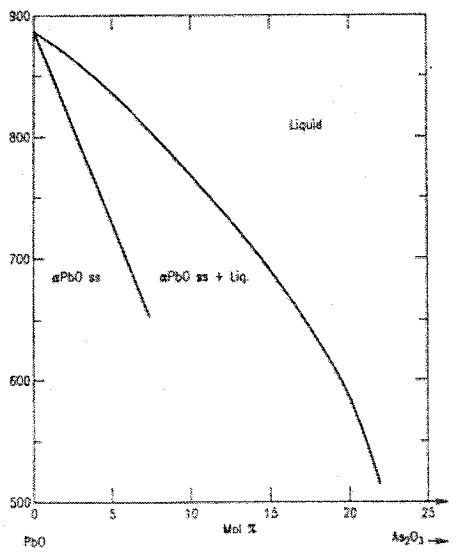

Figure 27. System PbO-As_2O_3 (after Roth et al., 1996, ref. 39)

In other related research on the topic, Maier[22] found by vapour-density determinations that arsenic trioxide gas has the composition As_4O_6.

McClincy and Larson[41] determined the vapour pressures of As_4 above dilute As-Pb alloys at 703°C, where:

0.52 wt% As	X_{As}= 0.0143	P_{As_4} = 0.0078 mm Hg	a_{As}=0.0261
1.00 wt% As	X_{As}= 0.0279	P_{As_4} = 0.0147 mm Hg	a_{As}=0.0306

Lastly, Itagaki[33] generated a family of curves (Figure 28) correlating wt% As with activity of As_2O_3 for the following equilibrium:

$$3\ PbO_{(l)} + 2\ As_{(l)} = 3\ Pb_{(l)} + As_2O_{3\ (l)} \qquad (20)$$

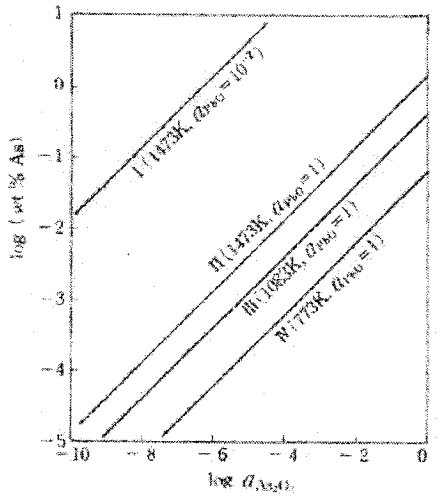

Figure 28. Correlation between the arsenic content in the crude lead and the activities of lead oxide and arsenic oxide in liquid oxide mixtures coexisting with the crude lead (after Itagaki, 1978, ref 33)

2.1.3 Pb-Sb-O System

QUICK FACTS:

Sb: MP 630.7 °C, BP 1587 °C

Sb_2O_3: MP 656 °C

The Pb-Sb system displays simple eutectic behaviour, as seen in the binary phase diagram, Figure 29.

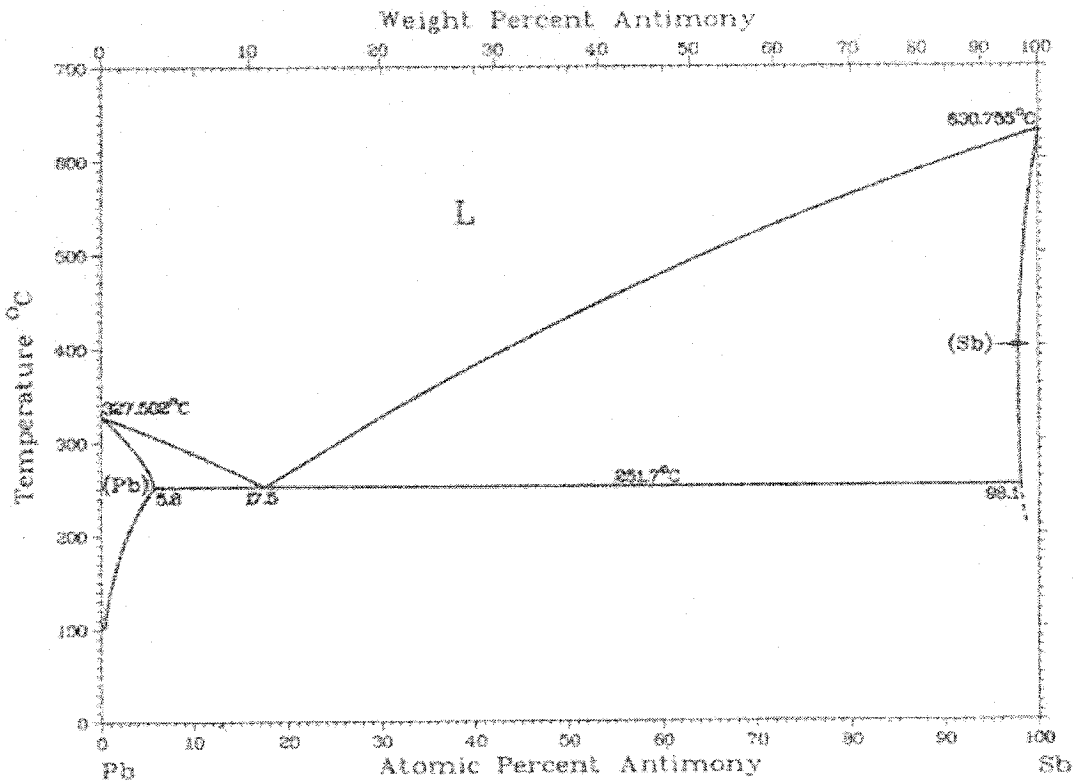

Figure 29. Pb-Sb binary phase diagram (after Massalski, 1990, ref 31)

As with the Pb-As system, much experimental work has been devoted to determining the activity of the components of the Pb-Sb system, at different temperatures.

Hultgren[42] found activity values for Pb and Sb in Pb-Sb liquid alloys at 905 K:

Where $x_{Sb} = 0$, $a_{Sb} = 0$, $\gamma_{Sb} = 0.779$. $x_{Pb} = 1.0$, $a_{Pb} = 1.0$, $\gamma_{Pb} = 1.00$

$x_{Sb} = 0.1$, $a_{Sb} = 0.082$, $\gamma_{Sb} = 0.817$ $x_{Pb} = 0.9$, $a_{Pb} = 0.898$, $\gamma_{Pb} = 0.998$

Moser et al.[43] determined equations for activity coefficients of lead and antimony (T in °C) which are in good agreement with the above values:

$$\ln \gamma_{Pb} = -\left(\frac{101}{T} + 0.063\right)(1 - X_{Pb})^{1.83} \qquad (21)$$

$\gamma_{Pb} = 1.00$ at 600°C, where $X_{Pb} = 0.967$ (≈ 98 wt%).

$$\ln \gamma_{Sb} = -\left(\frac{101}{T} + 0.063\right)\left[(1 - X_{Pb})^{1.83} - 2.205(1 - X_{Pb})^{0.83} + 1.205\right] \qquad (22)$$

$\gamma_{Sb} = 0.78$ at 600 °C, where $X_{Sb} = 0.033$ (≈ 2 wt%).

Taskinen and Teppo[44], and Seltz and DeWitt[45] generated activity curves for the Pb-Sb system at 748 K and saw that the negative deviations of the activities from Raoultian behaviour are small.

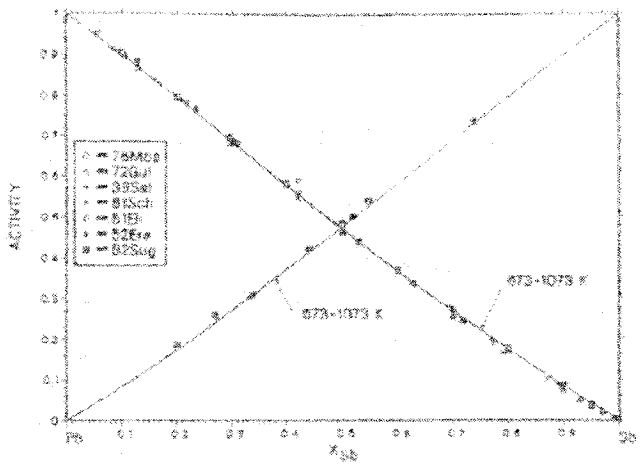

Figure 30. Antimony and lead activities in molten lead-antimony alloys at 673-1073K (after Taskinen and Teppo, 1992, ref . 44)

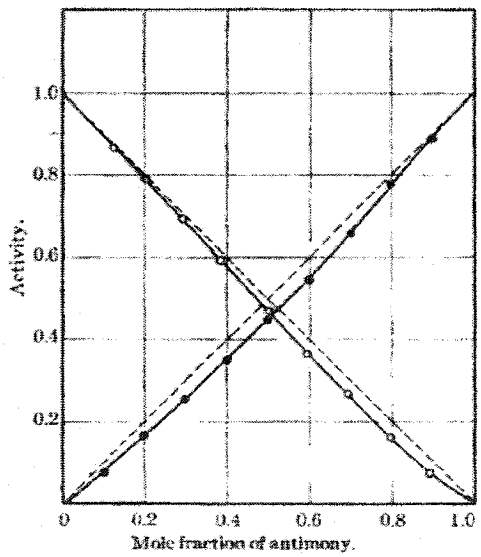

Figure 31. Activity curves for Pb and Sb (after Seltz, 1939, ref.45)

For the general antimony oxidation reaction,

$$\tfrac{4}{3}\,Sb_{(l)} + O_{2(g)} = \tfrac{2}{3}\,Sb_2O_{3(s)} \qquad \Delta G°_{600} = -317.90 \text{ kJ mol}^{-1}\ O_2 \qquad (23)$$

Taking the antimony and antimony oxide activities both as unity, the equilibrium O_2 partial pressure for this reaction would be 9.52×10^{-20} atm.

The reaction can also be written as:

$$2\,Sb_{(l)} + 3\,PbO_{(s)} = Sb_2O_{3\,(l)} + 3\,Pb_{(l)} \qquad \Delta G°_{600C} = -163.08 \text{ kJ mol}^{-1} \qquad (24)$$

However, using $X_{Sb} = 0.033$, using $\gamma_{Sb} = 0.78$ (Moser et al.[43]), $\gamma_{Sb_2O_3} = 0.324$ (average of values from McClincy et al. [52] and Zunkel et al. [53]), and $X_{Sb_2O_3} = 0.37$ (Zunkel[53]), $\Delta G_{600} = \Delta G°_{600} + RT \ln Q = -125.35$ kJ mol^{-1}, i.e., the reaction is spontaneous..

Zunkel's[53] results at 650 °C support the above conclusion with the following reaction expression and corresponding $\Delta G°$ value:

$$2\ Sb_{(1\ wt\%\ in\ Pb\ (l))} + 3\ PbO_{(l)} = Sb_2O_{3\ (l)} + 3\ Pb_{(l)} \qquad \Delta G°_{650C} = -30.37\ kJ \qquad (25)$$

FACT*Sage*™ makes no mention of specific complex Sb-Pb-O phases which may form, and when the slag is limited to an ideal solution, the following is obtained for a lead bullion containing antimony when contacted with oxygen:

0.02 Sb + 0.98 Pb + 0.5 O_2 =
(600,1,liq,#1) (600,1,liq,#1) (600,1,g,#1)

0.10013E-01 mol (0.99930 Pb *where* $\gamma_{Pb} = 1.0$
+ 0.58125E-04 Sb *where* $\gamma_{Sb} = 7.254$
+ 0.64440E-03 O *where* $\gamma_O = 4.751E\text{-}5$)
(600.00 C, 1 atm, Pb-liq)

+ 0.97999 mol (0.98980 PbO *where* $\gamma_{PbO} = 1.0$
+ 0.10204E-01 Sb_2O_3 *where* $\gamma_{Sb_2O_3} = 1.0$)
(600.00 C, 1 atm, Ideal#1)

DELTA G = -1.272E+05 J

This FACT*Sage*™ output indicates that the bullion containing 0.02 at% Sb will come to equilibrium with a PbO-Sb_2O_3 ideal solution slag with a PbO to Sb_2O_3 ratio of roughly 95:1.

In other studies of the Pb-Sb-PbO-Sb_2O_3 system, Itoh et al[46] found that both oxides exhibit slight negative deviation from Raoult's law. At 1173K (900°C):

$N_{Pb} = 0.9796$; $N_{Sb} = 0.0204$; $N_O = 0.00$; $X_{Sb} = 0.0204$.
metal phase

$$N'_{Pb} = 0.3703; \quad N'_{Sb} = 0.1049; \quad N'_{O} = 0.5248; \quad X'_{Sb} = 0.2207.$$

where N and N' denote mole fraction, $X_{Sb} = N_{Sb}/(N_{Pb}+N_{Sb})$ molar ratio in metal, $X'_{Sb} = N'_{Sb}/(N'_{Pb}+N'_{Sb})$ molar ratio in oxide

This trend can be seen clearly in the activity-molfraction plots below (Figure 32 and Figure 33).

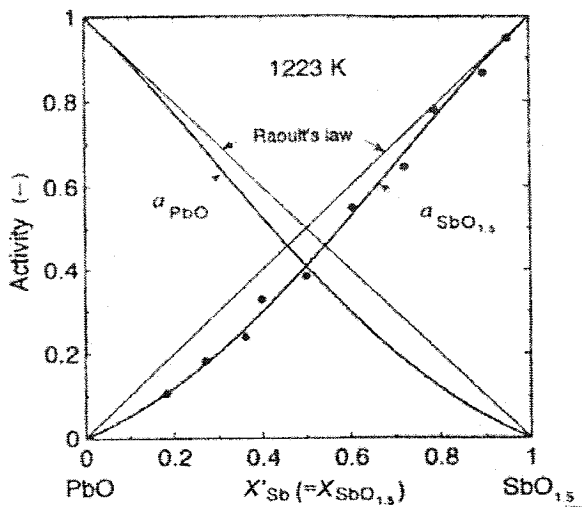

Figure 32. Activities of PbO and $SbO_{1.5}$ at 1223 K (after Itoh, 2001, ref. 46)

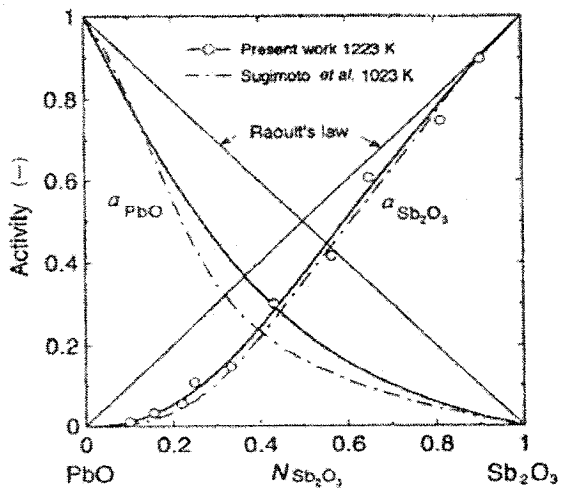

Figure 33. Activities of PbO and Sb_2O_3 at 1023 K (after Itoh, 2001, ref. 46)

Consultation of the various available pseudobinary and Pb-Sb-O ternary phase diagrams indicates that a number of complex Pb-Sb-O phases may exist, in the temperature range below the melting point of PbO (888 °C).

Milyan et al. [47] generated a ternary phase diagram from their work (Figure 34), which differs significantly from the Pb-Sb-O diagram found in the Phase Diagrams for Ceramists (Figure 35, reproduced from the work of Hennig and Kohlmneyer[48])

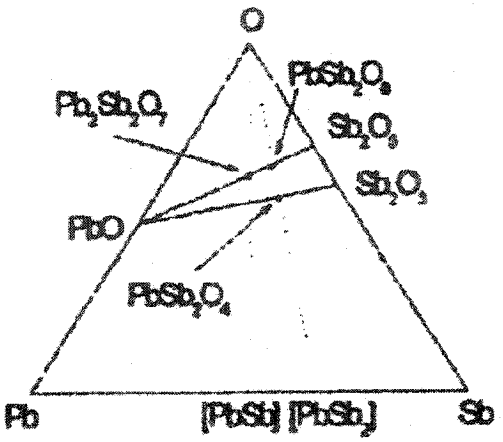

Figure 34. Pb-Sb-O ternary phase diagram (after Milyan et al., 1999, ref.47)

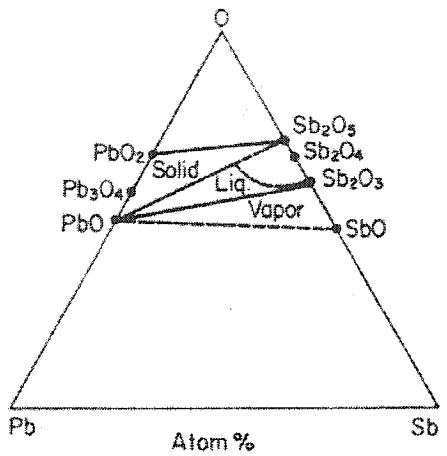

Figure 35. System Pb-Sb-O (after Roth et al., 1996, ref. 39)

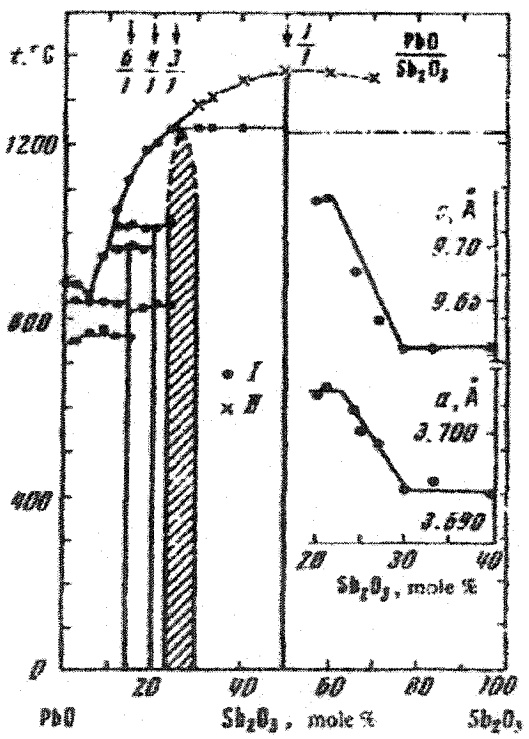

Figure 36. Equilibrium diagram of the PbO-Sb_2O_3 system in the presence of atmospheric oxygen (after Bush et al., 1978, ref 49)

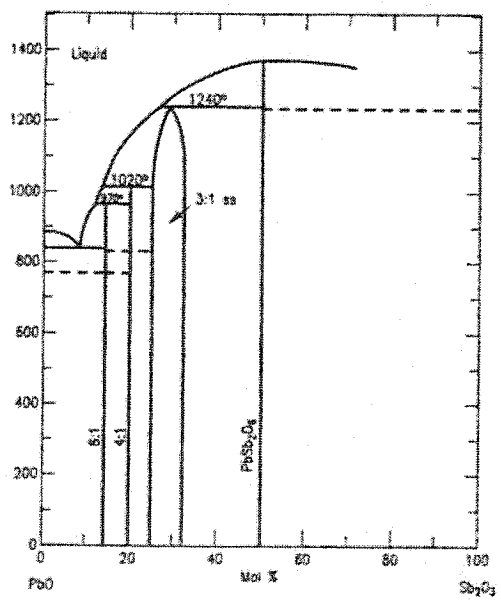

Figure 37. System PbO-Sb_2O_3-Sb_2O_5 (after Roth et al., 1996, ref. 39)

Bush and Venevtsev[49] found that intermediate compounds are formed in the PbO-Sb_2O_3 system, namely $PbSb_2O_6$, $Pb_{3+x}Sb_2O_{8+x}$ (with a homogeneity range of 23 – 30 mol% Sb_2O_3), $Pb_4Sb_2O_9$, and $Pb_6Sb_6O_{11}$. This pseudobinary phase diagram is presented in Figure 36 (and reproduced in Figure 37).

As can be seen, there are four intermediate compounds with ratios of the initial oxides, PbO:Sb_2O_3 of 1:1, 3:1, 4:1, and 6:1. It was assumed that Sb^{3+} is oxidized to Sb^{5+} during the formation of the compounds in the presence of atmospheric oxygen.

Maier[22] mentions several reactions involving complex species or higher order antimony oxides, for example:

$$2PbO{\bullet}Sb_2O_{3\,(s)} = Sb_4O_{6\,(g)} + 2PbO_{\,(s)} \qquad \Delta G°_{970K} = -6.7\ kJ \qquad (26)$$

$$2Sb_2O_{3\,(cubic)} + O_{2\,(g)} = 2\ Sb_2O_{4\,(s)} \qquad \Delta G°_{298K} = 162.4\ kJ \qquad (27)$$

$\Delta G°$ for this latter reaction indicates that Sb_2O_4 is more stable than Sb_2O_3. Maier[22] found that when mixtures of 69.5 wt% PbO and 30.5 wt% Sb_2O_3 were heated to this melting point (575 °C), minute particles of liquid lead were formed. Bush et al.[49] found that the oxidation of Sb_2O_3 (valentinite) to Sb_2O_4 (cervantite) takes place in the range from 480 to 780 °C.

Maier and Hincke[50] performed the original work on the Pb-Sb-O system (Figure 38), and found a rapid oxidation of both Sb_2O_3 to higher oxides, and of lead antimonites ($PbO{\bullet}Sb_2O_3$) to lead antimonates ($PbO{\bullet}Sb_2O_5$) upon heating in air.

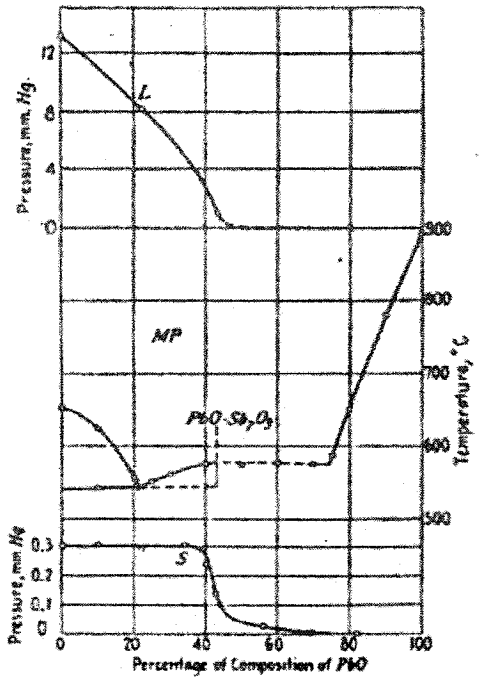

Figure 38. Melting point curve for $PbO\text{-}Sb_2O_3$ system. Curve MP is the melting point diagram. Curve L is the vapour pressure of liquid mixtures at 697°C. Curve S is the vapor pressure of solid mixtures at 539°C. (after Maier and Hincke, 1932, ref 50)

They summarized possible oxidation reactions as follows:

1 Bullion

(a) Sb by elementary oxygen
(b) Pb by elementary oxygen
(c) Sb by higher oxides of Sb or Pb
(d) Pb by higher oxides of Sb or Pb

2 Slag

(a) lower to higher oxides of Sb by elementary oxygen
(b) lower to higher oxides of Sb by lead oxide

It was found that compositions above 70 wt% PbO showed an oxidation of Sb_2O_3 to higher oxide, with the formation of metallic lead, and a vitreous slag phase. Moreover, it was found that antimony trioxide is volatilized rapidly only at compositions with lead content below that of the compound $PbO{\cdot}Sb_2O_3$.

Taloi[51] mathematically modeled metal-slag equilibrium in the $Pb\text{-}Sb\text{-}PbO\text{-}Sb_2O_3$ system at 700°C, producing the following antimony distributions,

Table 3. Values for metal-slag equilibrium in Pb-Sb-PbO-Sb_2O_3 system at 700 °C (after Taloi, 1992, ref. 51.)

$X_{Sb_2O_3}$	% Sb in Pb
0.186	0.127
0.212	0.290
0.260	0.707
0.292	1.04
0.375	1.89
0.398	2.14

McClincy and Larson[52] found that the activity of PbO in slags containing more than 63 mol% PbO deviated positively from ideality while a negative deviation was found for slags containing less PbO.

It was determined that activities in a 2-phase slag in PbO-Sb_2O_3 system at 650 °C were as follows (it is assumed that PbO activity in the 2-phase slag region does not vary significantly with temperature, and was estimated at 0.964):

$X_{Sb_2O_3}$ (slag) = 0.108; $P_{Sb_4O_6}$ = 0.0162 mm Hg; $\gamma_{Sb_2O_3}$ = 0.342; $\frac{a_{Sb_2O_3}}{a_{PbO}^3} = 0.0412$

$X_{Sb_2O_3}$ (slag) = 0.176; $P_{Sb_4O_6}$ = 0.0160 mm Hg; $\gamma_{Sb_2O_3}$ = 0.209; $\frac{a_{Sb_2O_3}}{a_{PbO}^3} = 0.0410$

McClincy et al[52] determined the activities of PbO and Sb_2O_3 in the PbO-Sb_2O_3 system at 700 °C, Figure 39, from which it can be seen that Sb_2O_3 deviates negatively from ideal Raoultian behaviour, while PbO activity deviates positively from ideality, first positively, and then negatively over the same range.

In their work, Zunkel and Larson[53] established that $\frac{a_{Sb_2O_3}}{a_{PbO}^3}$ is a constant independent of temperature in the two-phase slag region in the PbO-rich end of the PbO-Sb_2O_3 system.

Their plot of equilibrium antimony contents of Pb-Sb alloys in contact with PbO-Sb_2O_3 slags at 650°C is shown in Figure 40.

The results of Zunkel and Larson[53] on the PbO-Sb_2O_3 system can be interpreted in the following manner: (i) at low Sb_2O_3 contents of the slag, the activity of Sb increases and the activity of PbO decreases with increasing Sb_2O_3 concentration in the slag indicating a single-phase solid-solution slag, (ii) for Sb_2O_3 contents greater than the solid-solution slag region, the activities of both Sb_2O_3 and PbO remain constant indicating a two-phase slag region; and (iii) for Sb_2O_3 contents grater than the two-phase slag region, the activity of Sb_2O_3 continues to increase, and the activity of PbO continues to decrease with increasing Sb_2O_3 concentration in the slag indicating a single-phase liquid slag region.

They assumed that Henry's law was obeyed over a sufficiently wide range of both temperature and concentration for antimony dissolved in lead, that ΔC_p for the reaction is zero, and that the activity of lead is unity.

$$2\ Sb_{(1\ wt\%\ in\ Pb,\ l)} + 3\ PbO_{(l)} \leftrightarrow Sb_2O_{3\ (l)} + 3\ Pb_{(l)} \qquad \Delta G°_{650C} = -21.7\ kJ \qquad (28)$$

$$Pb_{(l)} + 2\ Sb_{(l)} + 2\ O_{2\ (g)} \leftrightarrow PbO{\bullet}Sb_2O_3 \qquad \Delta G°_{604C} = -612.8\ kJ \qquad (29)$$

The PbO-rich end of the PbO-Sb_2O_3 pseudobinary phase diagram generated by Zunkel et al[53] is presented in Figure 41 and Figure 42. It can be observed that a two-liquid zone exists for Sb_2O_3 molfractions slightly greater than the eutectic composition (21.6 %.)

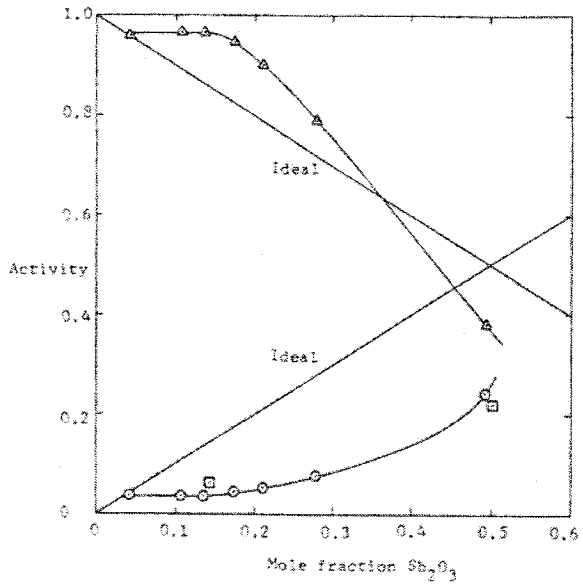

Figure 39. Activities of PbO and Sb_2O_3 in the PbO-Sb_2O_3 system at 700°C (after McClincy et al., 1968, ref. 52)

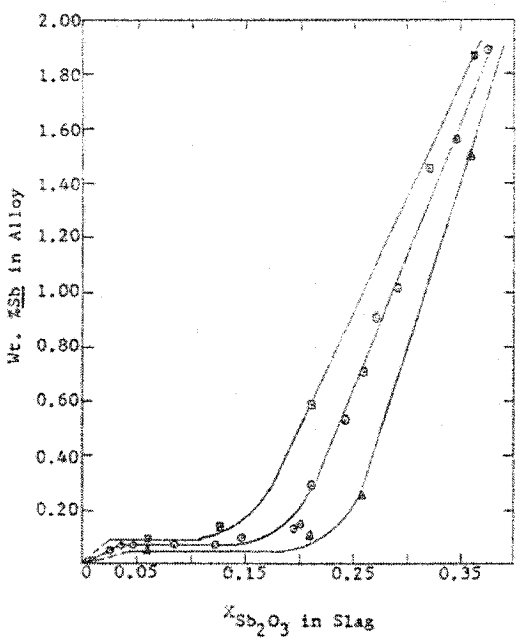

Figure 40. Equilibrium antimony contents of Pb-Sb alloys in contact with PbO-Sb_2O_3 slags at 650°(Δ), 700°(○) and 750°C (□) (after Zunkel et al., 1967, ref. 53)

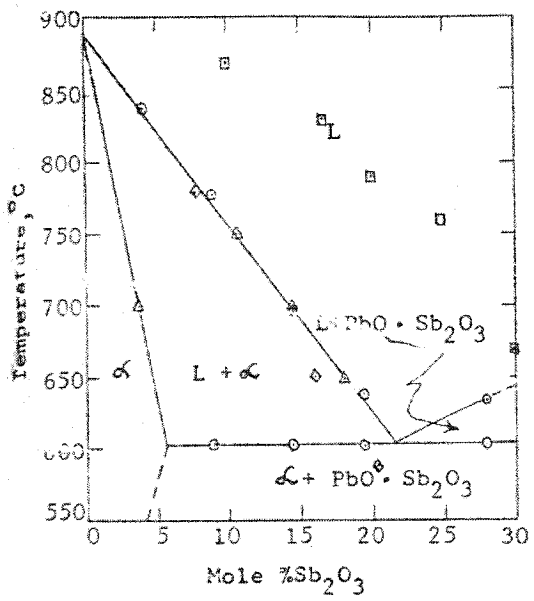

Figure 41. Phase diagram for the PbO-rich end of the PbO-Sb_2O_3 system (after Zunkel et al., 1967, ref. 53)

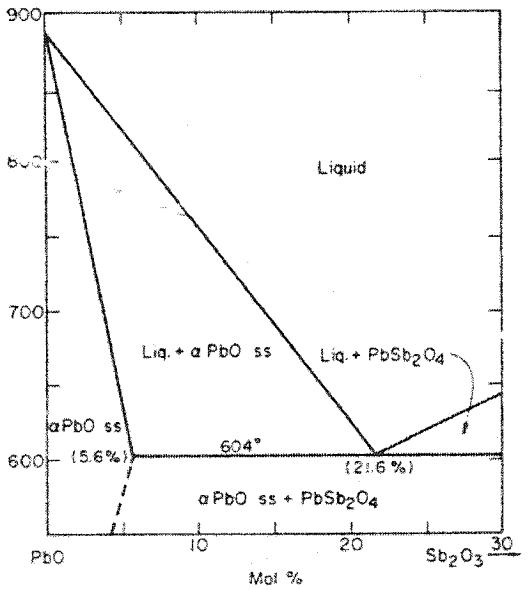

Figure 42. System PbO-Sb_2O_3 showing PbO-rich end (after Roth et al, 1996, ref. 39)

Other pseudobinary phase diagrams from the literature for the $PbO\text{-}Sb_2O_3$, $PbO\text{-}Sb_2O_4$, and $PbO\text{-}Sb_2O_5$ systems are presented below (Figure 43 - Figure 47).

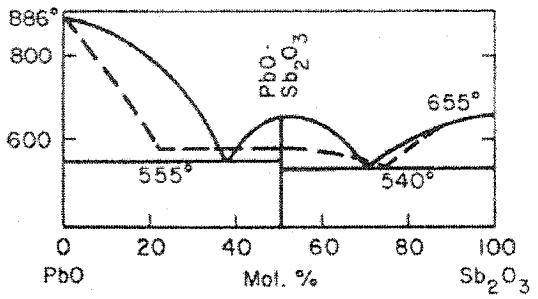

Figure 43. $PbO\text{-}Sb_2O_3$ (after Roth et al., 1996, ref. 39)

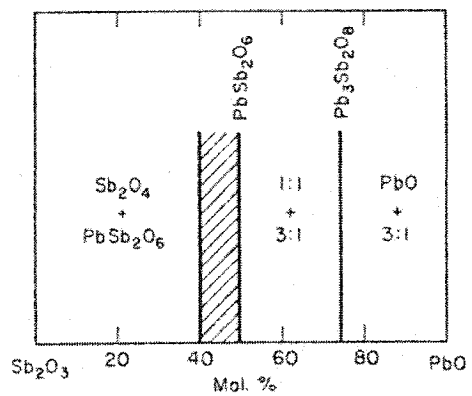

Figure 44. $PbO\text{-}Sb_2O_3$ (after Roth et al., 1996, ref. 39)

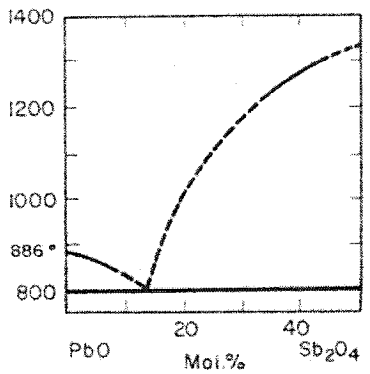

Figure 45. $PbO\text{-}Sb_2O_4$ (after Roth et al., 1996, ref. 39)

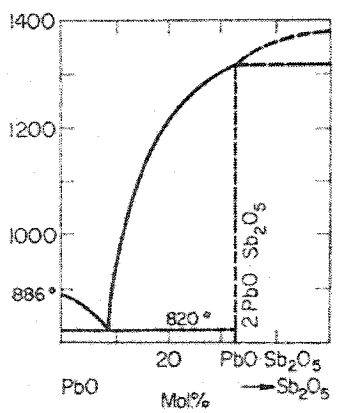

Figure 46. $PbO\text{-}PbO\cdot Sb_2O_5$ (after Roth et al., 1996, ref. 39)

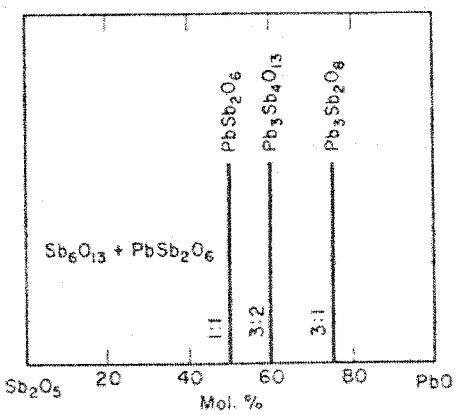

Figure 47. $PbO\text{-}Sb_2O_5$ (after Roth et al., 1996, ref. 39)

2.1.4 Pb-Sn-O System

QUICK FACTS:

Sn MP 232 °C, BP 2602 °C,

SnO_2 BP 1630°C

The Pb-Sn binary phase diagram is a simple eutectic, Figure 48.

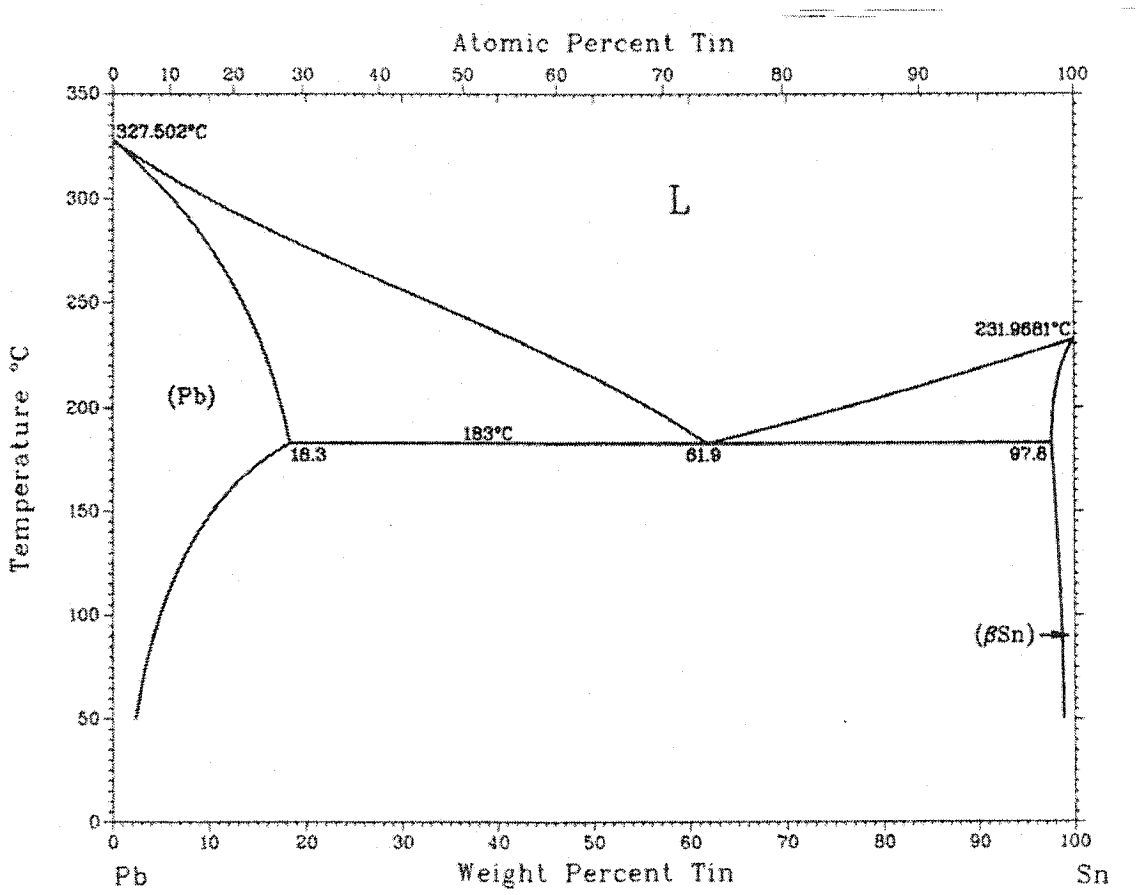

Figure 48. Pb-Sn binary phase diagram (after Massalski, 1990, ref 31)

Hultgren[42] determined activity values for Sn and Pb in Pb-Sn liquid alloys at 1050 K, finding a positive deviation from ideality in both cases, where:

$x_{Sn} = 0$; $a_{Sn} = 0$; $\gamma_{Sn} = 6.816$; $x_{Pb} = 1.0$; $a_{Pb} = 1.0$; $\gamma_{Pb} = 1.00$.

$x_{Sn} = 0.1$; $a_{Sn} = 0.346$; $\gamma_{Sn} = 3.458$; $x_{Pb} = 0.9$; $a_{Pb} = 0.931$; $\gamma_{Pb} = 1.035$.

In their studies, Das and Ghosh[54] found that in the range from 857 to 1100 K, activities of both tin and lead exhibited only moderate positive deviations from the respective Raoult's law lines and that their findings do not agree with the values reported in the literature, Figure 49.

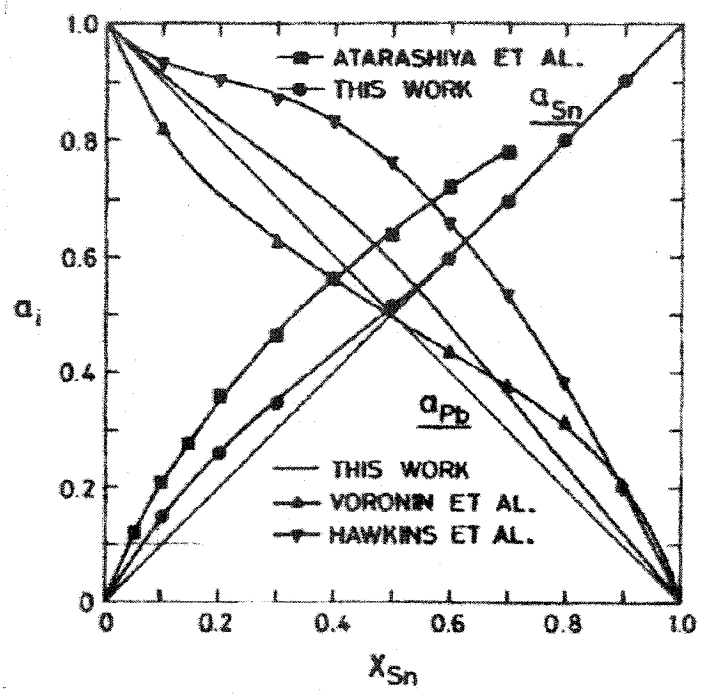

Figure 49. Das & Ghosh. Activity vs. composition relationships at 1050 K (after Das et al., 1972, ref.54)

Sivaramakrishnan and Kapoor[55] determined some thermodynamic properties of the Pb-Sn system at 500 °C, among which were the following:

$$N_{Sn} = 0.1, \gamma_{Sn} = 1.827, N_{Pb} = 0.9, \gamma_{Pb} = 1.009$$

Kurzina et al.[56] studied phase compositions of the lead-tin oxide system (Figure 50), and found that lead ortho- and metastannates, written as Pb_2SnO_4 and $PbSnO_3$, respectively, formed in the system at higher PbO content. The samples with 40 to 80 wt% PbO were found to contain small amounts of lead metastannate. The peaks corresponding to lead orthostannate were observed in the diffraction patterns of all the mixed Pb-Sn-O systems; the exothermic peaks at 415 to 480°C were attributed to the formation of lead meta- and

orthostannates. Lastly, it was observed that increasing lead oxide content in the samples increased Pb_2SnO_4 content.

Lastly, these workers claimed that over the entire range of the component ratios, bulk and surface properties of the samples were altered by the interaction of tin and lead oxides with the formation of multiphase systems.

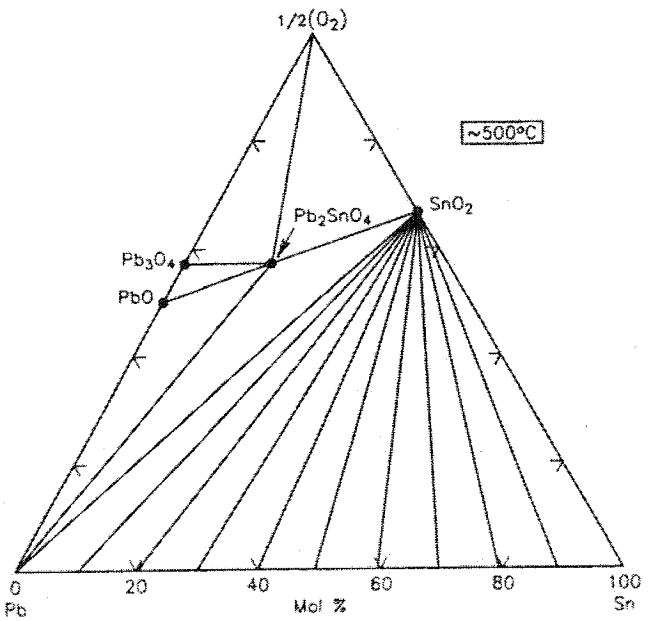

Figure 50. System Pb-Sn-O (after Kurzina et al., 2002, ref. 56)

FACT*Sage*™ makes no mention of specific complex Sn-Pb-O phases which may form, and when the slag is limited to an ideal solution, the following is obtained for a lead bullion containing tin is contacted with oxygen:

0.0026 Sn + 0.9974 Pb + 0.5 O_2 =
(600,1,liq,#1) (600,1,liq,#1) (600,1,g,#1)

0.26014E-02 mol (0.99973 Pb *where* $\gamma_{Pb} = 1.0$
+ 0.72882E-11 Sn *where* $\gamma_{Sn} = 2.591$
+ 0.27040E-03 O *where* $\gamma_{O} = 4.751E\text{-}5$)
(600.00 C, 1 atm, Pb-liq)

+ 0.9974	mol (0.99739	PbO(s)_litharge (red)	*where* $\gamma_{PbO} = 1.0$
	+ 0.26068E-02	SnO_2(s)_cussitite	*where* $\gamma_{SnO_2} = 1.0$)

DELTA G = -1.324E+05 J

This FACT*Sage*™ output indicates that the bullion containing 0.0026 at% Sn will come to be in equilibrium with an ideal slag solution with a PbO to SnO_2 ratio of roughly 380:1

2.1.5 Ellingham Plot Predictions

In this section, curves are plotted for Gibbs free energy for the oxidation reactions of Pb, As, Sb and Sn. Standard Gibbs free energy (ΔG°) values are used in the first plot, Figure 51, while in the second plot, Figure 52, the ΔG equation (30) curves take into account the activities of the metals. In the final plot, Figure 53, the ΔG curves take into account the activities of both the metal and oxide phases. Activity values used for the metallic and oxide phases are given in Table 4.

$$\Delta G = \Delta G^\circ + RT \ln \frac{a_{products}}{a_{reactants}} \qquad (30)$$

It can be observed in the second plot that the positions of the curves change relative to one another, but in comparing the first and last plots, there is little difference in positions, confirming that the preferential order of oxidation would be Sn, then Sb, then As, and finally Pb.

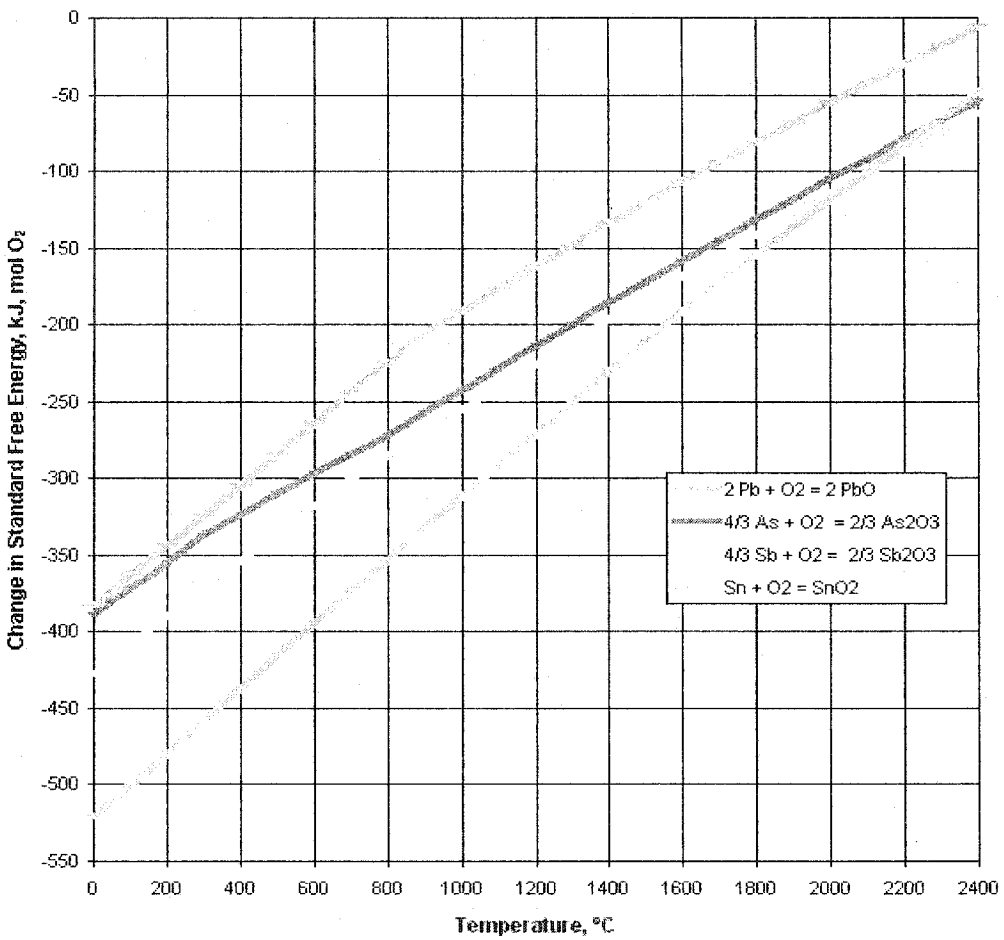

Figure 51. Ellingham plot - standard states

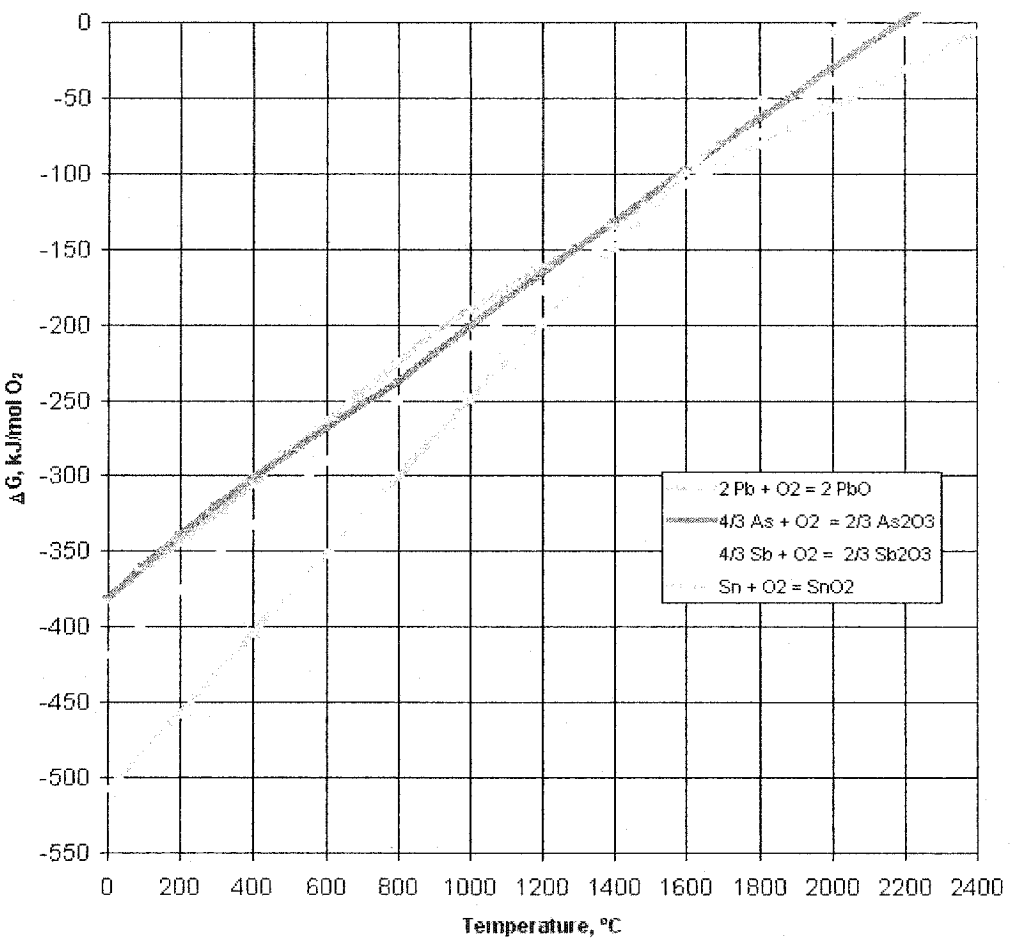

Figure 52. Ellingham plot - using metal activities

Table 4. Activity coefficient and mass fraction values used in Ellingham plots

Phase	Activity Coefficient, γ	Mole fraction, X	Phase	Activity Coefficient, γ	Mole fraction, X
$Pb_{(bullion)}$	1.00	0.963	$PbO_{(slag)}$	1.00	0.698
$As_{(bullion)}$	1.50	0.013	$As_2O_{3(slag)}$	2.24	0.112
$Sb_{(bullion)}$	0.78	0.024	$Sb_2O_{3(slag)}$	0.37	0.169
$Sn_{(bullion)}$	6.00	4.45×10^{-4}	$SnO_{2(slag)}$	1.00	0.021

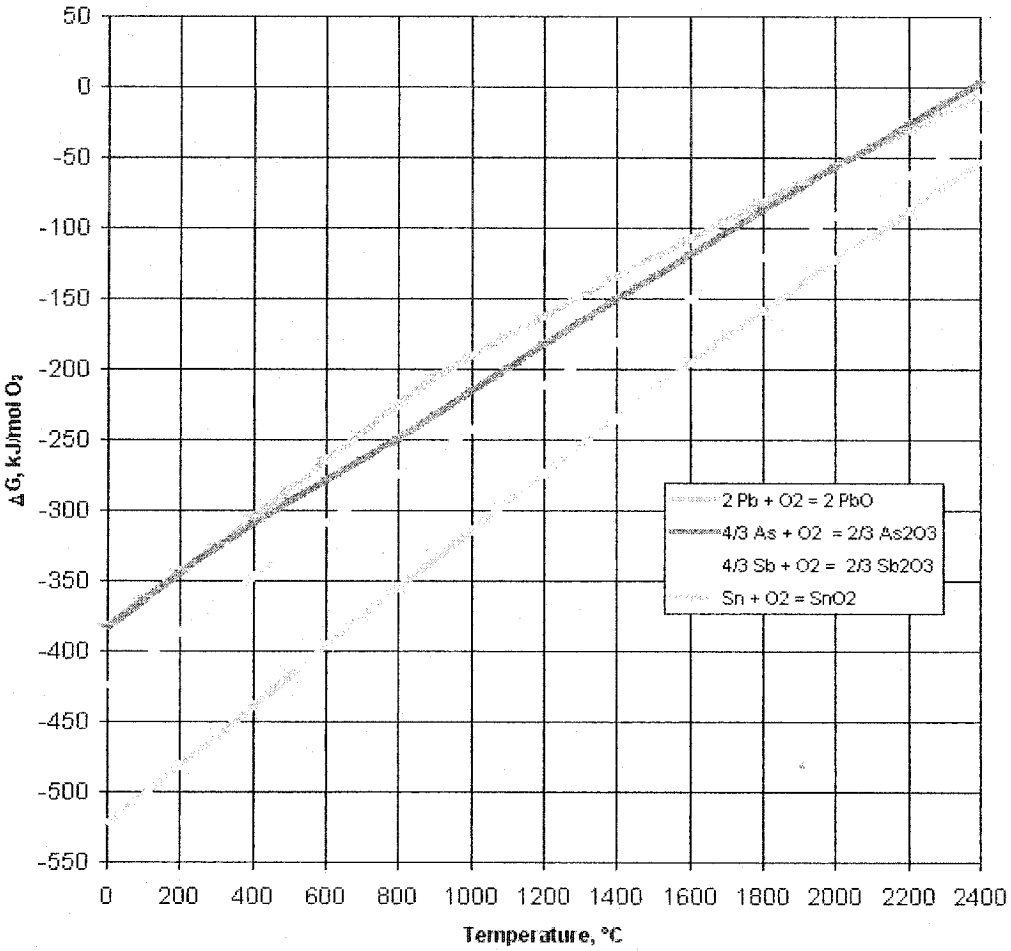

Figure 53. Ellingham plot - using metal and oxide activities

The thermodynamic software, FACT*Sage*™, gave the following results for a bullion containing As, Sb and Sn contacted with oxygen:

0.009 As	+	0.9684 Pb	+	0.5 O_2	+	0.02 Sb	+	0.0026 Sn	=
(600,1,liq,#1)		(600,1,liq,#1)		(600,1,g,#1)		(600,1,liq,#1)		(600,1,liq,#1)	

0.17091E-01 mol (0.99758		Pb	*where* $\gamma_{Pb} = 1.0$
+ 0.77028E-11		Sn	*where* $\gamma_{Sn} = 2.606$
+ 0.17111E-03		Sb	*where* $\gamma_{Sb} = 0.729$
+ 0.19769E-02		As	*where* $\gamma_{As} = 1.320$
+ 0.26733E-03		O	*where* $\gamma_{O} = 4.750E\text{-}5$)
(600.00 C, 1 atm, Pb-liq)			
+ 0.96843 mol (0.98236		PbO(s)_litharge (red)	*where* $\gamma_{PbO} = 1.0$
+ 0.46292E-02		As_2O_3(s)_claudetite	*where* $\gamma_{As_2O_3} = 1.0$
+ 0.10324E-01		Sb_2O_3(s2)_valen.ite	*where* $\gamma_{Sb_2O_3} = 1.0$
+ 0.26848E-02		SnO_2(s)_cussitite	*where* $\gamma_{SnO_2} = 1.0$)
(600.00 C, 1 atm, Ideal#1)			

Data on 1 product species identified with "T" have been extrapolated

DELTA G = -1.342E+05 J

This FACT*Sage*™ output indicates that an impure bullion would come to be in equilibrium with an As_2O_3-SnO_2-Sb_2O_3-PbO ideal solution slag, the latter composed mostly of PbO.

2.2 Kinetic Considerations: Effect of As, Sb, Sn and temperature on lead oxidation rates in stationary melts

2.2.1 Pure Lead

Much work has been done on the kinetics of oxidation of molten lead in still air employing different methods. The results are not all in agreement. Collected data is presented, Table 5.

Archbold and Grace[57] examined the interference colours of very thin oxide layers to calculate the oxidation of pure lead at temperatures from 453 °C to 643 °C in 10-minute experiments. It was found that a parabolic rate law was applicable. For a 2-minute experiment at 600 °C, an oxide thickness growth rate of 0.076 mm/min was obtained.

Bircumshaw[58] established that at 500 °C, 600 °C, and 700 °C, the early part of the oxidation process was consistent with the "parabolic" law though in several cases, this law ceases to be obeyed.

Workers at Metallgesellschaft[59] showed that 99.9999 wt% pure lead oxidizes at a rate of between 22.7 and 139 mm/min at 500 °C.

In gravimetric experiments conducted on electrolytic lead, Gruhl[60] found oxidation rates to be parabolic, at temperatures of 300 °C up to 525 °C. At temperatures above 600 °C (100 hour test), the rate of oxidation was found to be linear[61]. It was stated that at this temperature and above, lead oxidizes linearly with time because of "spitting" of the scale[62]. At 550 °C, a mass gain rate of approximately 0.129 mg/cm^2 hr was found after 100 hours, while at 600 °C, a mass gain rate of approximately 0.389 mg/cm^2 hr was found after 40 hours.

In a study using evaporated films of lead, Anderson and Tare[63] determined that the rates of oxidation at 548 °C and 503 °C were independent of oxide layer thickness (linear law) and proportional to the first power of oxygen partial pressure.

Table 5. Kinetics data for oxidation studies on pure lead.

						Reported Oxidation Rate	
Researcher	Pb	Experimental Time, secs	Experimental Time, hours	Temperature, °C	Graphical Data	μm/min	mg/cm^{2}hr
Metallgesellschaft	99.9999	500	0.14	500	y	65	
Archbold & Grace	"pure"	120	0.03	600	y	0.076	
Hoffman & Malich	pure	7200	2	520	y		1.392
Gruhl	pure	144000	40	600	y		0.389
Weyand	99.9999	10800	3	580	n		0.201
Krysko	B1	518400	144	480	y		0.199
Krysko	"commercial"	518400	144	480	y		0.190
Gruhl	pure	360000	100	550	y		0.129
Krysko	B2	518400	144	480	y		0.125
Krysko	99.9999	518400	144	480	y		0.100
Gruhl	pure	288000	80	500	y		0.060
Gruhl	pure	360000	100	400	y		0.056

				Converted Rate (0% porosity)		Converted Rate (50% porosity)	
Researcher	**Pb**	**Experimental Time, hours**	**Temperature, °C**	**μm/min**	**mg/cm²hr**	**μm/min**	**mg/cm²hr**
Metallgesellschaft	99.9999	0.14	500	65	*3646.500*	65	*1823.250*
Archbold & Grace	"pure"	0.03	600	0.076	*4.264*	0.076	*2.132*
Hoffman & Malich	pure	2	520	*0.02478*	1.392	*0.04956*	1.392
Gruhl	pure	40	600	*0.00692*	0.389	*0.01385*	0.389
Weyand	99.9999	3	580	*0.00358*	0.201	*0.00716*	0.201
Krysko	B1	144	480	*0.00354*	0.199	*0.00708*	0.199
Krysko	"commercial"	144	480	*0.00338*	0.190	*0.00676*	0.190
Gruhl	pure	100	550	*0.00230*	0.129	*0.00459*	0.129
Krysko	B2	144	480	*0.00223*	0.125	*0.00445*	0.125
Krysko	99.9999	144	480	*0.00178*	0.100	*0.00356*	0.100
Gruhl	pure	80	500	*0.00107*	0.060	*0.00214*	0.060
Gruhl	pure	100	400	*0.00100*	0.056	*0.00199*	0.056

Weber and Baldwin[62] found an averaged mass gain rate of approximately 0.333 mg/cm²hr at 600 °C, using 99.9936 wt% pure Pb in a 90-hour test. Specifically, it was established that liquid lead scales according to three successive parabolic relationships: the first parabola has a low constant, the second parabola has a much higher constant, while the third parabola has a constant only slightly smaller than the second.

For his doctoral thesis, Weyand[61] used a thermobalance to determine that molten lead (99.9999 wt% Pb) followed a cubic rate of oxidation between 350 °C and 400 °C, while a parabolic rate was found at temperatures above 400 °C. At a temperature of 580 °C, a mass gain of 0.201 mg/cm² hr was reported for a 3-hour test. At 550 °C, only PbO (orthorhombic) was found. In all cases, the oxide was preferentially oriented, with the (002) basal plane parallel to the melt surface. No significant pressure effects were found over a range of 730 mm to 1 mm Hg of oxygen.

2.2.2 Impurities

The effects of impurities on the oxidation kinetics in lead have been studied systematically by several workers[59,60,61,64,65,66,67,68]. More data exists on the influence of individual impurities (e.g. As, Sb, Sn) than on compound influences of several impurities. Data is presented in tabular form (Table 6) at the end of this section.

2.2.2.1 Lead Containing Arsenic

In his work, Krysko[66] used five types of commercial lead purchased on the open market, and tested them against high purity 99.9999 wt% Pb in oxidation experiments. All investigated samples when tested at 480±20 °C for 144 hours had a higher rate of oxidation than the high purity lead, varying by up to a factor of 2, from approximately 0.10 mg/cm^{2}hr to 0.19 mg/cm^2 hr. This demonstrated that the trace elements had a significant influence on the rate of oxidation. In another experiment on a commercial lead sample, an average mass gain of 0.199 mg/cm^2 hr was obtained. Following oxidation, the sample was cleaned and subjected to a re-oxidation; it yielded an average mass gain of about 0.125 mg/cm^2 hr. It was hypothesized that certain elements must have preferentially oxidized during the primary oxidation.

The workers at Metallgesellschaft[59] studied the growth of oxide layer on 99.994 wt% Pb with different additives. In a plot of oxide layer thickness (mm) vs. time (s), oxidation rates for 0.01 wt% As at 400 °C were roughly 3.5 times that of pure lead after 100 s at a rate of 166 mm/minute (extrapolated). At 500 °C for 10 seconds, the rate was found to be roughly 16.2 times that of pure lead, namely 2251 mm/minute (extrapolated). The most marked acceleration was found with lead containing 10 ppm As for blue-film formation (generally 1-10 s).

These same workers[59] showed the effect of As content (0 to 500 ppm) on the oxidation rate of a stationary melt in pure oxygen atmosphere at 420 °C, in 6-hour tests. On a plot of mass gain (mg) versus initial alloy content, a maximum value was found (0.86 mg/cm^2 hr) at very low content decreasing exponentially until about 0.116 mg/cm^2 hr at 150 ppm As. No change was seen thereafter for higher As contents. It was also concluded that when the initial As content in the lead is greater than or equal to 20 g/l (0.07 wt%), formation of a lead-arsenic-oxygen compound was expected in the oxide film.

2.2.2.2 Lead Containing Antimony

Hoffman and Malich[67,68] used gravimetry to obtain results on the effects of alloying additions on the oxidation rate of liquid lead in a 2-hour test at 520 °C. Results were

obtained for a range of antimony-alloyed lead (0.005 to 8.0 wt% Sb), but no clear pattern emerged from their studies: certain concentrations enhanced oxidation kinetics, while others suppressed the kinetics.

The workers at Metallgesellschaft[59] studied the oxide layer growth on 99.994 wt% Pb with Sb additives. On a plot of oxide layer thickness (mm) versus time (s), an extrapolated value of 208 mm/min was found for lead containing 0.01 wt% Sb at 400 °C following 100 s exposure; this was roughly 4.4 times that of pure lead. At 500 °C following an exposure time of 10 s, an extrapolated rate of 2875 mm/min was found, corresponding to approximately 20.6 times that of pure Pb. The most marked blue-film formation (1-10 s) was found at 0.002 – 0.005 wt% Sb. At higher temps (600 to 750 °C, 2.5 to 10 minutes) a maximum was found at 0.01 wt% Sb.

In gravimetric experiments conducted on electrolytic lead containing varying amounts of antimony at 400 °C, Gruhl[60] found that antimony slightly lowered the oxidation rate, ranging in an inconsistent way from 0.021 mg/cm^{2}hr from 0.1 wt% Sb to 0.043 mg/cm^{2}hr for 0.01 wt% Sb, as compared to 0.056 mg/cm^{2}hr for pure Pb (100 hour test). Experiments conducted at 500 °C showed the reverse trend, wherein small amounts of antimony increased (with increasing wt% Sb) the oxide growth rate from 0.153 mg/cm^{2}hr from 0.01 wt% Sb to 0.235 mg/cm^{2}hr for 0.1 wt% Sb, as compared to 0.060 mg/cm^{2}hr for pure Pb (100 hour test).

In his test on 1000 g lead baths, Green[75] found that there existed a specific antimony range (0.01 to 0.03 wt%) which corresponded to the maximum lead oxidation rate (Figure 55). As will be discussed further in Section 2.3.3, Port Pirie's continuous softener takes advantage of this range for optimal oxidation rates.

Researchers at Metallgesellschaft[59] asserted that the effect of Sb may be explained by an increase in the "vacant places" in the solid oxide structure, and that a decline in oxidation rate beyond the maximum in the 350 to 500 °C range would appear to be due to the occurrence of lead antimonite or antimony oxide in the oxide film. No uniform description

of oxidation pattern can be given for extended periods – it depended largely on operating conditions.

2.2.2.3 Lead Containing Tin

The workers at Metallgesellschaft[59] found that small concentrations of tin in pure lead reduced the oxidation rate, as a dense SnO_2 film was formed when wt% Sn was greater than 0.1%. At higher concentrations and with longer times, Sn concentrations greater than 100 ppm resulted in a further reduction in the oxidation rate, due to this same pure SnO_2 surface layer. Even very small tin additions (< 10 ppm) retarded the growth rate of the oxide film.

The effect of Sn content (0 to 500 ppm) on oxidation rate of stationary melts in pure oxygen atmosphere was studied at 420 °C in 6-hour tests. A plot of mass gain (mg) versus initial alloy content shows a maximum value (0.83 mg/cm^2 hr) at very low Sn content decreasing to about 0.046 mg/cm^2hr at 150 ppm Sn. There was no detectable change beyond this concentration with increasing Sn content[59].

Table 6. Kinetics data for oxidation studies on lead containing impurities

	Impurity Content, wt%						Reported Oxidation Rate		Converted Rate (0% porosity)		Converted Rate (50% porosity)	
Researcher	Pb	As	Sb	Sn	Expt'l Time, hours	Temp, °C	μm/min	mg/cm²hr	μm/min	mg/cm²hr	μm/min	mg/cm²hr
M			0.01		0.003	500	2875		2875	*161288*	2875	*80644*
M		0.01			0.003	500	2251		2251	*126281*	2251	*63141*
M			0.01		0.028	400	208		208	*11669*	208	*5834*
M		0.01			0.028	400	166		166	*9313*	166	*4656*
H & M			1		2	520		1.618	*0.02880*	1.618	*0.05760*	1.618
H & M			0.01		2	520		1.618	*0.02880*	1.618	*0.05760*	1.618
H & M				0.01	2	520		1.510	*0.02688*	1.510	*0.05376*	1.510
H & M			6		2	520		1.471	*0.02618*	1.471	*0.05237*	1.471
H & M			0.05		2	520		1.176	*0.02093*	1.176	*0.04187*	1.176
H & M			0.5		2	500		1.167	*0.02077*	1.167	*0.04155*	1.167
H & M			0.005		2	520		0.980	*0.01744*	0.980	*0.03489*	0.980
H & M			8		2	520		0.931	*0.01657*	0.931	*0.03314*	0.931
H & M			0.1		2	520		0.931	*0.01657*	0.931	*0.03314*	0.931
M		1 ppm?			6	420		0.860	*0.01531*	0.860	*0.03062*	0.860
M				1 ppm?	6	420		0.830	*0.01477*	0.830	*0.02955*	0.830
H & M			0.002		2	520		0.814	*0.01449*	0.814	*0.02898*	0.814
H & M			0.5		2	450		0.517	*0.00920*	0.517	*0.01841*	0.517
H & M			0.5		2	400		0.417	*0.00742*	0.417	*0.01485*	0.417
W & B	99.9927	0.33ppm	0.33ppm	0.33ppm	90	600		0.333	*0.00593*	0.333	*0.01185*	0.333
H & M			0.5		2	520		0.294	*0.00523*	0.294	*0.01047*	0.294
H & M				1	2	520		0.294	*0.00523*	0.294	*0.01047*	0.294
H & M				0.1	2	520		0.275	*0.00490*	0.275	*0.00979*	0.275
G			1		70	500		0.235	*0.00418*	0.235	*0.00837*	0.235
G			0.5		80	500		0.208	*0.00370*	0.208	*0.00740*	0.208
G			0.1		80	500		0.190	*0.00338*	0.190	*0.00676*	0.190
G			0.05		80	500		0.172	*0.00306*	0.172	*0.00612*	0.172
G			0.01		80	500		0.153	*0.00272*	0.153	*0.00545*	0.153
M		150 ppm			6	420		0.116	*0.00206*	0.116	*0.00413*	0.116
M				150 ppm	6	420		0.046	*0.00082*	0.046	*0.00164*	0.046
G			0.01		100	400		0.043	*0.00077*	0.043	*0.00153*	0.043
G			1		100	400		0.030	*0.00053*	0.030	*0.00107*	0.030
G			0.5		100	400		0.028	*0.00050*	0.028	*0.00100*	0.028
G			0.05		100	400		0.023	*0.00041*	0.023	*0.00082*	0.023
G			0.1		100	400		0.021	*0.00037*	0.021	*0.00075*	0.021
G				0.01	100	400		0.019	*0.00034*	0.019	*0.00068*	0.019
G				0.05	100	400		0.006	*0.00011*	0.006	*0.00021*	0.006
G				0.1 - 1.0	100	400		0.004	*0.00007*	0.004	*0.00014*	0.004

M = Metallgesellschaft
H & M = Hoffman & Malich
W & B = Weber & Baldwin
G = Gruhl

Hoffman and Malich[67, 68] studied the effects of alloying additions on the oxidation rate of liquid lead in a 2-hour gravimetry test at 520 °C. Results were obtained for several tin-lead alloys (0.01 to 1.0 wt% Sb), but again no clear pattern emerged from their studies: one concentration increased oxidation kinetics, while two others slowed the kinetics.

Konetski et al.[65] used a Pb-2.9 at% Sn alloy to determine that an oxide that forms on this alloy was highly enriched in tin compared to the bulk alloy because tin oxide was more stable than lead oxide. The amount of tin in the oxide increased with depth into the oxide, while the lead content decreased. Tin may also have been oxidized internally in these alloys in the solid state, most likely at grain boundaries.

In gravimetric experiments conducted on electrolytic lead containing varying amounts of tin at 400 °C, Gruhl[60] found tin to lower the oxidation rate: lead containing 0.01 wt% Sn resulted in a rate reduction from pure lead from about 0.056 mg/cm^{2}hr to 0.019 mg/cm^{2}hr. At 0.1 to 1 wt% Sn, the rate of oxidation was more significantly reduced, from about 0.056 mg/cm^{2}hr to 0.004 mg/cm^{2}hr.

2.3 Industrial Softening Observations

Since the behaviour of high-temperature chemical systems is often controlled by mass transfer kinetics rather than by the thermodynamic behaviour for that particular system, it is also worthwhile to investigate data from industrial practice as the latter gives an indication of the *actual* system behaviour.

2.3.1 Practice

In commercial lead softening, air, oxygen-enriched air, or oxygen is injected into an impure lead melt through a series of lances. The rapid exothermic oxidation reactions caused by the violent agitation normally produce enough heat during operation to maintain the reaction temperature without use of gas-fired burners[69].

At Noranda Inc., Brunswick Smelting in the early 1970's, air and oxygen-enriched air was originally introduced at 550°C to achieve fast process kinetics[14], but process changes over the years have necessitated higher softening temperatures (600 to 650 °C) in order to also maintain a sufficiently fluid, easily-tapped slag. Blanderer writes that 650 °C is the critical temperature for kettle softening[70], below which the reaction process is too slow, and above which the iron kettle corrodes. At Teck Cominco and elsewhere, the issue of temperature stems from several practical constraints: experience has shown that due to slow reaction kinetics below 610 to 620 °C, there is a risk of "losing" the reaction. The temperature must also be sufficiently high (> 590 °C) to keep the slag fluid. At the same time, excessive temperatures (> 650 °C) cause the oxygen lances to deteriorate rapidly and/or fail[16].

In one of Noranda's softening patents[71], it was claimed that in a continuous high temperature softening furnace with a well-mixed bath containing low amounts of sulphur,

arsenic, antimony and tin, it is very improbable that these elements will react directly with introduced oxygen. As such, the postulated reactions are the following[71]:

$$Pb_{(bullion)} + \tfrac{1}{2} O_2 \rightarrow PbO_{(slag)} \quad (31)$$

$$2\ PbO_{(slag)} + S_{(bullion)} \rightarrow 2\ Pb_{(bullion)} + SO_{2\ (gas)} \quad (32)$$

$$3\ PbO_{(slag)} + 2\ As_{(bullion)} \rightarrow 3\ Pb_{(bullion)} + As_2O_{3\ (slag)} \quad (33)$$

$$3\ PbO_{(slag)} + 2\ Sb_{(bullion)} \rightarrow 3\ Pb_{(bullion)} + Sb_2O_{3\ (slag)} \quad (34)$$

$$2\ PbO_{(slag)} + Cu_2S_{(matte)} \rightarrow 2\ Cu_{(bullion)} + 2\ Pb_{(bullion)} + SO_{2\ (gas)} \quad (35)$$

$$2\ PbO_{(slag)} + PbS_{(matte)} \rightarrow 3\ Pb_{(bullion)} + SO_{2\ (gas)} \quad (36)$$

The consequence of such a reaction scheme is that all reactions would occur between species dissolved in the lead and the solid PbO at solid / liquid interfaces at the slag / melt boundary.

2.3.2 Slagging & Slag Composition

Davey states that at temperatures over 600 °C, the order of formation of the oxides is SnO_2, As_2O_3, Sb_2O_3, PbO[9]. Elsewhere[72] it is written that the selective oxidation of As, Sb and Sn is accompanied by the "unavoidable" oxidation of lead, such that the product of softening is a mixture of PbO, Sb_2O_3, As_2O_3, and SnO_2.

Betterton[73] wrote in 1934 that "plumbite and/or plumbate of lead (Pb (II) and Pb (IV) respectively) are formed, which are very active in scorifying antimony, arsenic and tin". It is claimed that the bullion may be softened by the addition to the softening furnace of litharge or a high lead oxide containing slag[71].

Values for typical assays of the softener slags at Port Pirie's continuous softening unit have the following contents: 12.8 wt% Sb, 4.5 wt% As, 73 wt% Pb in equilibrium with a bullion containing 0.04 wt% Sb, 0.003 wt% As[74]. Assays of Brunswick's slag in Perez's article[14] were 6 to 7 wt% Sb, 13 to 15 wt% As and 65 wt% Pb.

It has been determined experimentally that metal having the composition of softened bullion is in equilibrium with a liquid oxide slag containing about 9 wt% Sb[21].

A plot summarizing work of several researchers shows the antimony content in the lead-antimony-oxide slag as a function of the antimony content in equilibrium with it (Figure 54).

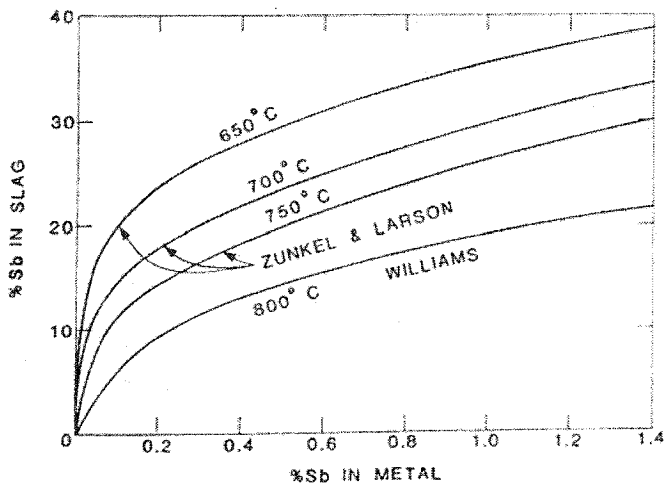

Figure 54. Distribution of antimony between slag and metal phases (after Davey, 1980, ref. 9)

In most publications, the slag is considered to be composed of PbO and Sb_2O_3 (and minor amounts of As_2O_3); however, at Port Pirie, this assumption does not account for the entire weight of the slag, based on elemental analysis for Pb, Sb, As, and Sn. Davey [9] writes that at Port Pirie, the composition analysis comes close to 100 % if the antimony oxide is considered to be Sb_2O_4.

It is very interesting to note that in the original Teck Cominco design, wt% Sb in the slag correlated better with wt% As in the feed than it did with wt% Sb in the feed, according to the following relations[15]:

wt% As slag = 2.6 + 16.7 (wt% As feed)

wt% Sb slag = 27.7 – 25.9 (wt% As feed)

wt% Pb slag = 56.7 + 9.2 (wt% As feed)

As an example, a feed with 0.5 wt% As produced a slag containing 11.0 wt% As, 15.0 wt% Sb, and 61.3 wt% Pb.

2.3.3 Softening Strategy

Williams[21] wrote that in the continuous process, the lead bath is maintained at a composition corresponding to a very high oxidation rate. As a result, the oxidation of the bath, which corresponds with the softening of the bullion, proceeds at a rate many times greater than was thought possible for bath softening. As seen in Figure 55 below, this corresponds to roughly 0.02 wt% Sb.

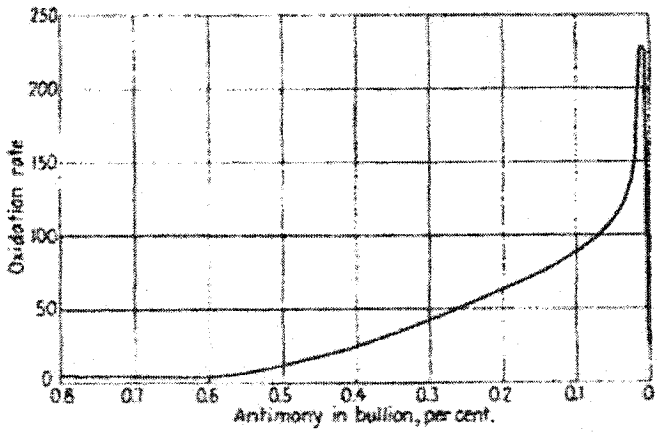

Figure 55. Oxidation rate versus antimony content (After Williams (1936), Ref. 21)

Thus, the addition of oxygen is controlled such that the arsenic and antimony in incoming bullion are oxidized with some lead in such proportions that more slag of the composition already existing in equilibrium with the bullion bath is formed[21]. In practice, the antimony content of the softened bullion is held in the range 0.02 to 0.05 wt% Sb, and the temperature maintained at 700 to 730 °C [74]. At the Broken Hill Associated Smelters (BHAS) at Port Pirie, Australia, the softener is run continuously by taking advantage of increased oxidation rates associated with this specific antimony concentration range, Figure 56.

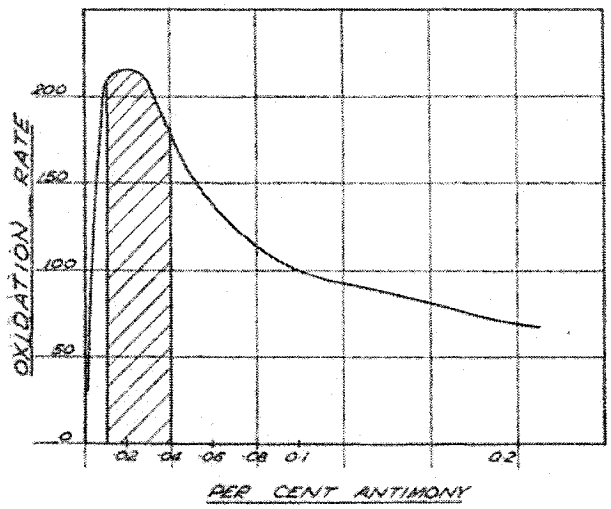

Figure 56. Oxidation rate as a function of antimony content (based on a standard test of 1000g bath) (after Green, 1950, ref 75)

In fact, Green[75] stated that only a continuous process can take full advantage of this observed phenomenon since batch softening only approaches this "zone" at the end point of its operation. It is later stated that antimony is the controlling element on oxidation rate, even when both antimony and arsenic are present in the bullion. In the author's reply to a question by Dr. F.D. Richardson regarding this phenomenon, Green stated that they "are unable to explain why this critical range in antimony composition should occur, and it was only discovered after an exhaustive analysis of various phenomena taking place in the course of development of the continuous process" [75].

In the related article, Green[75] reported on studies that were done to investigate the variables influencing oxidization during softening. He outlined them as follows:

(i) direct action of injected air on the metal bath

(ii) action of the furnace atmosphere on melt thrown up by the blowers

(iii) action of the slag as a "conveyor" of oxygen to the metal by the alternate oxidation and reduction of antimony and arsenic, as in the following reactions:

i. $Sb_2O_3 + O_{2\,(atm)} \rightarrow Sb_2O_5$

ii. $Sb_2O_5 \rightarrow Sb_2O_3 + O_2$ (to metal)

Two tests were performed at 900 °C in scorifiers in a muffle furnace to measure the rate of oxygen transfer to the melt when it was covered by a fluid oxide slag. One test was performed with pure litharge, and the other with litharge containing added percentages of arsenic and antimony trioxides. It was found that the presence of the Sb- and As- trioxides accelerated the rate of lead oxidation, presumably by the aforementioned mechanism[75].

2.4 Hypothesis

The most important variables contributing to the rate of oxidation of lead in the complex lead-impurity system were identified by the review of the relevant literature on the subject of the thermodynamics and kinetics of lead softening reactions. The four parameters selected for study are the temperature of the melt, and the initial weight percents of arsenic, antimony, and tin in lead bullion containing these impurity elements.

The working hypothesis, based largely on industrial observations, is that an "ignition temperature" exists, and that melt composition plays a significant role in the softening reactions and mass gain kinetics.

CHAPTER 3: EXPERIMENTAL METHODOLOGY

3.1 Experimental apparatus ("Hot Box")

For the purpose of investigating the behaviour of the lead alloys and reaction products during softening, a furnace hereafter referred to as the 'Hot Box', with a quartz glass viewing and illumination window was constructed. The collection of visual observations would provide information about the physical behaviour of the system that was intended to give insight into the chemical reactions occurring at or near the sample surface (i.e. the gas-liquid interface), the mass transfer mechanisms, and the role of the alloying elements (impurities) in the oxidation/softening reaction/process.

With this apparatus, the author was able to safely observe the high temperature activity occurring at the surface of 6.25 g lead (or alloyed lead) samples when oxygen was introduced to the furnace. The samples were brought to temperature under an almost inert gas atmosphere, and skimmed if necessary to expose a normally dross- or slag-free surface. The experiments were filmed for future examination and reference. An initial series of five (5) tests were performed in the Hot Box with varying amounts of arsenic, namely 0 wt%, 0.2 wt%, 0.4 wt%, 0.6 wt%, 0.8 wt%, to observe and record differences in oxidation behaviour.

Thereafter it was decided to gather two sets of data concurrently: one set of thermogravimetric (TGA) data, and the second, the visual data.

To this end, the Hot Box was modified into a homemade thermogravimetric apparatus by appending auxiliary components, e.g. analytical balance, scrubbing system and temperature controller. The retro-fitting took several months, and the result was a furnace that thermogravimetrically analyzed, under a controlled gas environment, a sample to which the researcher had skimming access, should skimming be required. In addition, the experiment could be visually recorded at the same time.

The modified Hot Box is presented in Figure 57, and its components are described below.

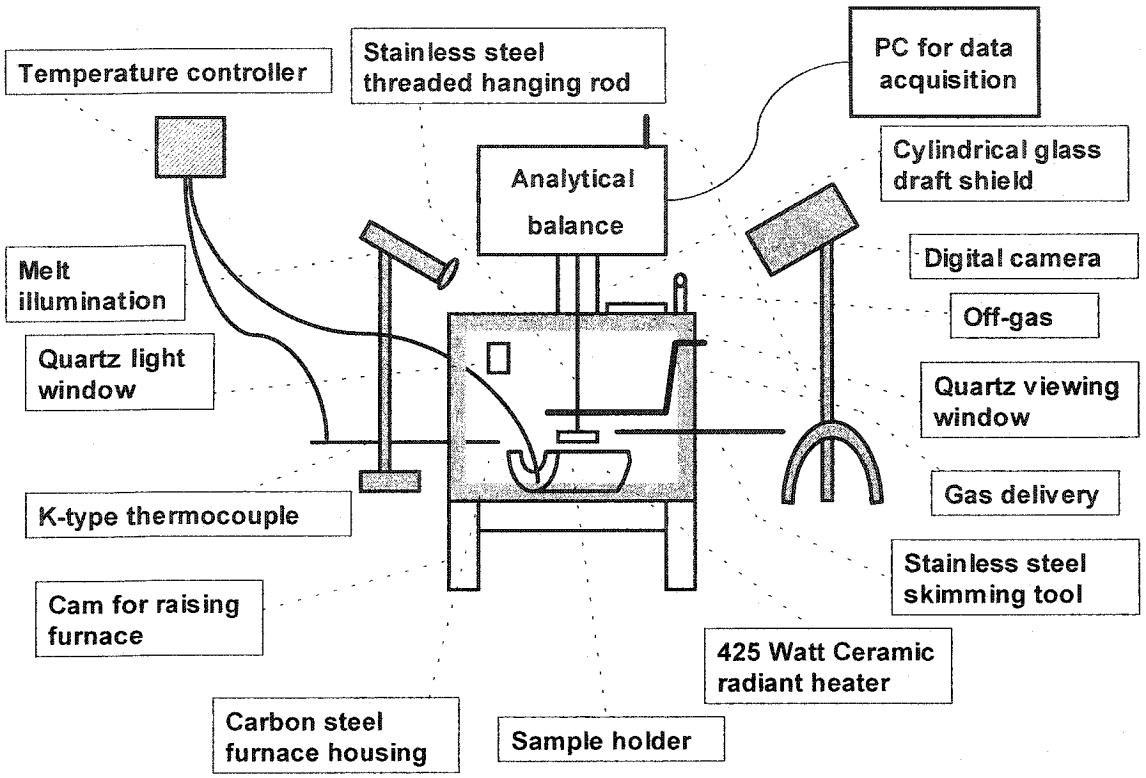

Figure 57. Experimental apparatus

A **Mettler AT200 analytical balance** was selected, which provided 165 readings per minute to 0.1 mg precision. This balance had "weigh-through" capacity, which meant that a hook on the underside of the weighing platform allowed samples to be suspended and weighed from the bottom. In practice (not illustrated in Figure 57), the balance was positioned for support on a 52 cm x 29 cm x 3 cm granite slab, which was placed on a steel shelf bolted to the laboratory wall. A 1.3 cm diameter hole was drilled through the granite slab and the shelf to allow the sample rod to hang through.

An **Omega 425 Watt semi-cylindrical vacuum-formed ceramic fibre radiant heater** was selected as the heating source (Figure 58). The heater had the following dimensions: A = 1.5 cm, B = 1.3 cm, C = 0.75 cm. A typing heating curve for the heater can be found in Appendix I.

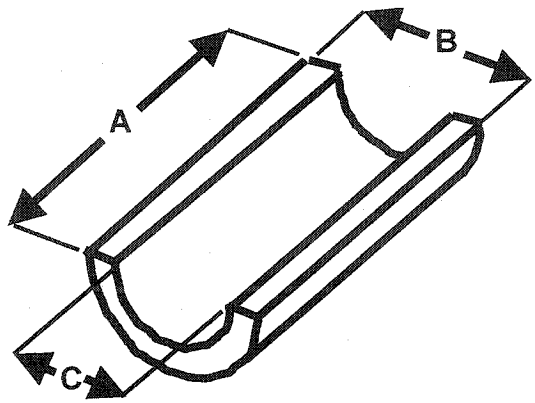

Figure 58. Schematic of cylindrical radiant ceramic heater. Dimensions A = 1.5 cm, B = 1.3 cm, C = 0.75 cm.

The **steel box** that housed the heater was constructed of 0.16 cm ($^1/_{16}$") welded carbon steel plate, and had dimensions of roughly 2.2 cm (l) x 1.65 cm (w) by 15 cm (h). The cover was removable, and was connected to the furnace by sixteen (16) shortened 0.6 cm (d) x 1.9 cm (l), 51 threads per cm (20 threads per inch) ("¼-20") machine bolts. Ceramic fibreboard (Fibre Cast) provided the seal between the cover and the furnace. The furnace was lined with roughly 2.5 cm of SiO_2-Al_2O_3 fibreboard insulation (Thermal Ceramics).

A 30 cm high x 7.5 cm OD blown-glass **cylinder** with a flat bottom served as a draft shield for the sample rod in the space between the balance and the furnace. The cylinder had a 0.65 cm diameter hole at the centre of the base. The seals between the cylinder and (i) the metal shelf and (ii) the Hot Box were manufactured from ceramic fibreboard

An adjustable **three-component hanging unit** was constructed to suspend the sample from the balance. This consisted of an upper latching mechanism, threaded onto a 32.5 cm section of 0.25 cm (d), 8 threads per cm (32 threads per inch) ("8-32") stainless steel threaded rod, to which a machined carbon-steel, C-shaped, sample holder was connected.

Quartz plates (Chemglass, USA) of dimensions (5 cm x 5 cm x 0.16 cm), (2.5 cm x 2.5 cm x 0.16 cm) were used for the viewing and light ports, respectively.

An **off-gas port**, fabricated into the furnace cover, directed any off-gases to a scrubbing unit, which consisted of six water-filled, 1-litre Erlenmeyer flasks connected in series. The off-gas from the last flask was directed gas into a fume hood.

Two (2) **Mini-Maglite**™ 2-cell AA flashlights provided the necessary illumination of the sample surface.

A **temperature-controlling unit** was fabricated in-house using a Watlow 935A temperature controller, a 120/240 VAC solid-state relay, and a k-type thermocouple. Following several calibration trials, the thermocouple lead was placed directly beside the sample holder for the most reliable readings (as the thermocouple could not be placed in the melt without affecting the mass readings.) Calibration curves are presented in Appendix I.

A stainless steel **skimming tool** was positioned at the same height as the suspended sample, so that the sample surface could be skimmed in cases where a solid oxide formed.

A carbon steel **cam** was constructed to support the furnace and to allow for easier assembly and disassembly of the unit.

A JVC GRDVL310 Digital **video camera** was used to record the experiments, which captured 30 frames/sec. The camera was equipped with a variable-speed shutter (1/500,1/250, 1/100, 1/60 sec.), and could deliver 110,000-pixel 2.5" high resolution.

A gas delivery system was set up because the control of the gas environment in TGA trials was very important for controlling melt oxygen exposure time. Gas was delivered to the system at two points (Figure 59). In all cases, the gas was delivered from the cylinder to the gas train via an Air Products dual stage regulator, ¼" ID reinforced PVC pipe, with Swagelok™ compression connectors.

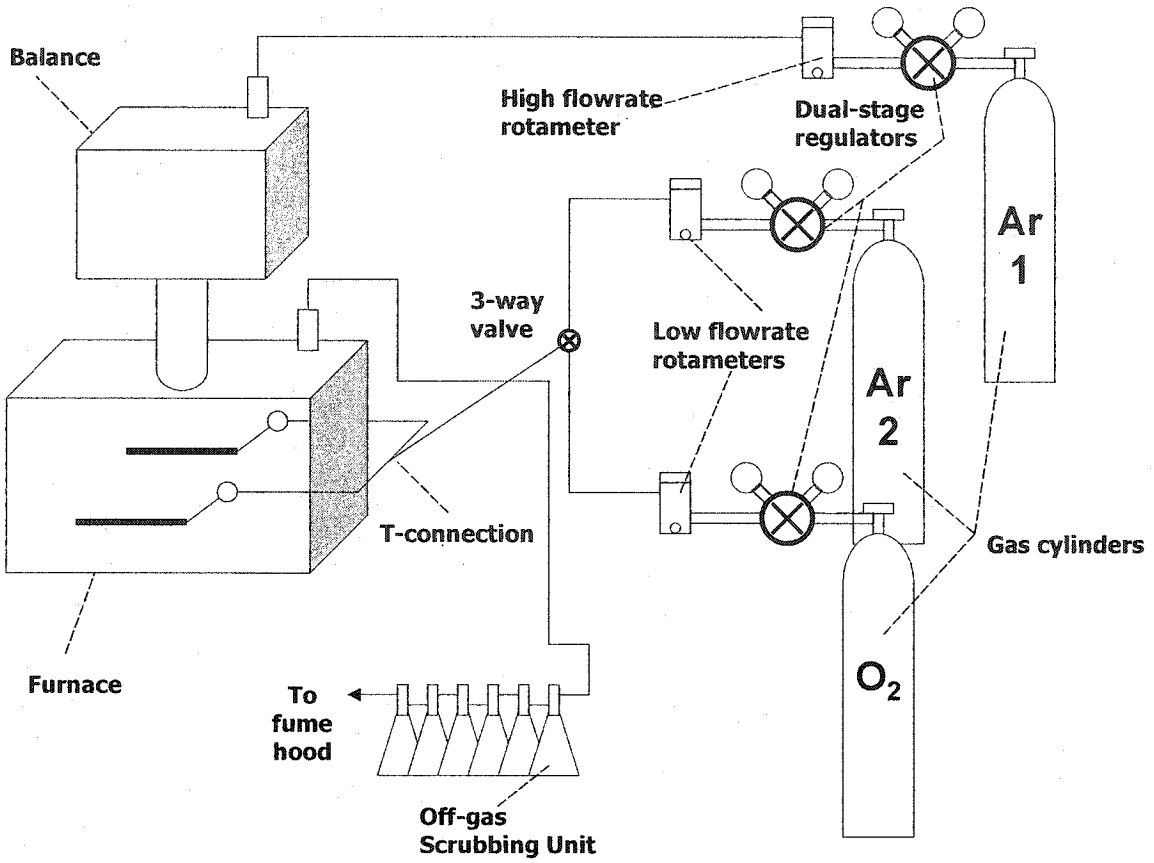

Figure 59. Gas delivery system

3.2 Experimental Procedures

3.2.1 Test Sample Preparation and Experimental Set-Up

Initially, master alloys were prepared by the following method: small pieces of 99.99% pure lead ingot were cut, and holes bored in them. A measured amount of the alloying element, e.g. pure As powder was placed in the hole. Additional pieces of lead were added as required to achieve the 350 g target mass, and the lot were put in a Leco mounting press, and made into 2.5 cm high x 4 cm diameter pucks. These pucks were placed in a closed steel crucible in a silicon carbide resistance furnace and the crucible and contents were heated to a prescribed temperature (e.g. 350 °C for Pb-Sn alloys), under argon by injecting the argon under the lid on the steel crucible. Determination of the alloying temperature was based on the constituent metals, their melting points, and the binary phase diagram, using a

temperature roughly 20 °C greater than the higher melting point metal. Also, argon was injected into the melt for 10 minutes to increase sample homogeneity. The furnace was turned off and the sample was allowed to cool naturally under argon. For arsenic alloys, good results were obtained, but concentration gradients were found across the frozen sample thickness with Sb- and Sn-Pb alloys when drillings from different parts of the master alloy button were tested by ICP and AA. For this reason, it was decided to use commercially produced alloys.

Appropriate quantities to achieve the desired nominal starting assays were freshly drilled from the commercial alloys (Table 7) in order to create 6.25 g of a test sample. An example calculation of sample preparation is presented in Appendix I. These drillings were packed into high-alumina rectangular dishes (Keratec Advanced Materials S.A., Spain), which measured 2.5 cm x 1.5 cm x 0.5 cm external dimensions, with a wall thickness of ~0.15 cm. The crucible was then placed in the hanging sample holder and the whole TGA-furnace apparatus was carefully assembled.

Table 7. Commercial alloy compositions. Full compositions are given in Appendix I.

Supplier	Description	wt% As	wt% Sb	wt% Sn	wt% Pb
Teck Cominco	**Alloy 425**	1.700	6.200	<1 ppm	92.05
Teck Cominco	**Alloy 414**	12.00	180 ppm	<1 ppm	87.98
Teck Cominco	**Alloy 422**	0.4300	2.050	3 ppm	97.50
Teck Cominco	**Alloy 423**	0.6300	3.140	3 ppm	96.20
ESPI Metals	**Pb5.0Sb**	0	5.000	1 ppm	95.00
Arbell Inc	**HiFlo Solder**	<10 ppm	40 ppm	63.43	36.54
Teck Cominco	**Refined Lead**	<1 ppm	10 ppm	<1 ppm	99.99

The gas delivery to the TGA-furnace apparatus was constructed in the following manner (Figure 59):

(i) Argon "1" (99.998% purity) purged the acrylic chamber which housed the balance. This gas flowrate was controlled by a medium flow rate (0 – 10 lpm) rotameter. The argon flow maintained a positive pressure in the glass cylinder to suppress rising heat, as well as any volatiles produced in the course of the test.

(ii) Oxygen (99.96 % purity) and argon "2" (99.998 % purity) flowrates were controlled by low flow (0.05 – 0.5 lpm) rotameters. The gas was directed to a three-way valve positioned outside the furnace. This flow fed a T-connection which split the flow to two 0.65 cm (¼") copper pipes, which connected to the side walls of the furnace. From these junctions, gas flowed through stainless steel conduits, which ran alongside the sample holder, roughly 1 cm above and 1 cm to the side. Six-1.5 mm holes were drilled in each tube, and the tubes were sealed at the ends.

To begin all tests, initial (sample + dish) mass was recorded and the system was purged with gas from argon cylinders 1 and 2 at roughly 10 and 0.1 lpm, respectively for 35 minutes via a medium flow rate (0 – 10 lpm) rotameter. The temperature controller was set to the desired set point, and once the set point was reached and was stable, the argon flow rates were lowered to at 1.0 and 0.15 lpm, respectively. Thereafter, the argon flowrate from cylinder 1 was kept constant.

When the sample had been brought to the desired temperature, it was skimmed if necessary and when possible the dross was shaken off the skimming tool, onto a thin ceramic blanket placed on the surface of the ceramic heater. This was necessary since the drosses that came into contact with the heater ceramic tended to chemically attack it.

Mass data acquisition was then initiated using Microsoft HyperTerminal®, and oxygen was introduced into the furnace through the two gas dispensers placed about 1 cm above and to the side of the melt at 100 cm^3/min via the three-way valve, and was maintained for the desired time period. Following exposure, argon cylinder 2 flow was resumed at 150 cm^3/min.

The appearance of the sample surface was visually recorded at intervals during the heating period, and continuously once the sample reached elevated temperatures, and during the initial period following oxygen introduction.

3.2.2 Stage I: Exploratory testing

The first series of experiments served to explore the effects of varying alloy components and contents and temperature, while perfecting the experimental method. The conditions for these tests are presented in Table 8.

Table 8. Stage I Experimental Design

		Initial Alloy Impurity Content, wt%			
Test Number	**Date**	**As**	**Sb**	**Sn**	**Temperature, °C**
DVTGA1	7-Oct-02				600 ± 20
DVTGA3	23-Oct-02	0.35			600 ± 20
DVTGA4	30-Oct-02	0.78			600 ± 20
DVTGA5	7-Nov-02		0.60		600 ± 20
DVTGA6	8-Nov-02		1.05		600 ± 20
DVTGA7	9-Dec-02		1.60		600 ± 20
DVTGA8	10-Dec-02		1.60		600
DVTGA9	17-Dec-02			0.30	600
DVTGA10	18-Dec-02			1.50	600
DVTGA11	19-Dec-02		1.80		500
DVTGA12	20-Dec-02	0.75			500
DVTGA13	20-Dec-02	0.53	0.53		600
DVTGA15	22-Dec-02	0.80		0.30	600
DVTGA16 Droplet Flow Test	7-Feb-03	0.80			600

3.2.3 Stage II: Factorial Design

A 2^4 experimental factorial design (with two replicates) was chosen to evaluate the following four parameters: weight percentage arsenic (wt% As), weight percentage antimony (wt% Sb), weight percentage tin (wt% Sn), and temperature (T, °C). The levels for the impurity elements chosen were based on the maximum levels found in the Teck Cominco lead softener feed bullion year-to-date 2002 values that were available at the time of planning.

The levels for temperature were selected to adequately highlight differences in reaction kinetics, i.e., 600 °C, as compared with 500 °C. Data is summarized in Table 9.

Table 9. High / low values used in factorial design.

Parameter	Name	High Value (+)	Low Value (-)
A	Initial nominal wt% As	0.90	0
B	Initial nominal wt% Sb	2.00	0
C	Initial nominal wt% Sn	0.26	0
D	Temperature, °C	600	500

Although a triple interaction effect was not expected, it was decided to employ a complete factorial design, which would consist of sixteen (16) experiments, Table 10.

Table 10. 2^4 experimental factorial design with two replicates. "0" refers to values intermediate between the High and Low values.

Experiment Design (ED) Number	A	B	C	D	AB	AC	AD	BC	BD	CD	ABC	ABD	ACD	BCD	ABCD
1	-	-	-	-	+	+	+	+	+	+	-	-	-	-	+
2	-	-	-	+	+	+	-	+	-	-	-	+	+	+	-
3	-	-	+	-	+	-	+	-	+	-	+	-	+	+	-
4	-	-	+	+	+	-	-	-	-	+	+	+	-	-	+
5	-	+	-	-	-	+	+	-	-	+	+	+	-	+	-
6	-	+	-	+	-	+	-	-	+	-	+	-	+	-	+
7	-	+	+	-	-	-	+	+	-	-	-	+	+	-	+
8	-	+	+	+	-	-	-	+	+	+	-	-	-	+	-
9	+	-	-	-	-	-	-	+	+	+	+	+	+	-	-
10	+	-	-	+	-	-	+	+	-	-	+	-	-	+	+
11	+	-	+	-	-	+	-	-	+	-	-	+	-	+	+
12	+	-	+	+	-	+	+	-	-	+	-	-	+	-	-
13	+	+	-	-	+	-	-	-	-	+	-	-	+	+	+
14	+	+	-	+	+	-	+	-	+	-	-	+	-	-	-
15	+	+	+	-	+	+	-	+	-	-	+	-	-	-	-
16	+	+	+	+	+	+	+	+	+	+	+	+	+	+	+
17	0	0	0	0	0	0	0	0	0	0	0	0	0	0	0
18	0	0	0	0	0	0	0	0	0	0	0	0	0	0	0

The experimental order was chosen randomly by drawing numbers from a hat. Table 11 summarizes the experimental conditions for the tests.

Table 11. Stage II Experimental Details (ED = "experimental design"). Note: Experiments 3 and 13 had to be re-done due to experimental mishaps. They were re-done as 3b and13b, respectively.

			Initial Alloy Impurity Content, wt%			
Test Number	**Description**	**Date**	**As**	**Sb**	**Sn**	**Temperature, °C**
DVTGA17	ED1	13-Feb-03	0.00	0.00	0.00	500
DVTGA18	ED2	17-Feb-03	0.90	0.00	0.26	600
DVTGA20	ED3b	18-Feb-03	0.45	1.00	0.13	550
DVTGA21	ED4	19-Feb-03	0.90	2.00	0.00	600
DVTGA22	ED5	19-Feb-03	0.45	1.00	0.13	550
DVTGA23	ED6	20-Feb-03	0.90	2.00	0.26	500
DVTGA24	ED7	20-Feb-03	0.00	2.00	0.26	500
DVTGA25	ED8	21-Feb-03	0.90	0.00	0.00	500
DVTGA26	ED9	22-Feb-03	0.00	0.00	0.26	600
DVTGA27	ED10	22-Feb-03	0.00	2.00	0.00	600
DVTGA31	ED11	03-Mar-03	0.00	2.00	0.26	600
DVTGA32	ED12	04-Mar-03	0.00	2.00	0.00	500
DVTGA35	ED13b	15-Mar-03	0.00	0.00	0.26	500
DVTGA36	ED14	15-Mar-03	0.90	0.00	0.26	500
DVTGA37	ED15	15-Mar-03	0.90	2.00	0.00	500
DVTGA38	ED16	16-Mar-03	0.00	0.00	0.00	600
DVTGA39	ED17	16-Mar-03	0.90	2.00	0.26	600
DVTGA40	ED18	16-Mar-03	0.90	0.00	0.00	600

3.2.4 Stage III: Industrial feed

A third series of tests were run concurrently with tests of Stage II. They served to evaluate actual Teck Cominco Softener feed and equivalent homemade alloys. Experimental conditions for Stage III tests are presented in Table 12.

Table 12. Stage III Experimental Details.

Test Number	Description	Date	Initial Alloy Impurity Content, wt%			Temperature, °C
			As	Sb	Sn	
DVTGA28	Teck Cominco Softener Feed	01-Mar-03	***0.22***	***1.12***	***0.10***	600
DVTGA29	Teck Cominco Softener Feed	02-Mar-03	***0.22***	***1.12***	***0.10***	500
DVTGA30	Teck Cominco Softener Feed	02-Mar-03	***0.22***	***1.12***	***0.10***	550
DVTGA33	Red Droplet Hunt	07-Mar-03	0.90	0.00	0.00	600
DVTGA41	Simulated Softener Feed	17-Mar-03	0.22	1.12	0.10	550
DVTGA42	Simulated Softener Feed	17-Mar-03	0.22	1.12	0.10	500
DVTGA43	Simulated Softener Feed	17-Mar-03	0.22	1.12	0.10	600
DVTGA44	Surface Temperature	24-Apr-03	0.90	0.00	0.00	600

Teck Cominco Softener Feed impurity compositions determined by atomic absorption (AA), and reproduced in trials 41-43.

3.2.5 Stage IV: Characterization of Reaction Products

To identify the products of oxidation, samples were analyzed by X-Ray Diffraction (XRD) using the Rigaku Rotaflex Rotating Anode System, with a copper K alpha lamp.

As the samples were only 6.25 g and with uneven surface topography (when the oxide did not grow homogeneously with respect to increasing thickness), it was not possible to perform XRD directly on the solid oxide surface, nor was it possible to separate enough of the oxide product from the metallic phase for XRD analysis. It was therefore decided to flatten the specimens in a mounting press in preparation for XRD analysis.

In addition to XRD, samples were also analyzed by Energy Dispersive X-Ray Analysis (EDX) using the JEOL JSME 840A Scanning Electron Microscope. The selected accelerating voltage for analysis of the surface oxide was 5 keV.

CHAPTER 4: RESULTS

4.1 Introduction

Each of the systems investigated, namely: Pb-O, Pb-As-O, Pb-Sb-O, Pb-Sn-O, Pb-As-Sb-O, Pb-As-Sn-O, Pb-Sb-Sn-O, Pb-As-Sb-Sn-O, Teck Cominco Lead Softener Feed, and Simulated Lead Softener Feed are discussed in turn, in a simple and concise manner.

For each system, thermogravimetric (TGA) curves are presented, using the same scale for all plots to facilitate visual comparison, and comments are made on the salient points. Observations made during the trials are reported to elucidate the softening reactions and pertinent photos are included to illustrate transition points. Lastly, the products of reaction, identified by X-Ray Diffraction (XRD) and Energy Dispersive X-Ray Analysis (EDX) are reported. Sample XRD and EDX spectra are included in Appendix I.

In total, results from twenty-four (24) experimental trials are presented. Results from the Experimental Design ("ED") tests were analyzed by linear regression against the four experimental parameters in order to identify significant relationships, while the Softener Feed and Simulated Softener Feed served as a basis for comparison of experimental alloys with actual industrial feed material.

4.2 Pb-O System

4.2.1 Thermogravimetric Curve & Experimental Data for the Pure Pb Tests

Thermogravimetric curves are presented for the trials run on nominally pure Pb at 500 °C and 600 °C, Figure 60. Experimental conditions and results are given in Table 13.

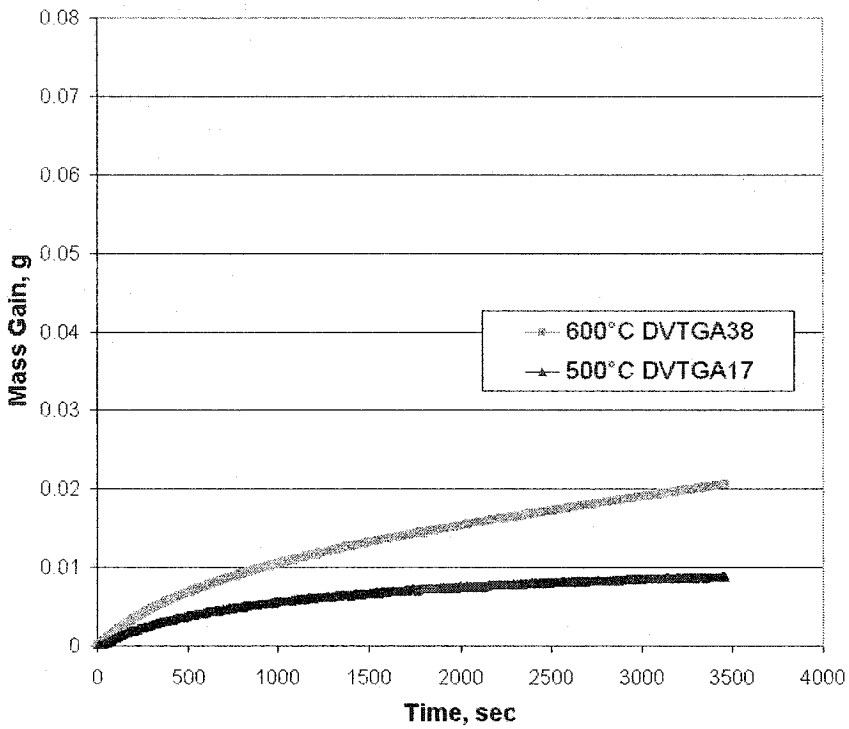

Figure 60. Pure Pb TGA curves for tests DVTGA 17 (500 °C) and DVTGA 38 (600 °C).

Table 13. Experimental conditions and results for DVTGA 17 (500 °C) and DVTGA 38 (600 °C).

Trial	DVTGA 17	DVTGA 38
Composition	Pure Pb	Pure Pb
Temperature (°C)	500	600
Time (minutes) until O_2 introduction	21	31
Mass Gain (g) prior to O_2 introduction	0.0063	0.0128
Average Rate Mass Gain (mg/cm^2hr) prior to O_2 introduction	7.49	10.31
Mass Gain (g) first 300 s	0.0027	0.0046
Mass Gain (g), 60 minute test	0.0088	0.0207
Total Mass Gain (g) (Heating PLUS 60 minutes)	0.0151	0.0335
Percentage of Mass Gained during Heating	41.7	38.2

4.2.2 Captured Images for Pure Pb Tests

4.2.2.1 DVTGA 17(500 °C) and DVTGA 38 (600 °C)

The images selected (below) serve to illustrate that the conditions of the melt at t =0 were such that a clean metal surface was not exposed in either trial since a reaction product that could not be removed was always present and acted as a barrier to mass transfer.

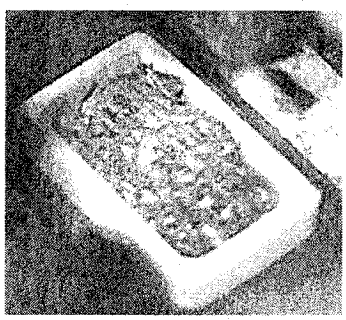

Figure 61. DVTGA 17 (500 °C) at t = 0.

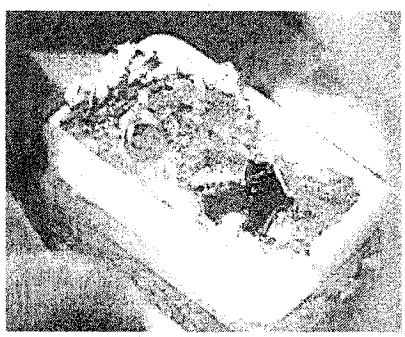

Figure 62. DVTGA 38 (600 °C) at t = 0.

4.2.3 Experimental Observations for the Pure Pb Tests

DVTGA 17 (500 °C): it was not possible to skim the sample surface, and it was therefore left to oxidize in an unskimmed state.

DVTGA 38 (600 °C): all the metal drillings oxidized, and it was not possible (even with mechanical agitation) to get a single, coherent bead of lead. It too was left to oxidize in an unskimmed state.

4.2.4 Oxide products Identified in the Pure Pb Tests

The elements identified by EDX for both samples were Pb and O.

4.2.5 Comments on the Pure Pb Tests

The main observable difference between the two tests was that the sample run at 600 °C gained more mass, indicating that temperature was a significant parameter.

4.3 Pb-As-O System

4.3.1 Thermogravimetric Curve & Experimental Data for the Pb-As Tests

Thermogravimetric curves are presented for the trials run on binary Pb-As alloys at 500 °C and 600 °C in Figure 63. Experimental conditions and results are given in Table 14.

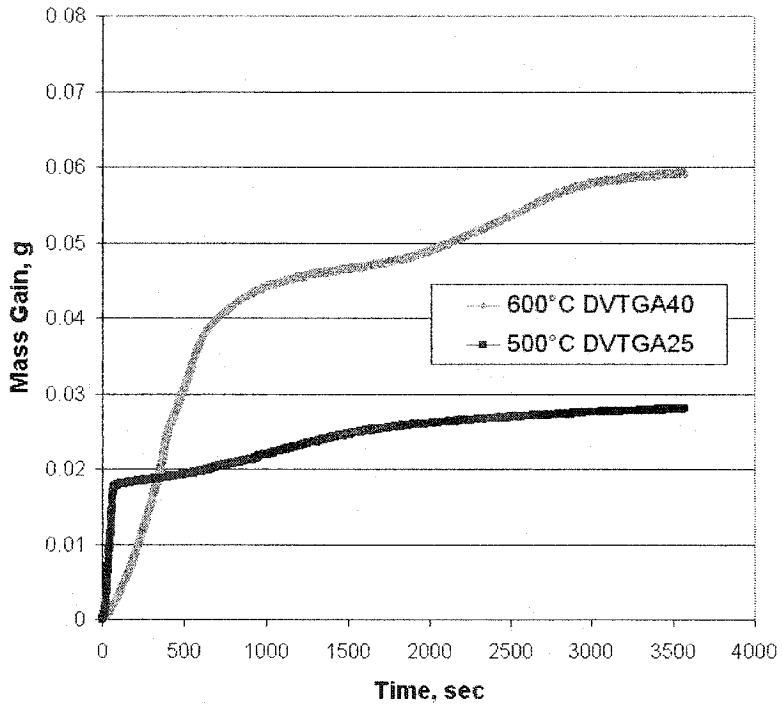

Figure 63. Pb0.90As TGA curves for tests DVTGA 25 (500 °C) and DVTGA 40 (600 °C).

Table 14. Experimental conditions and results for DVTGA 25 (500 °C) and DVTGA 40 (600 °C).

Trial	DVTGA 25	DVTGA 40
Composition	Pb0.90As	Pb0.90As
Temperature (°C)	500	600
Time (minutes) until O_2 introduction	22.9	30
Mass Gain (g) prior to O_2 introduction	0.0106	0.0051
Average Rate Mass Gain (mg/cm^{2}hr) prior to O_2 introduction	11.56	4.25
Mass Gain (g) first 300 s	0.0186	0.0157
Mass Gain (g), 60 minute test	0.0281	0.0593
Total Mass Gain (g) (Heating PLUS 60 minutes)	0.0387	0.0644
Percentage of Mass Gained during Heating	27.4	7.9

4.3.2 Captured Images for the Pb-As Tests

4.3.2.1 DVTGA 25 (500 °C)

The images selected for DVTGA 25 (500 °C), Figure 64 to Figure 69, illustrate the manner in which the oxide product on the melt surface was consumed, reduced, and/or volatilized during the heating period, thereby exposing a clean metallic surface. This phenomenon is referred to hereafter as "self-cleaning", and is addressed in the Discussion (Chapter 5:. As oxygen was introduced, there was more and more visible activity on the melt surface, and the TGA curve, Figure 63, indicated that mass gain was rapid. The inflection point in the curve corresponded to roughly t = 75 s, and thus the images leading up to Figure 69 show the surface gradually becoming covered by an oxide product by 75 s and which, by 120 s, had apparently changed in colour and morphology.

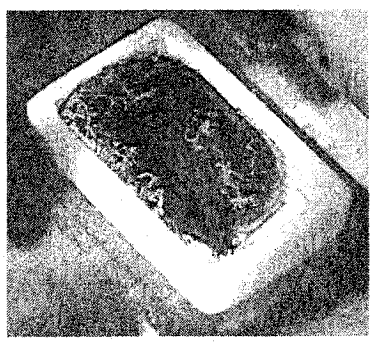

Figure 64. DVTGA25 (500 °C) at t = 240 s prior to O_2 introduction.

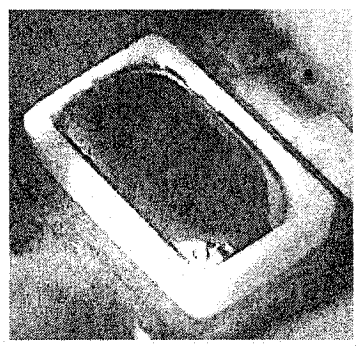

Figure 65. DVTGA25 (500 °C) at t = 60 s prior to O_2 introduction.

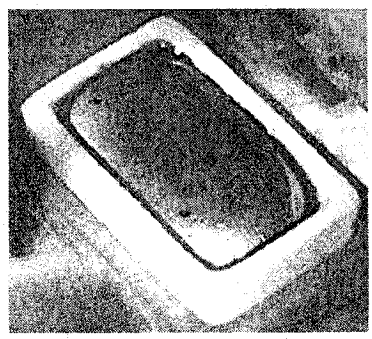

Figure 66. DVTGA25 (500 °C) at t = 30 s.

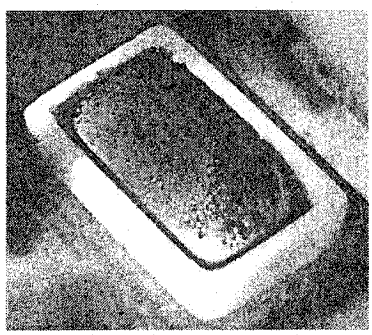

Figure 67. DVTGA25 (500 °C) at t = 60 s.

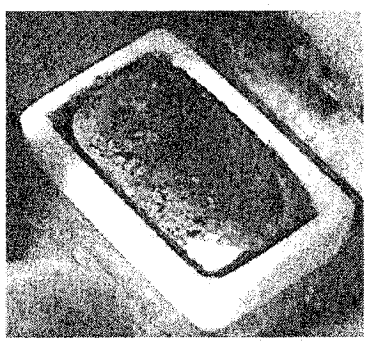

Figure 68. DVTGA25 (500 °C) at t = 75 s.

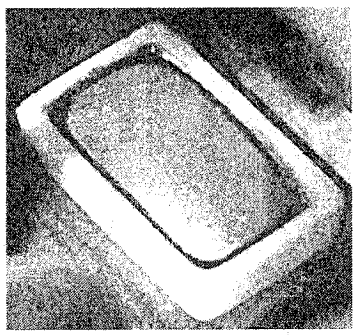

Figure 69. DVTGA25 (500 °C) at t = 120 s.

4.3.2.2 DVTGA 40 (600 °C)

The selected images for DVTGA 40 (600 °C), Figure 70 to Figure 77, show that the melt was also able to "self-clean" at 600 °C as well. Oxide product accretions seen in Figure 74 (t = 370 s) can be seen to grow in thickness and appear to play a role in the surface becoming covered by an oxide product, Figure 76. Figure 77 corresponds to the inflection point in the TGA curve (Figure 63) at roughly 500 s.

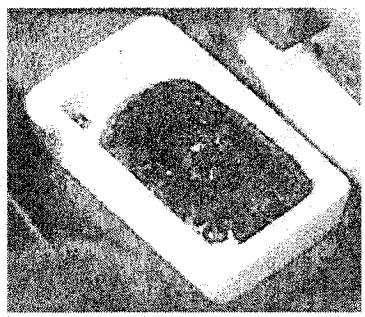

Figure 70. DVTGA40 (600 °C) at t = 180 s prior to O_2 introduction.

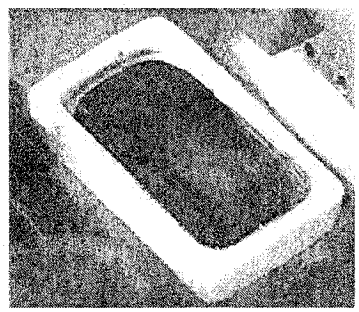

Figure 71. DVTGA40 (600 °C) at t = 0.

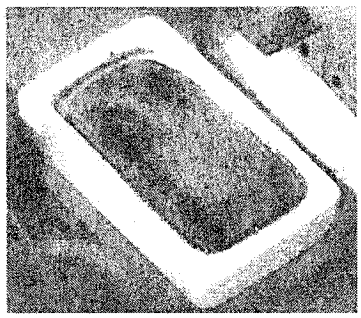

Figure 72. DVTGA40 (600 °C) at t = 60 s.

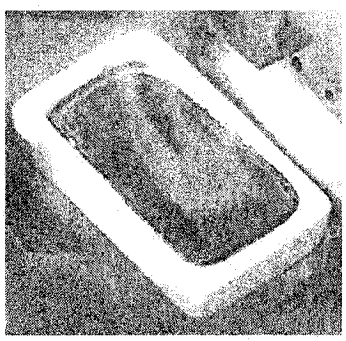

Figure 73. DVTGA40 (600 °C) at t = 180 s.

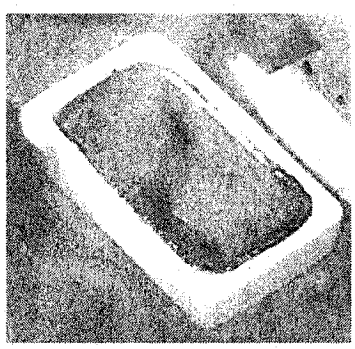

Figure 74. DVTGA40 (600 °C) at t = 370 s.

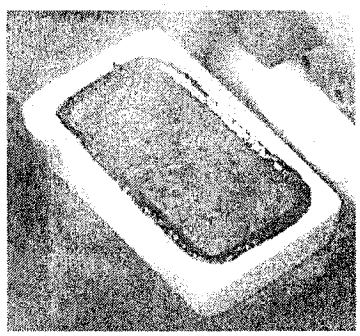

Figure 75. DVTGA40 (600 °C) at t = 400 s.

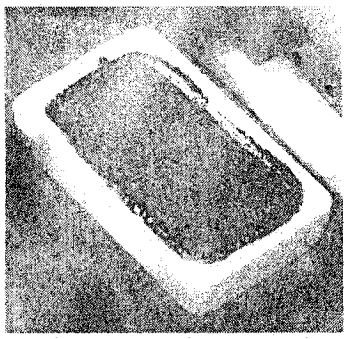

Figure 76. DVTGA40 (600 °C) at t = 500 s.

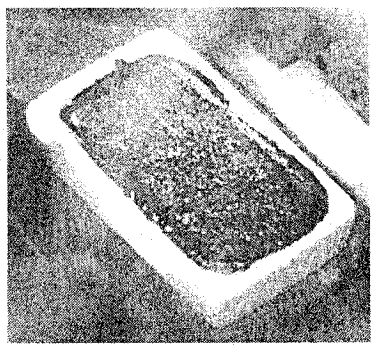

Figure 77. DVTGA40 (600 °C) at t = 580 s.

4.3.3 Experimental Observations for the Pb-As Alloys

DVTGA25 (500 °C): the melt was seen to "self-clean". Reddish droplets that were thought to be a complex Pb-As-O phase were observed to radiate outward from the centre of the melt and accumulated around the melt at the wall of the alumina dish. At a given moment, roughly t = 370 s, the surface began to slowly cover over, and finally, after 500 s, it was covered completely.

DVTGA40 (600 °C): reddish droplets similar to DVTGA 25 (500 °C) were observed to be radiating outward from the centre of the melt after the sample had 'self-cleaned'. Fuming was also observed at the sample surface and the fuming phase appeared to interact with the droplets, i.e., the source of the fume appeared to be the surface where the reddish droplets were moving.

4.3.4 Oxide products Identified in the Pb-As Tests

The oxide products identified by XRD for DVTGA25 (500 °C) were $Pb_8As_2O_{13}$ (dominant), $Pb_3As_2O_8$ (sub-dominant), and $Pb_4As_2O_9$ (sub-dominant), while the products identified for DVTGA40 (600 °C) were $Pb_8As_2O_{13}$ (dominant) and $Pb_4As_2O_9$ (sub-dominant).

4.3.5 Comments on the Pb-As Tests

The two samples were observed to show similar behaviours, though the surface of DVTGA 25 (500 °C) became covered in oxide product sooner in the course of the experiment.

DVTGA40 (600°C) appeared to gain significantly more mass over the course of the test. It is interesting that the products of oxidation are basically the same, with the exception of one species which was found only on the 500 °C sample.

4.4 Pb-Sb-O System

4.4.1 Thermogravimetric Curve & Experimental Data for the Pb-Sb Tests

Thermogravimetric curves are presented for the trials run on binary Pb-Sb alloys at 500 °C and 600 °C, Figure 78. Experimental conditions and results are given in Table 15.

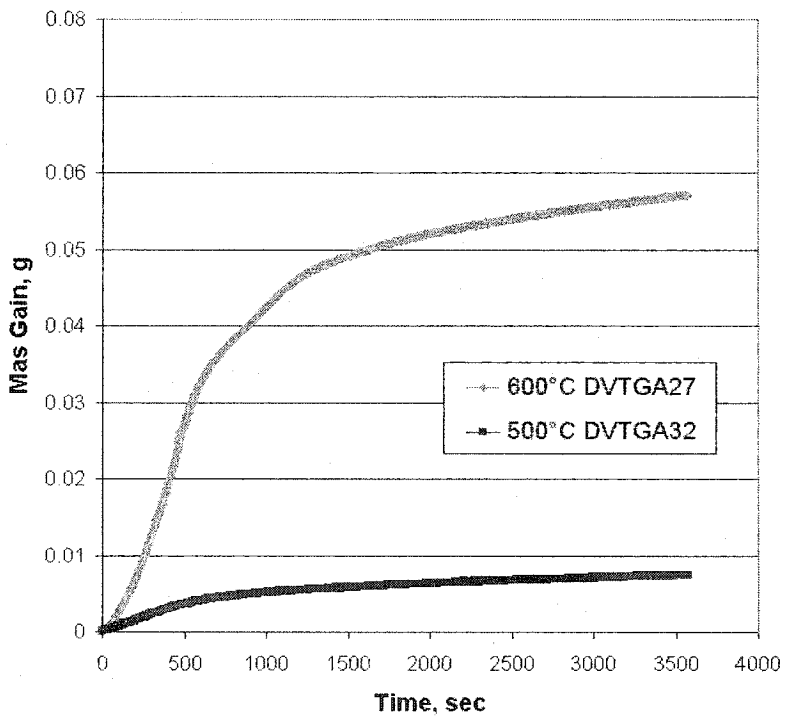

Figure 78. Pb2.00Sb TGA curves for tests DVTGA 32 (500 °C) and DVTGA 27 (600 °C).

Table 15. Experimental conditions and results for DVTGA 32 (500 °C) and DVTGA 27 (600 °C).

Trial	DVTGA 32	DVTGA 27
Composition	Pb2.00Sb	Pb2.00Sb
Temperature (°C)	500	600
Time (minutes) until O_2 introduction	26.5	26.5
Mass Gain (g) prior to O_2 introduction	0.0081	0.0030
Average Rate Mass Gain (mg/cm^{2}hr) prior to O_2 introduction	7.63	2.83
Mass Gain (g) first 300 s	0.0023	0.0125
Mass Gain (g), 60 minute test	0.0074	0.0571
Total Mass Gain (g) (Heating PLUS 60 minutes)	0.0155	0.0601
Percentage of Mass Gained during Heating	52.3	5.0

4.4.2 Captured Images for the Pb-Sb Tests

4.4.2.1 DVTGA 32 (500 °C)

The selected image of the sample surface for DVTGA32 (500 °C), Figure 79, is shown to contrast with DVTGA 27 (600 °C), Figure 80, at t = 0. The sample can be seen to be covered in oxide and the melt shape is seen to be uneven.

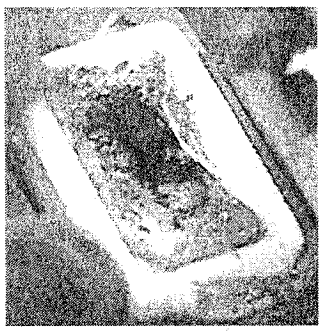

Figure 79. DVTGA32 (500 °C) at t= 0.

4.4.2.2 DVTGA 27 (600 °C)

The images selected for DVTGA27 (600 °C), Figure 80 to Figure 84, show the surface at t = 0 to be clean and free of oxide. With the introduction of oxygen, an oxide was observed to slowly accumulate at the edge of the melt on the crucible wall. By t = 500 s (Figure 83), the sample surface was fully covered by an oxide layer that continued to evolve, with commensurate mass gain, until the end of the test. Time t = 500 s corresponded to the

inflection point seen on the TGA curve, Figure 78, after which point a parabolic growth rate was observed.

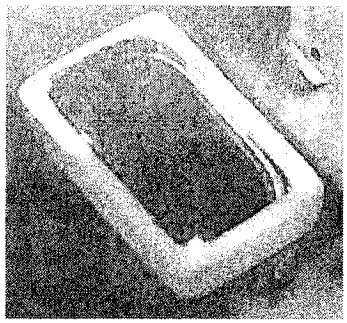

Figure 80. DVTGA27 (600 °C) at t = 0.

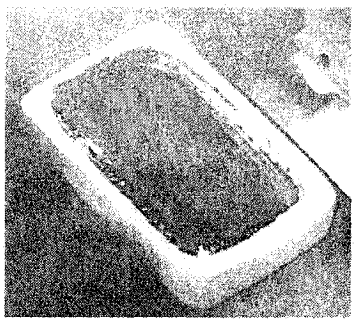

Figure 81. DVTA27 (600 °C) at t = 180 s.

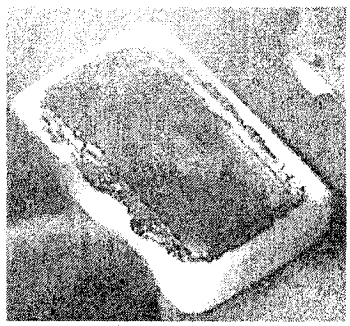

Figure 82. DVTGA27 (600 °C) at t = 365 s.

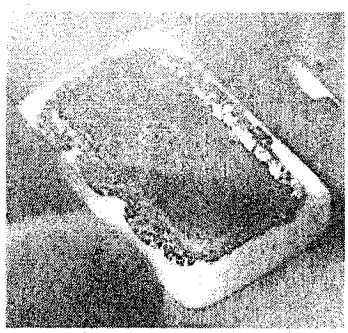

Figure 83. DVTGA27 (600 °C) at t = 500 s.

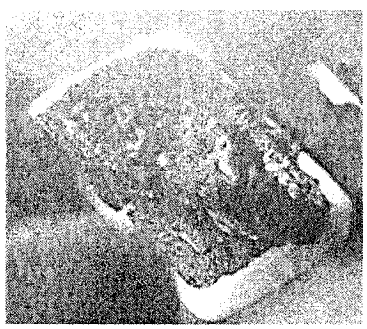

Figure 84. DVTGA27 (600 °C) at t = 600 s.

4.4.3 Experimental Observations for the Pb-Sb Tests

DVTGA32 (500 °C): a flaky oxide crust that had formed during melting was easily skimmed, however a second crust on the surface of the sample was difficult to skim. A white deposit was observed to collect on the viewing window glass.

DVTGA27 (600 °C): a liquid oxide phase formed on the sample surface. Fuming was also seen. The oxide phase was seen to wet the alumina crucible, as evidenced by the accretions which formed on the walls of the crucible, Figure 82 to Figure 84. A white deposit formed on the viewing window glass.

4.4.4 Oxide Products Identified in the Pb-Sb Tests

EDX revealed the presence of Pb, Sb and O on both samples.

4.4.5 Comments on the Pb-Sb Tests

Assuming all other experimental parameters to have been the same, it is interesting to note the effect of temperature on oxidation behaviour. The higher temperatures appeared to facilitate reduction or perhaps volatilization of the surface oxide phase, exposing a clean surface, and thereby contributing in a significant way to the difference in sample mass gains, as compared to samples where the surface is not completely exposed at t = 0. However, mass loss due to volatilization adds complexity to the analysis of the TGA data.

4.5 Pb-Sn-O System

4.5.1 Thermogravimetric Curve & Experimental Data for the Pb-Sn Tests

Thermogravimetric curves are presented for the trials run on binary Pb-Sn alloys at 500 °C and 600 °C in Figure 85. Experimental conditions and results are given in Table 16.

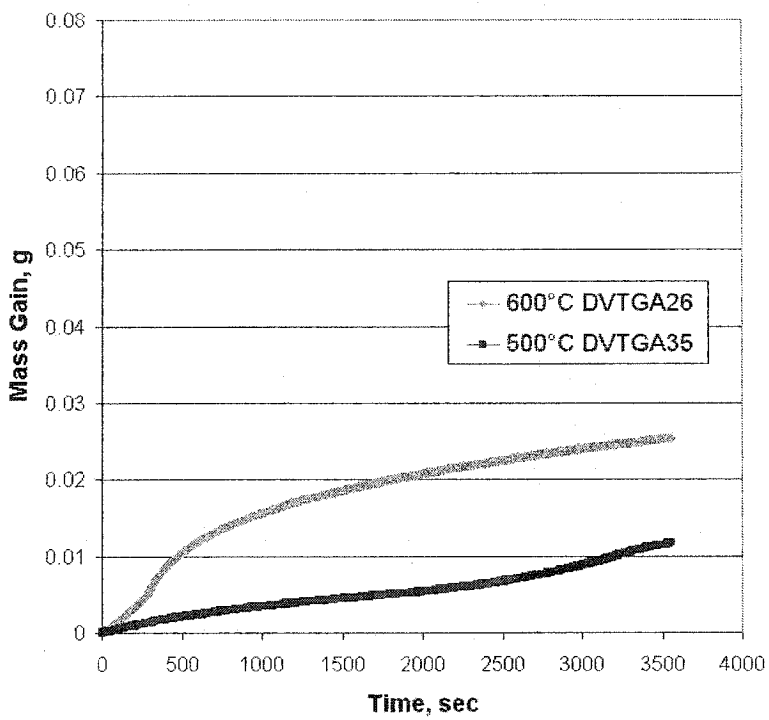

Figure 85. Pb0.26Sn TGA curves for tests DVTGA 35 (500 °C) and DVTGA 26 (600 °C).

Table 16. Experimental conditions and results for DVTGA 35 (500 °C) and DVTGA 26 (600 °C).

Trial	DVTGA 35	DVTGA 26
Composition	Pb0.26Sn	Pb0.26Sn
Temperature (°C)	500	600
Time (minutes) until O_2 introduction	25	29
Mass Gain (g) prior to O_2 introduction	0.0082	0.0164
Average Rate Mass Gain (mg/cm^{2}hr) prior to O_2 introduction	8.19	14.12
Mass Gain (g) first 300 s	0.0014	0.0056
Mass Gain (g), 60 minute test	0.0118	0.0255
Total Mass Gain (g) (Heating PLUS 60 minutes)	0.0200	0.0419
Percentage of Mass Gained during Heating	41.0	39.1

4.5.2 Captured Images for the Pb-Sn Tests

4.5.2.1 DVTGA 35(500 °C) and DV TGA 26

Both images, Figure 86 and Figure 87, were selected to show the shiny silver skin that remained following skimming of the sample surfaces just prior to oxygen introduction.

Although the crust that had formed on the sample surface during melting was very easily skimmed, it was not possible to skim the shiny silver skin.

Figure 86. DVTGA35 (500 °C) at t = 0.

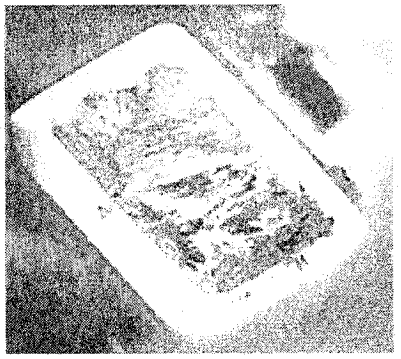

Figure 87. DVTGA26 (600 °C) at t = 0.

4.5.3 Experimental Observations for Pb-Sn Tests

DVTGA35 (500 °C): some crusty oxide pieces that had formed during melting were skimmed prior to oxygen introduction. The shiny silver skin that formed could not be skimmed and remained on the sample surface.

DVTGA26 (600 °C): some crusty oxide pieces that had formed during melting were skimmed prior to oxygen introduction. The shiny silver skin that could not be skimmed remained on the sample surface. Also, a black layer formed on the sample surface following oxygen introduction.

4.5.4 Oxide Products Identified in the Pb-Sn Tests

Analysis by XRD revealed PbO (massicot) as the dominant phase on the DVTGA 35 (500 °C) sample. EDX analysis of the different coloured DVTGA 26 (600 °C) oxide products showed Pb+O and Pb+Sn+O phases to be present.

4.5.5 Comments on the Pb-Sn Tests

Although there was difficulty in skimming both samples, and an unskimmable skin remained on both samples, it can be seen clearly in the different shapes of the TGA curves (Figure 85) that increasing temperature increased the rate and extent of mass transfer.

4.6 Pb-As-Sb-O System

4.6.1 Thermogravimetric Curve & Experimental Data for the Pb-As-Sb Tests

Thermogravimetric curves are presented for the trials run on ternary Pb-As-Sb alloys in Figure 88. Experimental conditions and results are given in Table 17.

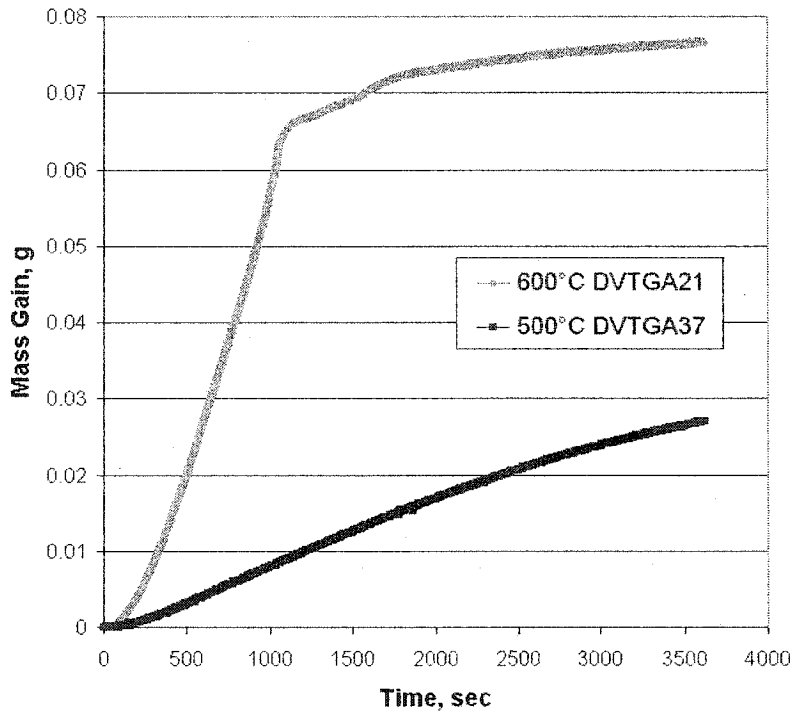

Figure 88. Pb0.90As2.00Sb TGA curves for tests DVTGA 37 (500 °C) and DVTGA 21 (600 °C).

Table 17. Experimental conditions and results for DVTGA 37 (500 °C) and DVTGA 21 (600 °C).

Trial	DVTGA 37	DVTGA 21
Composition	Pb0.90As 2.00Sb	Pb0.90As 2.00Sb
Temperature (°C)	500	600
Time (minutes) until O_2 introduction	23	31.5
Mass Gain (g) prior to O_2 introduction	0.0045	0.0011
Average Rate Mass Gain (mg/cm^{2}hr) prior to O_2 introduction	4.89	0.87
Mass Gain (g) first 300 s	0.0013	0.0086
Mass Gain (g), 60 minute test	0.0270	0.0766
Total Mass Gain (g) (Heating PLUS 60 minutes)	0.0315	0.0777
Percentage of Mass Gained during Heating	14.3	1.4

4.6.2 Captured Images for the Pb-As-Sb Tests

4.6.2.1 DVTGA 37(500 °C)

The images selected for DVTGA37 (500 °C), Figure 89 to Figure 91, show that the melt was able to almost completely "self-clean" during heating and melting, such that it was clear at time t = 0. Further, even after 60 minutes exposure to pure oxygen, the sample surface did not become completely covered by an oxide layer.

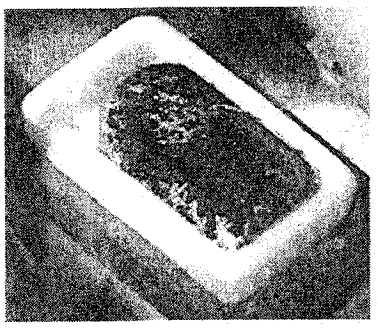

Figure 89. DVTGA37 (500 °C) at t = 300 s prior to O_2 introduction.

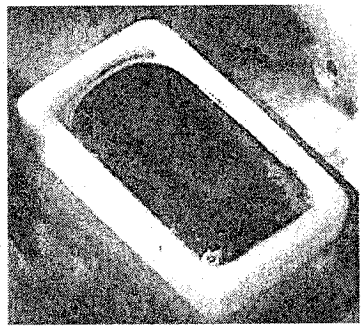

Figure 90. DVTGA37 (500 °C) at t = 0.

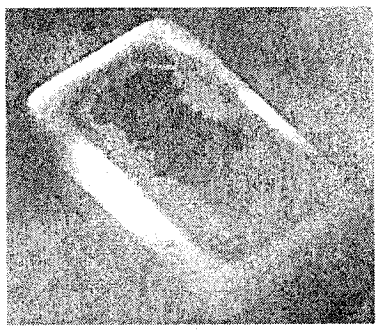

Figure 91. DVTGA37 (500 °C) at t = 3600 s.

4.6.2.2 DVTGA 21 (600 °C)

The images selected for DVTGA 21 (600 °C), Figure 92 to Figure 94, illustrate that again the melt surface has "self-cleaned" by time t = 0. Following oxygen introduction, an oxide product was observed to accumulate at the edge of the sample by the crucible wall. By t = 1050 seconds (Figure 94) the sample surface was completely covered by an oxide layer. This corresponds well with the inflection point on the TGA curve, Figure 88.

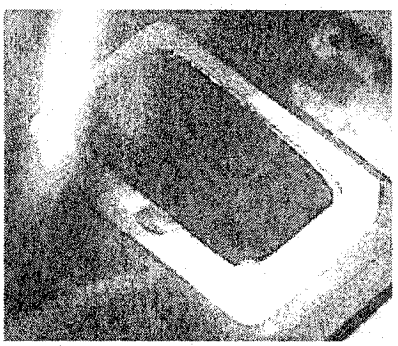

Figure 92. DVTGA21 (600 °C) at t = 0.

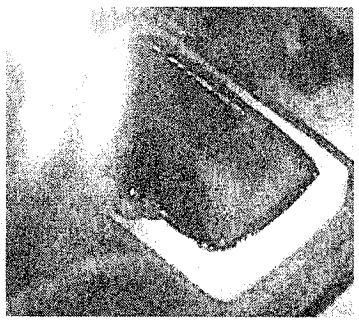

Figure 93. DVTGA21 (600 °C) at t = 500 s.

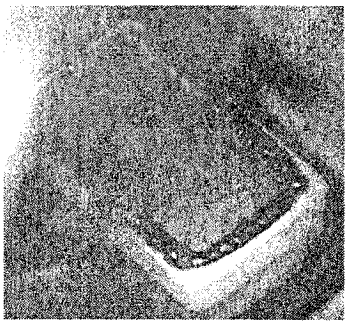

Figure 94. DVTGA21 (600 °C) at t = 1050 s.

4.6.3 Experimental Observations for the Pb-As-Sb Tests

DVTGA37 (500 °C): the sample surface 'self-cleaned'. The oxidation was *very* slow, and roughly 40% of the sample surface appeared to remain 'clean' throughout the experiment.

DVTGA21 (600 °C): the sample surface 'self-cleaned'. Reddish droplets were observed, as was a cloudiness on the viewing window glass.

4.6.4 Oxide Products Identified in the Pb-As-Sb Tests

Using EDX, Pb, As and O were detected on DVTGA 37, while on DVTGA21 (600 °C) Pb, As, Sb and O were detected.

4.6.5 Comments on the Pb-As-Sb Tests

The effect of temperature on mass gain was clear from the mass gain curves, Figure 88. This is further supported by the fact that in the 500 °C sample, the kinetics were sufficiently slow that the surface never became completely covered by an oxide layer.

4.7 Pb-As-Sn-O System

4.7.1 Thermogravimetric Curve & Experimental Data for the Pb-As-Sn Tests

Thermogravimetric curves are presented for the trials run on ternary Pb-As-Sn alloys at 500 °C and 600 °C in Figure 95. Experimental conditions and results are given in Table 18.

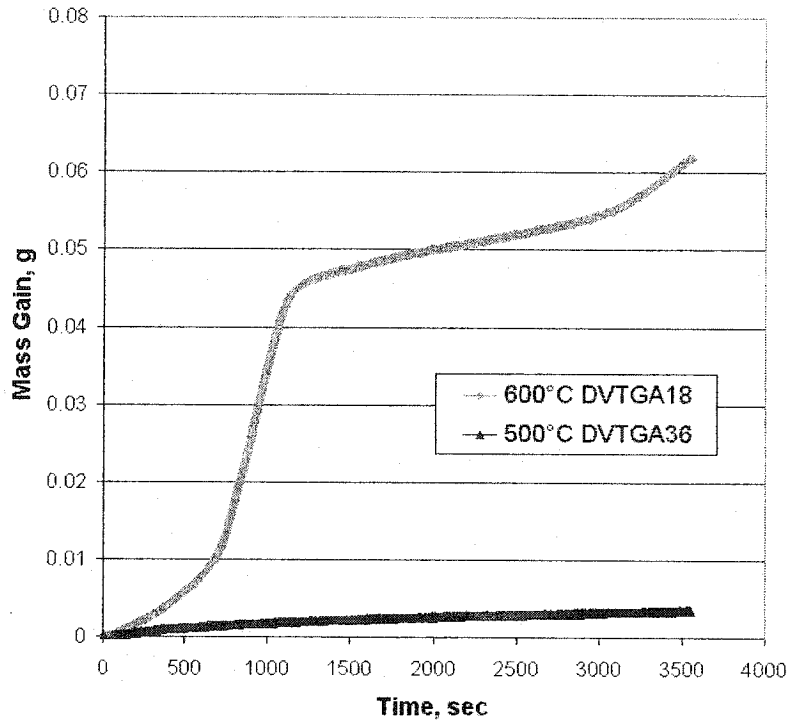

Figure 95. Pb0.90As0.26Sn TGA curves for tests DVTGA 36 (500 °C) and DVTGA 18 (600 °C).

Table 18. Experimental conditions and results for DVTGA 36 (500 °C) and DVTGA 18 (600 °C).

Trial	DVTGA 36	DVTGA 18
Composition	Pb0.90As 0.26Sn	Pb0.90As 0.26Sn
Temperature (°C)	500	600
Time (minutes) until O_2 introduction	23.5	30
Mass Gain (g) prior to O_2 introduction	0.0054	0.0080
Average Rate Mass Gain (mg/cm^{2}hr) prior to O_2 introduction	5.74	6.66
Mass Gain (g) first 300 s	0.0007	0.0028
Mass Gain (g), 60 minute test	0.0035	0.0619
Total Mass Gain (g) (Heating PLUS 60 minutes)	0.0089	0.0699
Percentage of Mass Gained during Heating	60.7	11.4

4.7.2 Captured Images for the Pb-As-Sn Tests

4.7.2.1 DVTGA 36 (500 °C)

This image, Figure 96, was selected to show the condition of the sample surface at time t = 0. An oxide can be seen at the edge of the sample, and the sample does not appear to fill the alumina crucible.

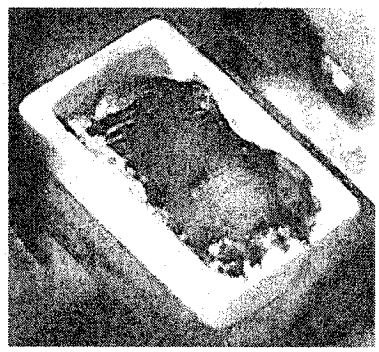

Figure 96. DVTGA36 (500 °C) at t = 0.

4.7.2.2 DVTGA 18 (600 °C)

Whereas the DVTGA 18 (600 °C) sample surface strongly resembled that of DVTGA 36 (500 °C) at time t = 0, it can be seen in the images, Figure 97 to Figure 99, that the oxidation behaviour over the course of the experiment was not the same. In fact, at roughly t = 735 s (Figure 98), an underlying phase thought to be arsenic oxide was seen to penetrate or "break through" the surface oxide phase. It was thought that this underlying phase chemically reacted with the initial phase. The time at which the break-through was seen to occur corresponded with the inflection point on the mass gain curve, Figure 95.

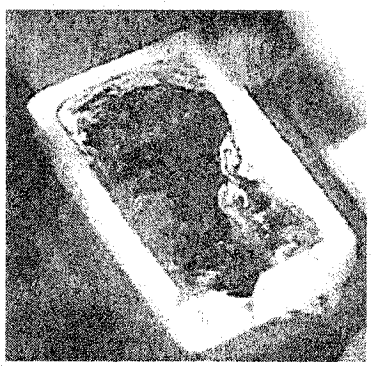

Figure 97. DVTGA18 (600 °C) at t = 0.

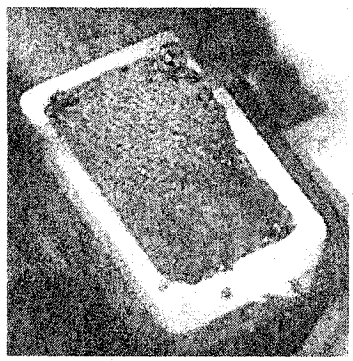

Figure 98. DVTGA18 (600 °C) at t = 735 s.

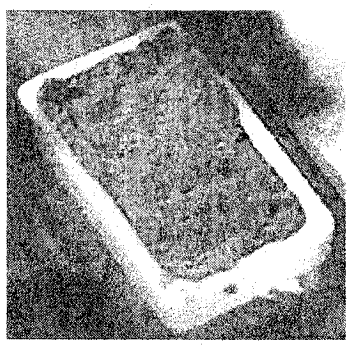

Figure 99. DVTGA18 (600 °C) at t = 1070 s.

4.7.3 Experimental Observations for the Pb-As-Sn Tests

DVTGA 36 (500 °C): The sample was difficult to skim since it was possible to skim a mass of reaction product away but there remained a skin on the surface, that quickly became brown and black following oxygen exposure.

DVTGA 18 (600 °C): As in DVTGA 36 (500 °), the sample surface was difficult to skim, and soon turned a brownish/blackish colour following exposure to oxygen. At approximately 840 s, reddish droplets could clearly be seen breaking through the existing oxide layer from below, and forming a new oxide phase.

4.7.4 Oxide Products Identified in the Pb-As-Sn Tests

XRD analysis of the DVTGA 36 (500 °C) sample identified only Pb metal, while analysis by EDX showed Pb, As, Sn and O to be present. XRD analysis of DVTGA 18 (600 °C) identified $Pb_3As_2O_8$ as the dominant oxide product.

4.7.5 Comments on the Pb-As-Sn Tests

Once again, the higher temperature caused the formation of a complex liquid Pb-As-O phase which broke through from beneath the existing, presumably tin-bearing, oxide layer. The consequence of this phenomenon was a greatly enhanced mass transfer, as evidenced by the section of the mass gain curve between t = 735 s and t = 1000 s, Figure 95.

4.8 Pb-Sb-Sn-O System

4.8.1 Thermogravimetric Curve & Experimental Data for the Pb-Sb-Sn Tests

Thermogravimetric curves are presented for the trials run on ternary Pb-Sb-Sn alloys at 500 °C and 600 °C in Figure 100. Experimental conditions and results are given in Table 19.

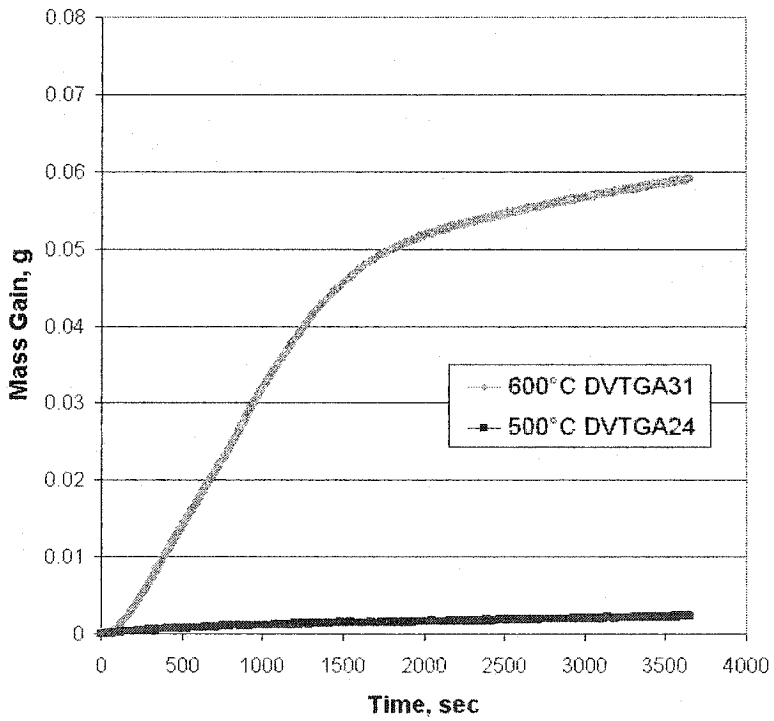

Figure 100. Pb2.00Sb0.26Sn TGA curves for tests DVTGA 24 (500 °C) and DVTGA 31 (600 °C).

Table 19. Experimental conditions and results for DVTGA 24 (500 °C) and DVTGA 31 (600 °C).

Trial	DVTGA 24	DVTGA 31
Composition	Pb2.00Sb 0.26Sn	Pb2.00Sb 0.26Sn
Temperature (°C)	500	600
Time (minutes) until O_2 introduction	23.5	31
Mass Gain (g) prior to O_2 introduction	0.0058	0.0087
Average Rate Mass Gain (mg/cm^2hr) prior to O_2 introduction	6.16	7.01
Mass Gain (g) first 300 s	0.0005	0.0068
Mass Gain (g), 60 minute test	0.0023	0.0591
Total Mass Gain (g) (Heating PLUS 60 minutes)	0.0081	0.0678
Percentage of Mass Gained during Heating	71.6	12.8

4.8.2 Captured Images for the Pb-Sb-Sn Tests

4.8.2.1 DVTGA 24 (500 °C)

The image selected, Figure 101, shows the condition of the sample surface at time t = 0. The shiny silver skin, characteristic of the tin-bearing lead alloys in the present work, can be seen. It can be seen in Figure 101 that the melt is intermixed with oxide.

Figure 101. DVTGA24 (500 °C) at t = 0.

4.8.2.2 DVTGA 31

The images selected, Figure 102 and Figure 103, show the effect of temperature on the surface conditions at t = 0 by which time the sample surface had almost completely "self-

cleaned" and the melt had completely filled the alumina crucible. In the upper left corner of the images, a white deposit on the viewing glass window can be seen.

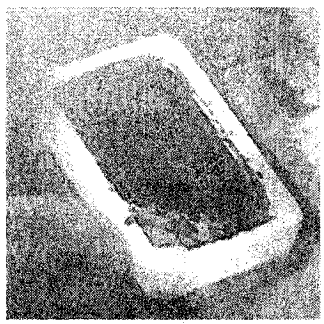

Figure 102. DVTGA31 at t = 0.

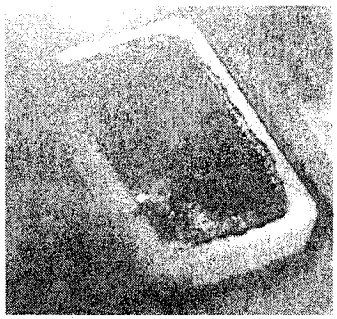

Figure 103. DVTGA31 at t = 340 s.

4.8.3 Experimental Observations for the Pb-Sb-Sn Tests

DVTGA 24 (500 °C): It was possible to skim a crusty layer that formed during heating and melting, but a shiny skin remained on the sample surface.

DVTGA 31 (600 °C): It was possible to skim most of the sample surface. The viewing glass window became clouded by a white product. Significant mass gain was observed.

4.8.4 Oxide Products Identified in the Pb-Sb-Sn Tests

XRD analysis of the DVTGA 24 (500 °C) sample identified only Pb metal, while analysis by EDX showed Pb, Sn and O to be present. EDX analysis of DVTGA 31 (600 °C) sample surface identified Pb, Sb and O.

4.8.5 Comments on the Pb-Sb-Sn Tests

The effect of temperature can be observed here in its contribution to the rate and extent of mass gain, Figure 100. The sample surface "self-cleaned" at 600 °C, whereas at 500 °C there was no evidence of this behaviour.

4.9 Pb-As-Sb-Sn-O System

4.9.1 Thermogravimetric Curve & Experimental Data for the Pb-As-Sb-Sn Tests

Thermogravimetric curves are presented for trials run on two types of quaternary Pb-As-Sb-Sn alloys (Figure 104 and Figure 105), with both alloys tested at 500 °C and 600 °C. Experimental conditions and results are given in Table 20.

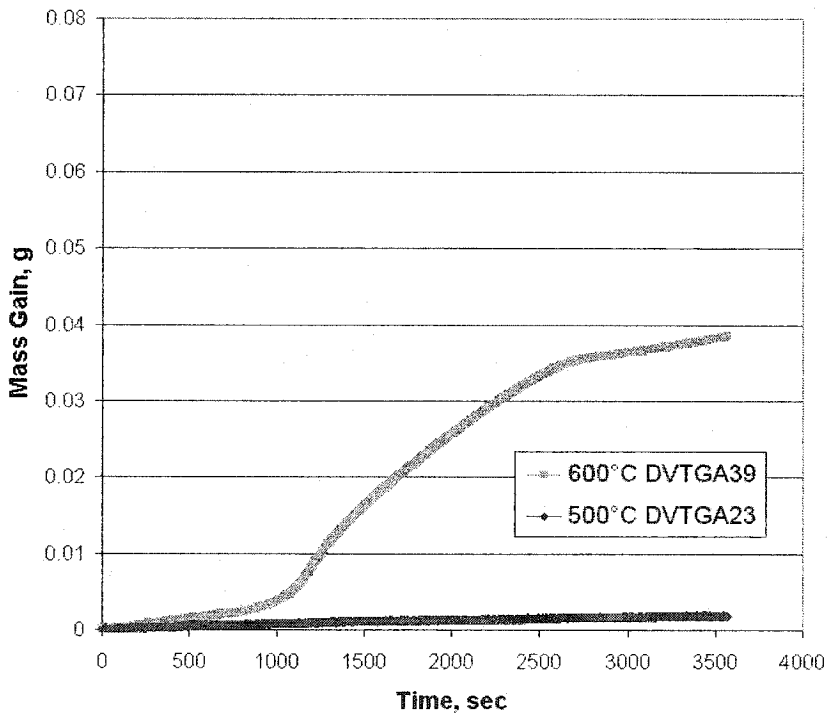

Figure 104. Pb0.90As2.00Sb0.26Sn TGA curves for DVTGA 39 (500 °C) and DVTGA 23 (600 °C)

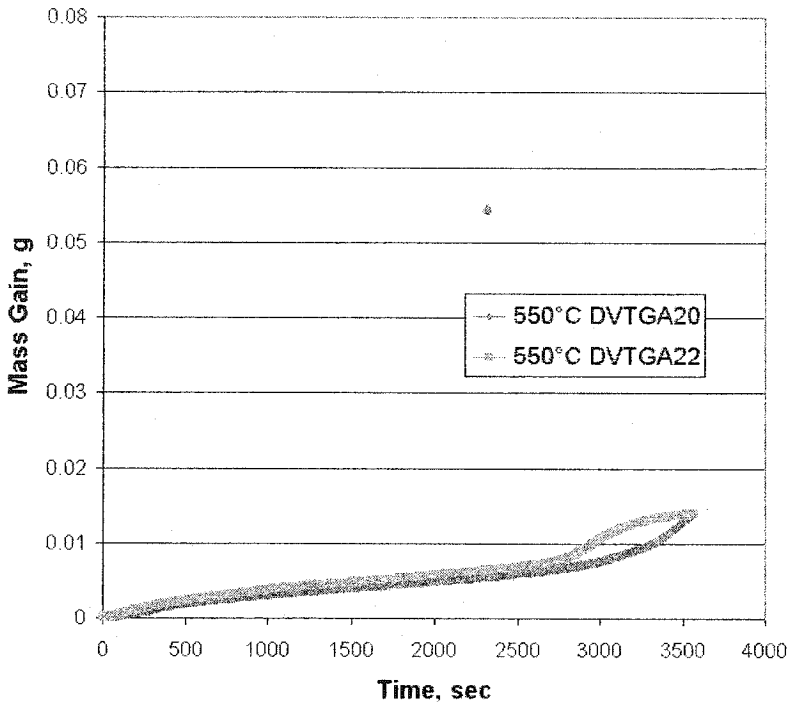

Figure 105. Pb0.45As1.00Sb0.13Sn TGA curves for DVTGA 20 (550 °C) and DVTGA 22 (550 °C)

Table 20. Experimental conditions and results for DVTGA 23 (500 °C), DVTGA 39 (600 °C), DVTGA 20 (550 °C) and DVTGA 22 (550 °C).

Trial	DVTGA 23	DVTGA 39	DVTGA 20	DVTGA 22
Composition	Pb0.90As 2.00Sb0.26Sn	Pb0.90As 2.00Sb0.26Sn	Pb0.45As 1.00Sb0.13Sn	Pb0.45As 1.00Sb0.13Sn
Temperature (°C)	500	600	550	550
Time (minutes) until O_2 introduction	32	36	28	26.5
Mass Gain (g) prior to O_2 introduction	0.0077	0.0063	0.0070	0.0053
Average Rate Mass Gain (mg/cm^2hr) prior to O_2 introduction	6.01	4.37	6.24	4.99
Mass Gain (g) first 300 s	0.0003	0.0009	0.0010	0.0016
Mass Gain (g), 60 minute test	0.0019	0.0376	0.0140	0.0139
Total Mass Gain (g) (Heating PLUS 60 minutes)	0.0096	0.0439	0.0210	0.0192
Percentage of Mass Gained during Heating	80.2	14.4	33.3	27.6

4.9.2 Captured Images for the Pb-As-Sb-Sn Tests

4.9.2.1 DVTGA 23 (500 °C)

The image selected, Figure 106, shows the condition of the sample surface at time t = 0. The shiny silver skin characteristic of tin-bearing lead alloys can be seen, which, at T = 500 °C, proved by the somewhat limited mass gain, to be an effective barrier to mass transfer, Figure 104.

Figure 106. DVTGA23 (500 °C) at t = 0.

4.9.2.2 DVTGA 39 (600 °C)

Although DVTGA 39 (600 °C) resembles DVTGA 23 (500 °C) at time t = 0, unexpected "break-through" behaviour was observed at roughly t = 1220 s and resulted in significant mass gain thereafter. For this reason, the two images, Figure 107 and Figure 108, were selected to show the "break-through" of a second oxide phase through the initial one.

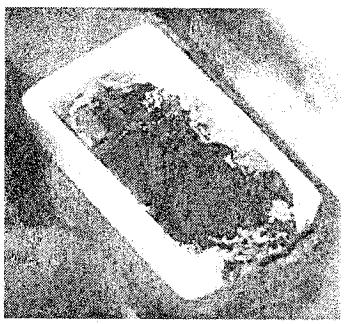

Figure 107. DVTGA39 (600 °C) at t = 0.

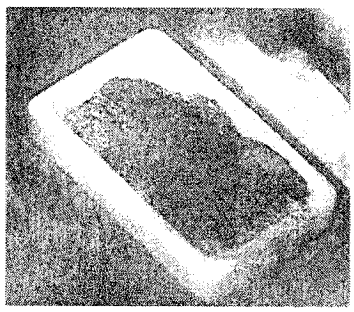

Figure 108. DVTGA39 (600 °C) at t = 1220 s.

4.9.2.3 DVTGA 20 (550 °C) and DVTGA 22 (550 °C)

These two tests were performed as replicates as described in the factorial design table (Table 10). It can be seen that the mass gain curves were coincident for the most part indicating that there was a high degree of reproducibility for the tests. Their overall mass gains proved to be intermediate between DVTGA 23 (500 °C) and DVTGA 39 (600 °C), though the concentration of impurity elements was exactly half. The surface morphology was also very similar to that DVTGA 39 (500 °C), Figure 106. The images, Figure 109 and Figure 110, were selected to show the condition of the sample surface immediately prior to oxygen introduction and to give more meaning to the mass gain curves, Figure 105. A similar type of shiny silver skin can be seen; similar to that described in tests on other tin-bearing alloys, e.g. DVTGA 25 (500 °C) and DVTGA 36 (600 °C).

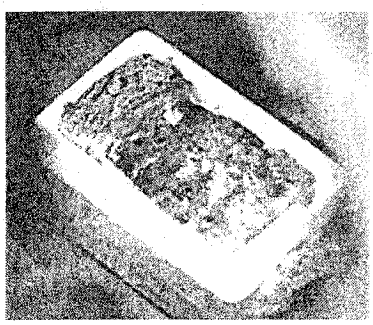

Figure 109. DVTGA20 (550 °C) at t = 0.

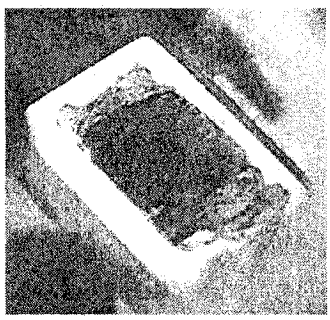

Figure 110. DVTGA22 (550 °C) at t = 0.

4.9.3 Experimental Observations for the Pb-As-Sb-Sn Tests

DVTGA23 (500 °C): a crust that formed during heating and melting was readily skimmed, but a skin remained on the sample surface. White deposits were observed on the viewing window glass.

DVTGA 39 (600 °C): a crust that formed during heating and melting was readily skimmed, but a skin remained on the sample surface. At t = 30 minutes, red droplets were observed to be "breaking through" the existing oxide layer from below.

DVTGA 20 (550 °C): a crust that formed during heating and melting was readily skimmed, but a skin remained on the sample surface. White deposits were observed on the viewing window glass.

DVTGA 22 (550 °C): a crust that formed during melting and heating was readily skimmed, but a skin remained on the sample surface. White deposits were observed on the viewing window glass.

4.9.4 Oxide Products Identified in the Pb-As-Sb-Sn Tests

XRD analysis of the DVTGA 23 (500 °C) sample identified only Pb (metal), while analysis by EDX showed Pb, As, Sn and O to be present.

XRD analysis identified complex oxide phases in the three remaining samples. On DVTGA 39 (600 °C), $Pb_5Sb_4O_{11}$ (dominant), Pb_4SbO_6 (sub-dominant) and $Pb_3As_2O_8$ (sub-

dominant) were identified. On DVTGA 20 (550 °C), $Pb_3As_2O_8$ was identified as the dominant phase. Finally, on DVTGA 22 (550 °C), $Pb_3As_2O_8$ was identified as the dominant phase, and Pb_4SbO_6 was identified as sub-dominant.

4.9.5 Comments on the Pb-As-Sb-Sn Tests

It was interesting to find that in samples which showed very little mass gain, that a number of complex oxide phases were identified by XRD, especially $Pb_3As_2O_8$ and Pb_4SbO_6, which were identified in both the 550 ° and 600 °C samples. A difference can be seen in the mass gains between the samples run at 550 °C, Figure 105, as compared to DVTGA 39 (600 °C) in Figure 104.

The most noteworthy observation regarding DVTGA 39 (600 °C) was the effect of temperature causing the formation of a complex liquid Pb-As-O phase which broke through from beneath the existing, presumably tin-bearing, oxide layer. The consequence of this phenomenon, as with DVTGA 18 (600 °C), was a mass transfer conduit, as evidenced by the mass gain curve, Figure 104.

4.10 Teck Cominco Lead Softener Feed

4.10.1 Thermogravimetric Curve & Experimental Data for the Teck Cominco Lead Softener Feed Tests

Thermogravimetric curves are presented for the trials run on Teck Cominco Lead Softener Feed at 500 °C, 550 ° C and 600 °C in Figure 111.

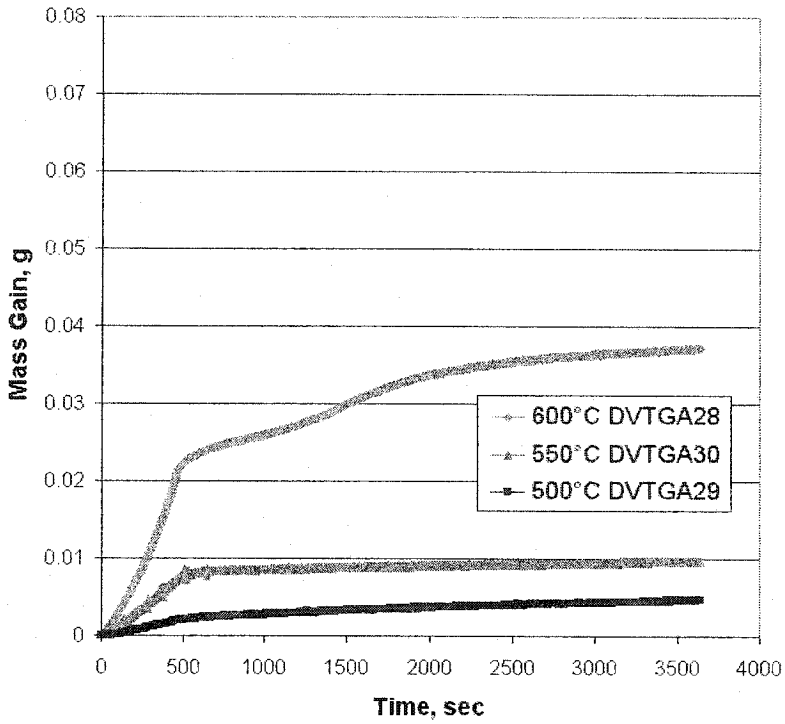

Figure 111. Teck Cominco Lead Softener Feed TGA curves for DVTGA 29 (500 °C), DVTGA 30 (550 °C) and DVTGA 28 (600 °C).

4.10.2 Captured Images for the Teck Cominco Lead Softener Feed Tests

4.10.2.1 DVTGA 29 (500 °C)

The images selected, Figure 112 and Figure 113, were chosen to show that the surface of the sample was roughly 50% clean at time t = 0 and that the oxide layer that formed following oxygen introduction visibly grew from the outside in, eventually covering the whole sample surface at roughly t = 600 s. This full coverage corresponded to the inflection point in the mass gain curve, Figure 111. The image in Figure 113 shows the surface just before it was completely covered. This type of behaviour was not observed as clearly in other tests.

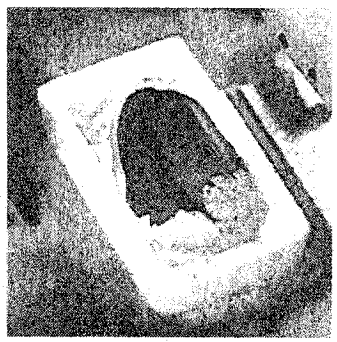

Figure 112. DVTGA29 (500 °C) at t = 0.

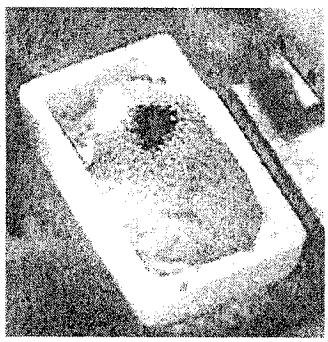

Figure 113. DVTGA29 (500 °C) at t = 600 s.

4.10.2.2 DVTGA 30 (550 °C)

The images selected, Figure 114 to Figure 117, show a phenomenon similar to that described for DVTGA 29 (500 °C). The sample surface was almost completely "self-cleaned" by time t = 0. The oxide layer that formed following oxygen introduction grew from the outside in and eventually covered the whole sample surface at roughly t = 600 s and corresponded to the inflection point in the mass gain curve, Figure 111.

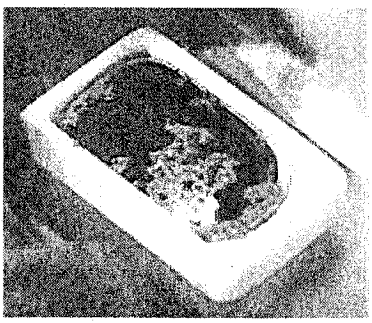

Figure 114. DVTGA30 (550 °C) at t = 120 s prior to O_2 introduction.

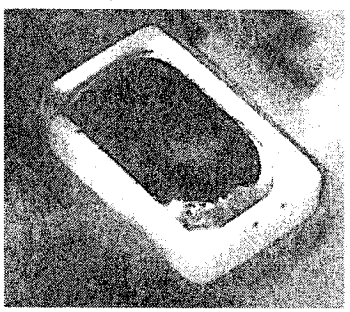

Figure 115. DVTGA30 (550 °C) at t = 0.

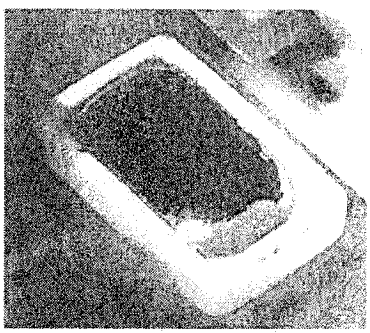

Figure 116. DVTGA30 (550 °C) at t = 210 s.

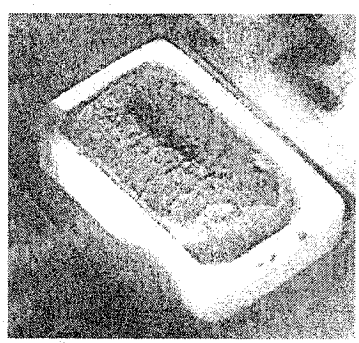

Figure 117. DVTGA30 (550 °C) at t = 595 s.

4.10.2.3 DVTGA 28 (600 °C)

The images selected, Figure 118 to Figure 121, show a phenomenon similar to that described for DVTGA 30 (550 °C). The sample surface was almost completely "self-cleaned" by time t = 0. The oxide layer that formed following oxygen introduction in this test very suddenly covered the whole sample surface at about time t = 450 s. Such rapid coverage was in contrast to DVTGA (550 °C), which was covered more gradually. The sudden covering corresponded to the inflection point in the mass gain curve, Figure 111.

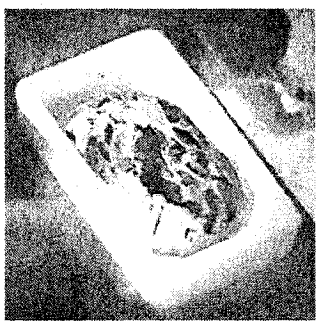

Figure 118. DVTGA28 (600 °C) at t = 420 s prior to O_2 introduction.

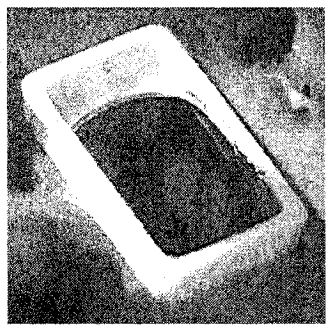

Figure 119. DVTGA28 (600 °C) at t = 0.

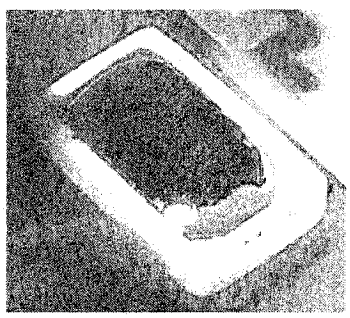

Figure 120. DVTGA28 (600 °C) at t = 210 s.

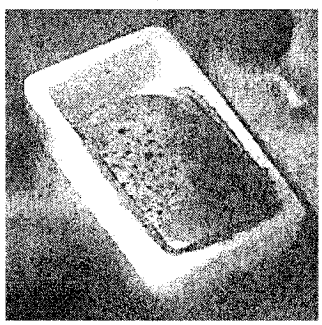

Figure 121. DVTGA28 (600 °C) at t = 450 s.

4.10.3 Experimental Observations for the Teck Cominco Lead Softener Feed Tests

DVTGA29 (500 °C): It was not possible to skim the surface completely; 50% of the surface remained covered by a resilient, seemingly "elastic" oxide. The oxide appeared to be composed of fragmented pieces of thin solid oxide, connected by an underlying skin.

The "hole" in the surface oxide layer, the latter which formed from the outside in, closed up *very* slowly over 15 minutes. Oxidation kinetics were *very* slow at 500 °C through or perhaps under this "elastic" layer.

DVTGA 30 (550 °C) Skimming was successful in removing most of the surface oxide at the end of heating and melting. A dark-coloured liquid oxide was observed following oxygen introduction. The "hole" in the surface oxide layer, the latter which grew from the outside in, closed up gradually. This phenomenon had not been seen previously. It was wondered if there were other agents at work in this melt, e.g., Bi and Cu, that are known to be present in the commercial material.

DVTGA 28 (600 °C) The surface appeared to 'self-clean' at around 550 °C. No skimming was necessary. The surface covered over suddenly with a gold-red oxide layer after about 7.5 minutes following oxygen introduction.

4.10.4 Oxide Products Identified in the Teck Cominco Lead Softener Feed Tests

EDX analysis of the sample surfaces identified Pb, As and O on DVTGA 29 (500 °C), Pb, As, Sb and O on DVTGA 30 (550 °C), and Pb, As, Sb and O on DVTGA 28 (600 °C).

4.10.5 Comments on the Teck Cominco Lead Softener Feed Tests

The most striking feature in this series of three tests was the effect of temperature, specifically between 550 °C and 600 °C, as evidenced by the mass gain curves for the latter temperatures, Figure 111. The oxidation behaviour in these tests had not been seen in previous synthetic alloy tests, and it was thought that the other impurity elements, e.g., Bi and Cu, in the bullion may have played a role in this behaviour. It was encouraging to the author to observe mass gain histories for the industrial material that strongly resembled that behaviour which was previously observed in prepared quaternary alloys. It is most interesting to compare the shape of mass gain curves for DVTGA21 (600 °C), Figure 88, with that for DVTGA28 (600 °C), Figure 111, since the curve shapes are similar, including the inflections points.

4.11 Simulated Lead Softener Feed

4.11.1 Thermogravimetric Curve & Experimental Data for the Simulated Lead Softener Feed Tests

Thermogravimetric curves are presented for the trials run on Simulated Lead Softener Feed at 500, 550 and 600 °C in Figure 122.

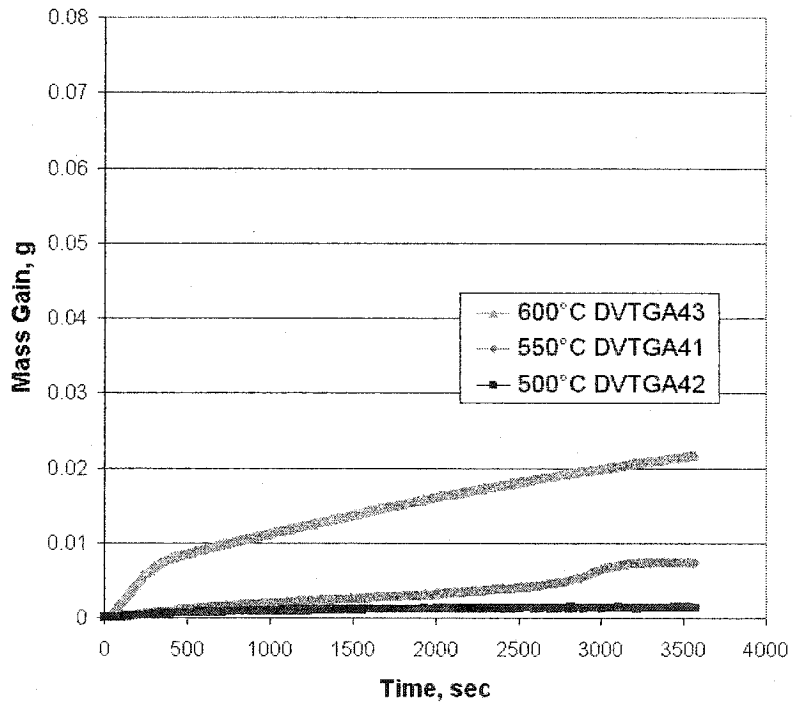

Figure 122. Simulated Lead Softener Feed (Pb0.22As1.12Sb0.10Sn) TGA curves for DVTGA 42 (500 °C), DVTGA 41 (550 °C) and DVTGA 43 (600 °C).

4.11.2 Captured Images for the Simulated Lead Softener Feed Tests

4.11.2.1 DVTGA 42 (500 °C) and DVTGA 41 (550 °C)

Both images, Figure 123 and Figure 124, were selected to show the shiny silver skin that remained following skimming of the sample surfaces, characteristic of tin-bearing lead alloys. Although a crust that had formed on the sample surface was skimmed, it was not possible to skim the thin skin which lay below and remained.

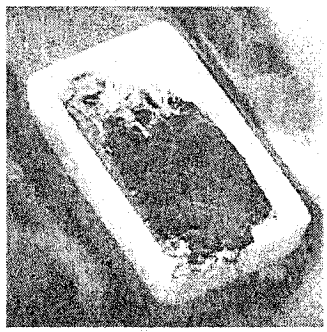

Figure 123. DVTGA42 (500 °C) at t = 0.

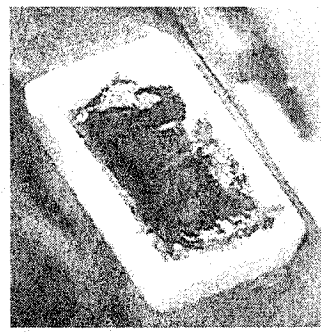

Figure 124. DVTGA41 (550 °C) at t = 0.

4.11.2.2 DVTGA 43 (600 °C)

The images selected, Figure 125 to Figure 127, show the condition of the sample surface at time t = 0, as well as well as the progression that was observed in the oxidation at the surface. The sample became nearly completely covered by around t = 350 s. Figure 127 shows the sample surface just before complete coverage. Careful study of the video recording revealed a series of irregularly shaped holes in the oxide layer which closed up one by one.

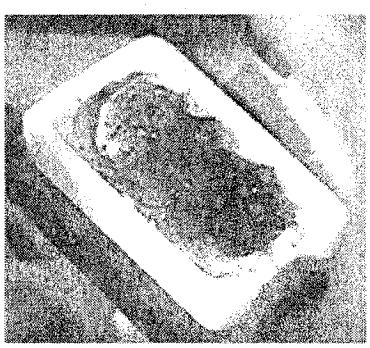

Figure 125. DVTGA43 (600 °C) at t = 0.

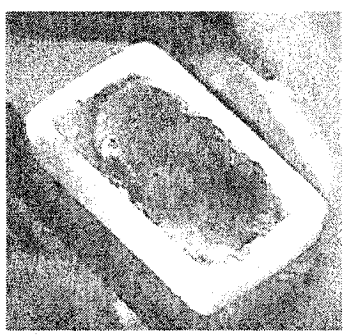

Figure 126. DVTGA43 (600 °C) at t = 75 s.

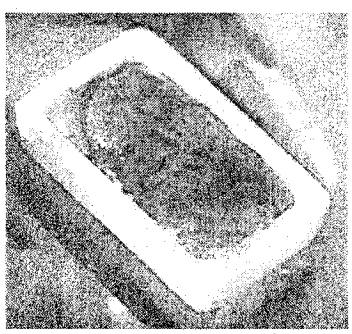

Figure 127. DVTGA43 (600 °C) at t = 225 s.

4.11.3 Experimental Observations for the Simulated Lead Softener Feed Tests

DVTGA 42 (500 °C): it was possible to skim a dry crust and a heterogeneous, viscous phase that formed during melting and heating, but a shiny skin remained on the sample

surface. Soon after oxygen introduction, the film present on the surface became black in colour.

DVTGA 41 (550 °C): it was possible to skim a crust that formed during melting and heating, but a shiny skin remained on the sample surface. Soon after oxygen introduction, the film present on the surface became black in colour.

DVTGA 43 (600 °C): it was not possible to completely skim the sample surface. After 2.5 minutes, small red pools formed on the surface of the already-existing solid goldish oxide layer. This phenomenon had not been observed before and was only seen in this test.

4.11.4 Oxide Products Identified in the Simulated Lead Softener Feed Tests

XRD analysis of the oxide phase from DVTGA 42 (500 °C) identified only Pb metal, while analysis by EDX showed Pb, As, and O to be present.

XRD analysis of the remaining two samples identified $Pb_5Sb_4O_{11}$ (dominant) and PbO (sub-dominant) in DVTGA 41 (550 °C), and $Pb_5Sb_2O_8$ as the dominant phase, while PbO, $PbSb_2O_5$ and Pb_4SbO_6 were identified as sub-dominant phases on DVTGA 43 (600 °C).

4.11.5 Comments on the Simulated Lead Softener Feed Tests

It was puzzling that the mass gain curves for the Simulated Softener Feed, Figure 122, were so different from those for the Teck Cominco Softener Feed, Figure 111. This may have been the influence of the impurity elements present in the industrial feed. There is also a small possibility that chemical analysis of Teck Cominco Softener Feed was somehow incorrect or otherwise corrupted, which would mean that the prepared Simulated Softener Feed was not as close to the chemical composition of the Teck Cominco Lead Softener Feed as believed.

4.12 General Curve Comparison

Collections of TGA curves were plotted together to present more clearly the variation of the mass gain data as a function of sample components and composition. The first

collection (Figure 128) plots six curves for tests run at 500 °C, while the second (Figure 129) presents six curves for TGA tests run at 600 °C.

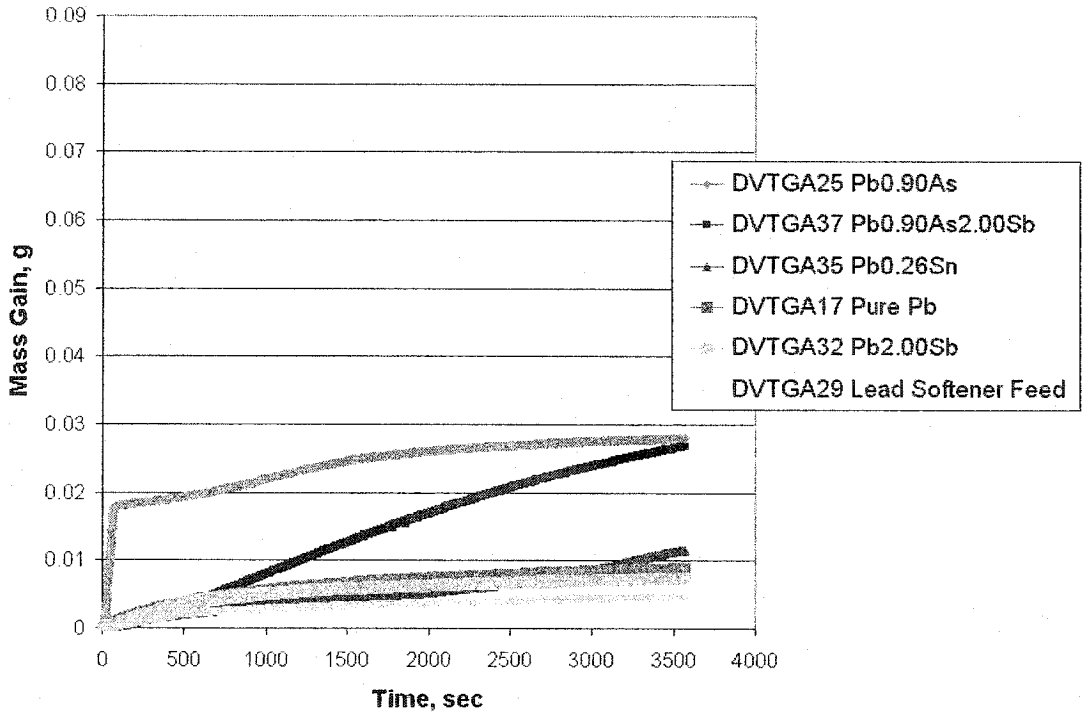

Figure 128. TGA curves for trials conducted at 500 °C.

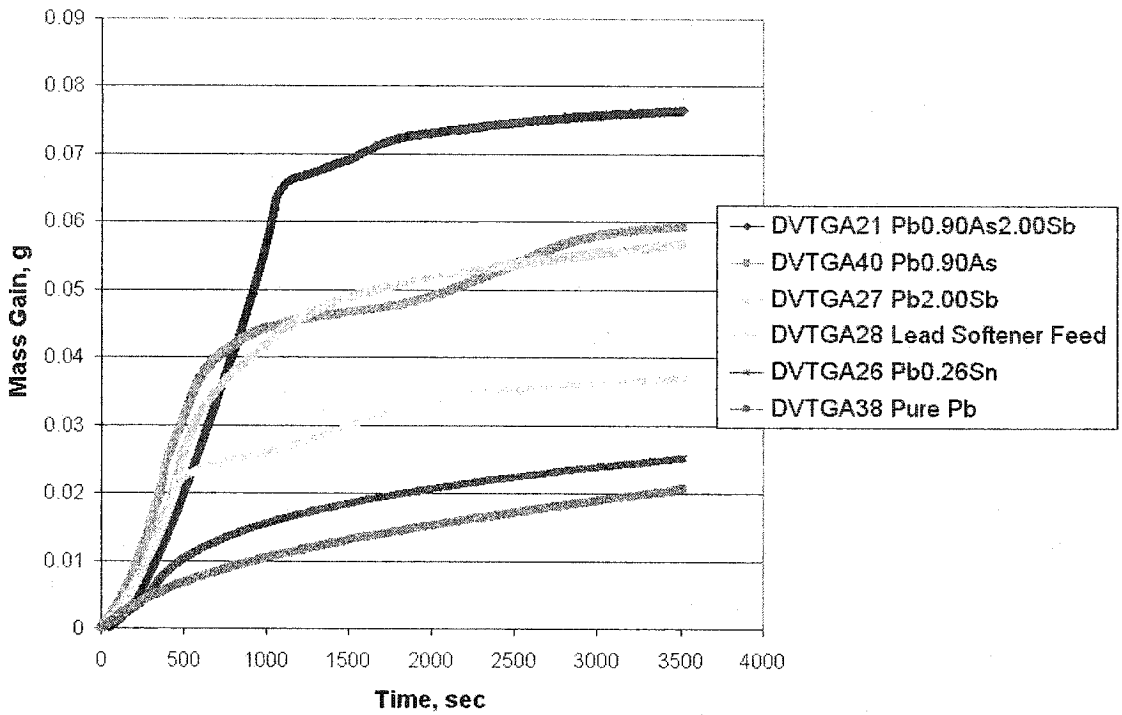

Figure 129. TGA curves for trials conducted at 600 °C.

4.13 Statistical Analysis on TGA tests

Linear regression analyses were performed to evaluate the effect of the four parameters, namely,

A = initial nominal wt% As

B = initial nominal wt% Sb

C = initial nominal wt% Sn

D = melt temperature (°C)

on the responses obtained for a selection of dependent variables. The responses evaluated were:

1. Mass Gain evaluated at time = 300 seconds from oxygen introduction
2. Mass Gain for 60 minutes oxygen exposure
3. Average Rate of Mass Gain prior to oxygen introduction
4. Total Mass Gain
5. Percentage of Mass Gained prior to oxygen introduction

As described in the previous chapter, the four (4) parameters were tested in a complete 2^4 factorial experimental design. The parameters and the summary of responses are given below, Table 21.

Table 21. Summary of responses used in linear regression analysis

Trial	Composition	Temperature, °C	Time until O_2 introduction, mins	Mass Gain prior to O_2 introduction, g	Avg Rate Mass Gain (pre-O_2 introduction), mg/cm^{2}hr	Mass Gain First 10 secs, g	Mass Gain First 20 secs, g	Mass Gain First 30 secs, g	Mass Gain First 40 secs, g
DVTGA 17	Pure Pb	500°C	21	0.0063	7.49	0.0000	0.0001	0.0002	0.0003
DVTGA 38	Pure Pb	600°C	31	0.0128	10.31	0.0001	0.0003	0.0005	0.0005
DVTGA 35	Pb0.26Sn	500°C	25	0.0082	8.19	0.0001	0.0002	0.0002	0.0002
DVTGA 26	Pb0.26Sn	600°C	29	0.0164	14.12	0.0001	0.0001	0.0003	0.0005
DVTGA 32	Pb2.00Sb	500°C	26.5	0.0081	7.63	0.0002	0.0002	0.0004	0.0003
DVTGA 27	Pb2.00Sb	600°C	26.5	0.003	2.83	0.0001	0.0004	0.0006	0.0008
DVTGA 24	Pb2.00Sb0.26Sn	500°C	23.5	0.0058	6.16	0.0000	0.0000	0.0000	0.0000
DVTGA 31	Pb2.00Sb0.26Sn	600°C	31	0.0087	7.01	0.0001	0.0001	0.0002	0.0000
DVTGA 25	Pb0.90As	500°C	22.9	0.0106	11.56	0.0006	0.0020	0.0046	0.0085
DVTGA 40	Pb0.90As	600°C	30	0.0051	4.25	0.0002	0.0005	0.0007	0.0011
DVTGA 36	Pb0.90As0.26Sn	500°C	23.5	0.0054	5.74	0.0000	-0.0002	-0.0002	-0.0001
DVTGA 18	Pb0.90As0.26Sn	600°C	30	0.008	6.66	0.0000	0.0000	0.0001	0.0002
DVTGA 37	Pb0.90As2.00Sb	500°C	23	0.0045	4.89	-0.0001	0.0000	-0.0002	-0.0001
DVTGA 21	Pb0.90As2.00Sb	600°C	31.5	0.0011	0.87	0.0000	0.0001	0.0000	0.0000
DVTGA 23	Pb0.90As2.00Sb0.26Sn	500°C	32	0.0077	6.01	0.0000	0.0000	0.0000	0.0000
DVTGA 39	Pb0.90As2.00Sb0.26Sn	600°C	36	0.0063	4.37	0.0000	0.0000	0.0000	0.0000
DVTGA 20	Pb0.45As1.00Sb0.13Sn	550°C	28	0.007	6.24	0.0000	0.0000	0.0000	-0.0001
DVTGA 22	Pb0.45As1.00Sb0.13Sn	550°C	26.5	0.0053	4.99	0.0001	0.0002	0.0002	0.0002

Trial	Composition	Temperature, °C	Mass Gain First 50 secs, g	Mass Gain First 60 secs, g	Mass Gain First 120 secs, g	Mass Gain First 300 secs, g	Mass Gain, 60 mins test, g	Total Mass Gain (Heat-up PLUS 60 mins), g	Percentage of Mass Gained during Heat-up
DVTGA 17	Pure Pb	500°C	0.0004	0.0005	0.0013	0.0027	0.0088	0.0151	41.7
DVTGA 38	Pure Pb	600°C	0.0007	0.0009	0.0022	0.0046	0.0207	0.0335	38.2
DVTGA 35	Pb0.26Sn	500°C	0.0002	0.0003	0.0006	0.0014	0.0118	0.0200	41.0
DVTGA 26	Pb0.26Sn	600°C	0.0006	0.0008	0.0018	0.0056	0.0255	0.0419	39.1
DVTGA 32	Pb2.00Sb	500°C	0.0004	0.0004	0.0008	0.0023	0.0074	0.0155	52.3
DVTGA 27	Pb2.00Sb	600°C	0.0011	0.0014	0.0034	0.0125	0.0571	0.0601	5.0
DVTGA 24	Pb2.00Sb0.26Sn	500°C	0.0000	0.0001	0.0002	0.0005	0.0023	0.0081	71.6
DVTGA 31	Pb2.00Sb0.26Sn	600°C	0.0001	0.0002	0.0014	0.0068	0.0591	0.0678	12.8
DVTGA 25	Pb0.90As	500°C	0.0112	0.0150	0.0181	0.0186	0.0281	0.0387	27.4
DVTGA 40	Pb0.90As	600°C	0.0014	0.0018	0.0045	0.0157	0.0593	0.0644	7.9
DVTGA 36	Pb0.90As0.26Sn	500°C	-0.0001	0.0000	0.0002	0.0007	0.0035	0.0089	60.7
DVTGA 18	Pb0.90As0.26Sn	600°C	0.0001	0.0002	0.0008	0.0028	0.0619	0.0699	11.4
DVTGA 37	Pb0.90As2.00Sb	500°C	0.0000	0.0000	0.0002	0.0013	0.0270	0.0315	14.3
DVTGA 21	Pb0.90As2.00Sb	600°C	0.0001	0.0002	0.0015	0.0086	0.0766	0.0777	1.4
DVTGA 23	Pb0.90As2.00Sb0.26Sn	500°C	0.0000	-0.0001	0.0001	0.0003	0.0019	0.0096	80.2
DVTGA 39	Pb0.90As2.00Sb0.26Sn	600°C	0.0001	0.0002	0.0003	0.0009	0.0376	0.0439	14.4
DVTGA 20	Pb0.45As1.00Sb0.13Sn	550°C	-0.0001	0.0000	0.0003	0.0010	0.0140	0.0210	33.3
DVTGA 22	Pb0.45As1.00Sb0.13Sn	550°C	0.0002	0.0003	0.0006	0.0016	0.0139	0.0192	27.6

Results are presented by dependent variable evaluated, giving the overall regression fit, and parameter significance details (i.e., t-score and corresponding probability value).

4.13.1 Analysis 1: Mass Gain Evaluated at t = 300 s from Purposeful Oxygen Injection

It can be stated with 99% confidence that the tin content, parameter C (t = -3.52, P = 4.2E-03), reduced average mass gain over the first 300 seconds of oxygen exposure. Overall fit for the analysis, F = 3.1E-03.

4.13.2 Analysis 2: Mass Gain, 60 minutes Oxygen Exposure

Looking at the mass gain over the sixty (60) minute test, it can be stated with 99.99% confidence that temperature, parameter D (t = 5.46, P = 8.5E-05), was significant. With a confidence interval of 91%, it can be stated that arsenic content, parameter A (t = 1.83, P = 8.8E-02), was also significant. Overall fit for the analysis, F = 4.0E-04.

4.13.3 Analysis 3: Average Rate of Mass Gain Prior to Oxygen Introduction

It can be stated that antimony content at 99.9% confidence, parameter B (t = -4.81, P = 7.0E-04), and arsenic content at 99% confidence, parameter A (t = -3.27, P = 8.4E-03), reduced the average rate of mass gain in the heating period prior to oxygen exposure at which time it has been estimated that there was oxygen present in the order of 200 ppm. Also significant at 99% confidence was the synergistic effect between tin and temperature, parameter CD (t = 3.27, P = 8.5E-03). This suggests that the effect of the tin content depends on temperature, that is, the tin content appears to be more significant at higher temperatures and less significant at lower temperatures. Further investigation would be required to expound this interactive effect. Overall fit for the analysis, F = 1.1E-03.

4.13.4 Analysis 4: Total Mass Gain

Temperature, parameter D (t = 6.47, P = 2.1E-05), was found to be the only significant parameter for the total mass gain for the heating period **plus** the 60 minute test, and was indisputably significant at 99.99% confidence. With higher temperatures, there was greater mass gain. Overall fit for the analysis, F = 2.0E-04.

4.13.5 Analysis 5: Percentage of Mass Gained prior to Oxygen Introduction

Looking at the percentage of mass gained in the test **prior** to purposeful oxygen introduction, as compared to the mass gained during the 60 minutes exposure time, and as opposed to Analysis 3, it can be stated with 99.999% confidence that higher temperatures, parameter D (t = -17.0, P = 2.7E-06) reduced the fraction of mass gained prior to oxygen introduction. In other words, at higher temperatures, proportionally more mass gain

occurred after purposeful oxygen introduction. It also meant that at lower temperatures, this percentage of mass gained was statistically higher.

It can also be stated with 99.99% confidence that a higher tin content, parameter C (t = 9.38, P = 8.4E-05) resulted in most of a sample's mass being gained during the heating period.

There were also two interactive effects that were significant at the 99.9% confidence interval and that were detected, but which would require further investigation to describe in greater detail. Specifically, the effect of antimony content depended on temperature, parameter BD (t = -7.26, P = 3.0E-04), i.e., a high antimony content at higher temperatures, may reduce the fraction of mass gained prior to oxygen introduction, while a low antimony content at lower temperatures may increase the fraction of mass gained prior to oxygen addition.

In a corresponding way, the effect of tin content also depended on temperature, parameter CD (t = -6.07, P = 9.0E-04), i.e., a high tin content at higher temperatures decreases the fraction of mass gained prior to oxygen introduction, while a low tin content at lower temperatures will increase the fraction of mass gained prior to oxygen introduction. Overall fit for the analysis, F = 3.8E-05.

4.14 Discussion of Errors

There are several identifiable sources of error which may have contributed to the range of results obtained, for example, the range of 0.0019 g (DVTGA23 (600 °C)) to 0.0766 g (DVTGA 21 (500 °C)) in mass gain for sixty minutes' oxygen exposure

Ideally, all metals and alloys used in the experimental trials should have been homogeneous and free of oxide. Also it may have been helpful to transfer samples into the furnace chamber under an inert gas atmosphere, and more importantly that this atmosphere be maintained during the heating period. However, there were practical cost and logistics limitations, which could not be avoided.

A large source of error derives from the imperfect seals on the TGA setup, which resulted in oxygen contamination of the gas phase and heat oxidation of the charge during the heating period. The effects were compounded in the following way: when the sample drillings of say, pure Pb, were exposed to oxygen from the ambient atmosphere before being introduced into the chamber, a very thin PbO layer formed on the surface. The drillings were heated and melted in an environment that contained unfortunately 200 ppm O_2, causing further oxidation of the drillings*. Once melted and even superheated, the drillings would be distinct, and mechanical mixing was not sufficient to separate the melt from the oxide to allow the oxide to be skimmed, if possible. Another problem was that the melt did not always fully fill the crucible, which meant that the melt surface area exposed to oxidation was not consistent from test to test and that the calculations for rate of mass gain per unit surface area are inaccurate, however, the maximum error associated with this issue was thought to be 20 % based on the actual melt surface area, and rates of mass gain which are given in mg $cm^{-2} hr^{-1}$.

Another source of error was the gas phase products of reaction, which were not recorded by the digital balance. For example, Pb2.00Sb sample DVTGA 27 (600 °C) showed evidence of fuming and the viewing window glass became cloudy from the white deposits. This means that there was mass loss from this sample to the gas phase and thus the values for mass gain were incorrect. This was an unfortunate consequence, but since no absolute values have been stated in this study on the kinetics of oxidation, this error was not taken into account.

The mass gain data acquired on the PC were averaged over time; specifically, the digital balance sent mass readouts without corresponding time values. Therefore, it was necessary to calculate the average delay between readings to construct the mass gain vs. time curves. Since the number of readouts sent over a sixty minute period was not consistent from test to test, the calculated delay between readings differed slightly from trial to trial. The

* This value of 200 ppm was obtained as an average of the total mass gained on all the samples during the heating period, taking into account the varying durations of heating required for the different samples.

maximum error associated with this issue was 5 %, which would be seen only in the shape (compression) of the mass gain curves, and the final value for mass gained.

As mentioned in the Experimental Methodology (Section 3.2.5), it was decided to flatten the specimens in a mounting press – a technique which often proved to be adequate in obtaining a flat surface without burying the oxide beneath the metallic phase, but sometimes this burying did occur, and no oxide phases could be identified. Another issue in this regard is that the compound database of the XRD apparatus used was outdated and incomplete. It was utilized because, in comparison to the alternative system, a) the oxide phase did not need to be separated from the metallic phase; b) there was no minimum mass of oxide required (i.e., the total sample mass exceeded the instrument's minimum mass requirement); and c) metallic phases could be analyzed, in addition to oxide phases. Sometimes the spectrum that was produced could not be matched with a spectrum in the database. As the investment of time on the identification of oxide phases could not be justified by the author based on the scope of the project as conceptualized, no further investigation was done. The purchase of a new, updated database was not entertained as an option.

Another challenge was that the Pb (metal) signal in the XRD characterization was sometimes overwhelming, and hence Pb was the only identifiable phase. Finally, phases that account for less than 5 wt% are not detected in XRD analysis. This was problematic specifically in the case of tin, which had an initial maximum concentration of 0.26 wt% in the alloy.

CHAPTER 5: DISCUSSION

5.1 Pure Pb

In order to establish a baseline for comparison, the Pb-O system (Figure 60) is first considered. It can be seen that oxidation followed parabolic rate laws, which, along with linear and logarithmic rate laws, are among the most commonly encountered in the high temperature oxidation of metals[76]. In such instances, a compact, dense oxide film or scale is formed on a metal surface, and the oxide acts to physically separate the reactants from one another and reaction progression depends on solid-state diffusion of the reactants through the oxide[76].

Rates of diffusion are commonly expressed in terms of a diffusion coefficient, D, which is defined by Fick's first law[77],

$$J = -D\left(\frac{\partial c}{\partial x}\right)_t \qquad (37)$$

where J is the instantaneous flow rate per unit area of the diffusing species across a plane, c is the concentration of the diffusing species at the plane, and $\partial c/\partial x$ is the concentration gradient of the diffusing species normal to the plane. Therefore D is the flow rate per unit area at unit concentration gradient at the plane, and is given in units of length^2/time, commonly, cm^2/sec. Diffusion across the oxide film takes place due to the statistical effect of lattice jumps – the effect is manifested as activity.

In the present study, it was found that it was not possible to skim the oxide film from the pure lead samples at 500 °C or 600 °C since as quickly as the film was removed it formed again under the conditions of the experiment. In addition, roughly 40% of the total mass gained by those samples was gained during 'Heating' (i.e., before purposeful oxygen introduction). As lead reacts quite readily with oxygen ($P_{O_2,\ equilibrium}$ = 1.71 x 10^{-16} atm at 600 °C), it is understandable that with at least 200 ppm O_2 present in the furnace chamber

during heating, a good part of the oxide layer was formed prior to purposeful oxygen introduction, and further growth was limited by the rate of mass transfer through the oxide layer.

The effects on the oxidation mechanism and kinetics of each of the four parameters investigated, namely: (A) initial nominal wt% As, (B) initial nominal wt% Sb, (C) initial nominal wt% Sn, and (D) melt temperature are discussed in the following sections.

5.2 Parameter A: Arsenic

5.2.1 Statistical Analysis of the Effect of Arsenic

Regression analysis indicated that increases in the arsenic content reduced the average rate of mass gain in the heating period prior to purposeful oxygen exposure when there was oxygen present at roughly 200 ppm. This effect is likely related to the Pb-As-O defect structure, but a deeper explanation would require more complex thermodynamic data, such as an Sb-Pb-O-As-Sn solid-liquid-gas phase diagram. With a confidence interval of 92%, it was also found that increased arsenic content was significant in increasing mass gain during the sixty (60) minute test.

5.2.2 Discussion of Other Arsenic-Related Behaviour

When lead samples containing 0.9 wt% As were studied, behaviour quite distinct from that for pure lead was observed. Droplets of a reddish liquid oxide phase were observed in the trials at 500 °C and 600 °C, both before and after oxygen introduction.

Also, the sample was observed to "self-clean" - that is, a clean metallic surface was exposed during the heating period as a result of the oxide on the surface being consumed. It was postulated that the mechanism involved As_2O_3 fluxing solid PbO on the surface, and perhaps the action of the complex oxide product as a "conveyor" of oxygen to the metal by the alternate oxidation and reduction of arsenic as it alternated between the +3 and +5 states. In this way, it appeared that arsenic, to the extent that it could remove oxygen at the metal interface through this fluxing reaction, continually refreshed the gas-metal interface[78], i.e., it removed the oxide layer which acted as a resistance to mass transfer.

Since the separate As and Pb oxidation reactions and the fluxing reactions happen **very** quickly at these temperatures (as compared to what can be perceived by the human eye or even by a digital video recorder which captures 30 frames per second), it is not possible to comment on the thermodynamic prediction that As oxidizes preferentially to lead oxidation was supported.

It should be noted that one experimental trial was devoted to determining the increase in the surface temperature when the reddish droplets were present and flowing outwards from the sample centre. In DVTGA44, it was found that at the moment of greatest surface droplet activity, roughly 4.5 minutes after oxygen was purposefully introduced, the surface temperature had risen to 632 °C, 27 °C above the set point temperature, that was determined experimentally to have been 605 °C. Two minutes later, the temperature had returned to its previous range.

The observed presence of complex liquid phase oxides such as the reddish droplets described above, suggests that mass transfer across the gas-liquid interface would be greatly facilitated, since diffusion rates in liquid oxides are rapid compared to those in solid oxides (although no diffusion data are available for this system), and liquid oxides would not be as effective as diffusion barriers in oxidation of metals[76]. This was observed as shown in Figure 63, wherein the rate of oxidation is greater than in the case of pure Pb, Figure 60. Furthermore, the temperature rise described in the previous paragraph suggested that one or more exothermic chemical reaction(s) took place, and that for that period of time in which the exothermic reaction(s) dominated, the increased temperature further increased both the mass transfer and chemical kinetics at the interface.

It may also be true that the presence of arsenic and presumably some oxygen in liquid solution with lead had an effect on the melt surface tension. In related work (on the topic of liquid binary-metallic solvents), Belton and Tankins[79] wrote that the large depression of the surface tension of liquid iron is related to the presence of trace amounts of electronegative solutes such as oxygen, sulfur, and selenium. They suggest that, by analogy with aqueous systems, this phenomenon "points to the possible existence of polar

molecules in the liquid metal", adding that "the effect of these solutes on surface tension is at least three orders of magnitude greater than other metal solutes"[79]. As surface tension is a physical phenomenon, the effect of a reduced surface tension on a melt's reactivity would be indirect – that is, a lower surface tension would result in the melt spreading and filling the crucible, and in this way providing greater surface area for reaction.

In addition, Marangoni convection is caused by a gradient in the surface tension γ along a free liquid vapour interface.[80] This driving force must overcome the resistance of the fluid to flow, characterized by the viscosity, η. The dimensionless Marangoni number, *Ma*, expresses this competition. It is defined as

$$Ma = \frac{L_s \rho c_p \delta\gamma}{\lambda\eta} \tag{38}$$

where L_s is a characteristic length, ρ is the density, c_p is the specific heat, $\delta\gamma$ is the difference in surface tension along L_s, and λ is the thermal conductivity. Marangoni convection may be contributing to enhancement of mass transfer rates

In work on both copper[81] and steel[82] melts, it has also been found that the surface tension value of the melt is sensitive to temperature and surface-active solute concentration, and as such, thermal and/or concentration gradients on the melt surface are the two major factors that create Marangoni flow.

Examining the mass gain curve for DVTGA40 (Pb0.90As, 600 °C), Figure 63, it can be seen that the curve appeared to have several oxidation stages, including a linear section ($370 < t < 580$ s), and a stage where the rate of mass gain was increasing ($1580 < t < 2450$ s). By comparison, the DVTGA 25 (Pb0.90As, 500 °C) sample, Figure 63, gains more than 50 % of its total mass in the first 70 seconds, and followed a mainly parabolic growth rate thereafter. The interesting feature was that both the 500 and 600 °C tests produced a "clean" surface onto which pure oxygen was purposefully introduced, and yet the 500 °C sample gained mass at a higher rate. This was an unexpected effect from the point of view of temperature's impact on oxidation mass gain kinetics.

For the lead-arsenic tests, the final oxide products were found to be $Pb_8As_2O_{13}$ (dominant), $Pb_3As_2O_8$ (sub-dominant), and $Pb_4As_2O_9$ (sub-dominant) for the 500 °C, and $Pb_8As_2O_{13}$ (dominant) and $Pb_4As_2O_9$ (sub-dominant) for the 600 °C sample. Consultation of the PbO-As_2O_5 pseudobinary phase diagram, Figure 23, indicates that these phases cannot be formed under equilibrium conditions below temperatures of the order of 800 °C. Regrettably, in the absence of a complete Pb-As-O ternary phase diagram, it is difficult to comment further on this issue. As mentioned in an earlier section, another PbO-As_2O_3 pseudobinary, Figure 27, indicated that a liquid oxide phase exists under some conditions, such as at 600 °C where $X'_{As} > 0.33$ (where X'_{As} is the molar ratio of As/(As+Pb) in the oxide phase).

When arsenic was added to Pb-Sb alloys, e.g. Pb0.90As2.00Sb (DVTGA 37 (500 °C) and DVTGA 21 (600 °C)), it had the effect of decreasing the initial rate of mass gain, regardless of temperature, though it increased the overall magnitude of mass gained in both cases.

When arsenic was added to Pb-Sn alloys, e.g. Pb0.90As0.26Sn (DVTGA 35 (500 °C) and DVTGA 26 (600 °C)) the presence of As had the effect of depressing oxidation in the 500 °C sample. For the 600 °C sample, it appeared to only slightly lower the initial rate of mass gain (e.g. first 150 seconds), but it dramatically increased the overall mass gain. Complex lead-arsenic oxides ($Pb_3As_2O_8$) were observed to penetrate through the layer of tin oxide, perhaps facilitating mass transfer to the melt surface. This same phenomenon was also observed in the Pb0.9As2.00Sb0.26Sn (DVTGA 39, 600 °C) sample, and the same Pb-As-O species was detected by XRD as an oxide product in both Pb0.45As1.00Sb0.13Sn (DVTGA 20 and DVTGA 22 (550 °C)) trials.

The effect of impurity elements on the rate of oxidation of lead has been explained by others[59] in terms of the valence model. The explanation rests on the claim that solid PbO is an n-type semiconductor and that during diffusion in crystalline solids, atoms or defects jump between sites within the crystal structure. Additions of higher valence elements such

as antimony, arsenic, and tin act to dope the PbO to create more site for "jumps" to occur, thereby increasing the diffusion and oxidation rates through the oxide.

In examining the contribution of fuming/volatilization in the As-Pb-O system, we find in the literature that other possible arsenic oxidation reaction pathways are the following:

$$4\,\underline{As}_{(1\ wt\%\ in\ Pb\ (l))} = As_{4\,(g)} \qquad \Delta G^{\circ}_{650} = 87.8\ kJ\ mol^{-1}\ ^{(37)} \qquad (39)$$

$$As_{4\,(g)} + 3\,O_{2\,(g)} = 2\,As_2O_{3\,(l)} \qquad \Delta G^{\circ}_{600} = -888.9\ kJ\ mol^{-1}\ O_2 \qquad (40)$$

Which yield an overall reaction of

$$4\,\underline{As}_{(1\ wt\%\ in\ Pb\ (l))} + 3\,O_{2\,(g)} = 2\,As_2O_{3\,(l)} \qquad \Delta G^{\circ}_{600} \approx -801.1\ kJ\ mol^{-1}\ O_2 \qquad (41)$$

Using $\Delta G_{650} = \Delta G^{\circ}_{650} + RT\ lnQ$, p_{As_4} can be determined with (Equation (39)) using the same activity coefficient and molfraction as in section 2.1.2. An As_4 partial pressure of 2.89E-11 atm is obtained, which would suggest that oxidation of arsenic in the gaseous phase would not be expected to be significant.

It is of interest to mention here that volatilization of oxides has also been shown to play a key role in As-Sb-O systems. Whereas at 600 °C, the vapour pressure of $Sb_4O_{6\,(g)}$ above $Sb_2O_{3\,(s)}$ is about 2.8 x 10-3 atm, at the same temperature, the vapour pressure of $As_4O_{6\,(g)}$ above $As_2O_{3\,(s)}$ is about 39.7 atm. In their study [83], Li and Hager found that arsenic oxide gas, $As_4O_{6\,(g)}$ enhanced the volatilization of antimony trioxide, $Sb_2O_{3\,(s)}$ through the following series of vapour complex formation reactions:

$$0.75\,As_4O_{6\,(g)} + 0.5\,Sb_2O_{3\,(s)} = As_3SbO_{6\,(g)} \qquad (42)$$

$$0.50\,As_4O_{6\,(g)} + 1.0\,Sb_2O_{3\,(s)} = As_2Sb_2O_{6\,(g)} \qquad (43)$$

$$0.25\,As_4O_{6\,(g)} + 1.5\,Sb_2O_{3\,(s)} = AsSb_3O_{6\,(g)} \qquad (44)$$

However, the study of the gaseous phases was beyond the scope of the original project design, and is therefore addressed here in only a general way for the Pb-As-O and Pb-Sb-O alloys.

5.3 Parameter B: Antimony

5.3.1 Statistical Analysis of the Effect of Antimony

In terms of the regression analysis, it was found that the presence of antimony significantly reduced the average rate of mass gain in the heating period, during which there was oxygen present in the order of 200 ppm. This effect is likely related to the Pb-Sb-O defect structure, but as mentioned in the section dealing with arsenic, a more sophisticated analysis would require more complex thermodynamic data, such as an Sb-Pb-O-As-Sn solid-liquid-gas phase diagram. One significant interaction effect was also detected: for the response of mass fraction gained prior to oxygen introduction, the effect of antimony content depended on temperature. For example, a high antimony content at higher temperatures reduced the fraction of mass gained prior to the purposeful oxygen introduction.

5.3.2 Discussion of Other Antimony-Related Behaviour

Comparing the Pb2.00Sb mass gain curves (DVTGA 32 (500 °C) and DVTGA 27 (600 °C), Figure 78) with those of pure lead (DVTGA 17 (500 °C) and DVTGA 38 (600 °C), Figure 60), it can be observed that temperature is a key contributor; the 600 °C curve has a much higher initial rate of mass gain and the overall mass gain is almost three (3) times greater. Although a small amount of a liquid phase thought to be a Pb-Sb oxide was observed during the experiment, no such phase was identified by XRD.

When antimony was added to Pb-As alloys, i.e., Pb0.90As2.00Sb (DVTGA 37 (500 °C) and DVTGA 21 (600 °C)), a phenomenon denoted as "compound behaviour" was observed: it appeared that a Pb-As phase was oxidizing distinctly from a Pb-Sb phase, which was also oxidizing. In the early stage of the trial run at 600 °C, reddish droplets were observed at the same time as a white fume phase. The 500 °C sample never appeared to become fully covered by a solid oxide layer, and thus the mass gain kinetics were

roughly linear with time over the 60 minute exposure period. The mass gain for these tests curves were visibly different from either the simply binary Pb-As or the Pb-Sb curves. Still, it is difficult to say that antimony actually oxidized preferentially to arsenic, as predicted by the Ellingham diagram (Figure 53), though it appeared that it did not.

When antimony was added to Pb-Sn alloys, e.g. Pb2.00Sb0.26Sn (DVTGA 24 (500 °C) and DVTGA 31 (600 °C)), a small increase in the initial rate of mass gain was observed for the 600 °C sample, and a significant increase in overall mass gain was recorded. This was likely due to the morphology of Pb-Sb-O oxide layers, as compared to Pb-Sn-O, the latter seemingly more limiting to mass transfer. In terms of the 500 °C sample, flattening of the mass gain curve was observed – the average rate of mass gain from t = 0 is roughly 4% of the rate of mass gain of the 600 °C sample.

In the trials performed on quaternary Pb0.90As2.00Sb0.26Sn alloys (DVTGA 39 (600 °C) and DVTGA 23 (500 °C)), very little difference can be seen between the 500 °C sample (DVTGA 23 (500 °C) as compared to the Pb0.90As0.26Sn sample, DVTGA 36 (500 °C). However, a dampening effect was observed in the 600 °C sample curve (DVTGA 39 (600 °C), wherein the initial slope was less steep, and the overall mass gain was smaller as compared to the Pb0.90As0.26Sn sample (DVTGA 18 (600 °C)). In these quaternary Pb-As-Sb-Sn samples, complex reaction products were formed, including $Pb_5Sb_4O_{11}$ and Pb_4SbO_6. It was interesting that a complex Pb-Sb-O phase (i.e., Pb_4SbO_6) was also observed on the Pb0.45As1.00Sb0.13Sn sample (DVTGA 22), which was run at only 550 °C, since it indicates that formation of a complex, identifiable Pb-Sb-O phase was not necessarily accompanied by "self-cleaning" behaviour or significant mass gain.

Very much to the surprise of the author, pseudobinary and ternary phase diagrams identified through an exhaustive search of the literature and presented in Chapter 2 revealed no matches with the complex Pb-Sb-O oxides identified by XRD here.

5.4 Parameter C: Tin

5.4.1 Statistical Analysis of the Effect of Tin

Regression analysis of the trials run according to the factorial design produced a number of conclusions relating to tin content. Firstly, tin content reduced the average mass gain over the first 300 s of oxygen exposure. It was also found that a synergistic effect between tin and temperature existed, suggesting that the effect of tin was more significant at higher temperatures than at lower temperatures. It was shown that a higher tin content resulted in most of a sample's mass being gained during the heating period, suggesting the formation of a passive, protective tin oxide layer after t_0 across which mass was transfer was impeded. Finally, regression analysis showed that the effect of tin content also depended on temperature; for example, a high tin content at higher temperatures decreased the fraction of mass gained prior to oxygen introduction, while a low tin content at lower temperatures increased the fraction of mass gained prior to oxygen introduction.

5.4.2 Discussion of Other Tin-Related Behaviour

Because tin was present in small amounts, mass transfer limitations might have prevented tin at the interface from oxidizing preferentially. However, during trials on samples containing tin, a unique oxide layer was consistently observed from the start of the reaction, indicating that this did not occur.

Comparing the Pb0.26Sn (DVTGA 35 (500 °C) and DVTGA 26 (600 °C)) curves, Figure 85, with the pure Pb curves, Figure 60, no remarkable difference was observed. During the tests, it was not possible to skim the samples, as both had a residual "skin" which could not be removed.

When tin was added to the Pb-As alloys, i.e., Pb0.90As0.26Sn (DVTGA 36 (500 °C) and DVTGA 18 (600 °C)), Figure 95, it appeared to slow oxidation in the 500 °C sample and it affected the shape of the 600 °C sample curve. It was thought that the presence of tin gave rise to a surface film which delayed the access of oxygen to the underlying melt, and thus to the arsenic in solution.

When tin was added to the Pb-Sb alloys, i.e., Pb2.00Sb0.26Sn (DVTGA 24 (500 °C) and DVTGA 31 (600 °C)), it had virtually no effect on the overall mass gain, though it did affect the rate of oxidation in the 600 °C sample over the first 1500 seconds.

Finally, when tin was added to the Pb-As-Sb alloys, i.e., Pb0.90As2.00Sb0.26Sn (DVTGA 23 (500 °C) and DVTGA 39 (600 °C)) it had the effect of lowering the rate of mass gain significantly, resulting also in a lower total mass gain, for both the 500 and 600 °C samples. As in the case of the Pb-As samples, it was hypothesized that the decrease can be accounted for by the presence of a thin surface oxide layer.

No tin oxide phase was detected in any of the XRD analyses of the samples (Pb0.26Sn 600 °C). As tin constituted at most 0.26 wt%, and the detection limit for XRD is roughly 5 wt%, this was as expected. However, tin was detected by EDX on the Pb0.26Sn (600°C), Pb0.90As0.26Sn (500 °C), Pb2.00Sb0.26Sn (500 °C), and Pb0.90As2.00Sb0.26Sn (500 °C) tests. The three latter trials were the three tests in which the samples gained most of their mass during the heating period (Table 21). The small amounts of tin in solution must have been preferentially oxidized early in the test; it is remarkable that a lead-tin oxide layer could be so impervious to mass transfer, yet be so thin as to be undetectable by XRD.

Researchers[59] have found that small concentrations of tin produce a marked reduction in the lead oxidation rate in tests run at 420 °C, in particular because a dense SnO_2 film is produced with Sn contents $\geq$ 0.1 wt%. In other work[84], it has been found that oxidized samples of Pb-2.9 at% Sn at 90 °C develop an "oxide inversion layer", wherein the amount of preferentially oxidized tin increases with depth into the sample, reaches a maximum, and then decreases to its bulk value. This phenomenon occurs in solid alloys in which the solvent is more noble than the solute[84].

5.5 Parameter D: Temperature

5.5.1 Statistical Analysis of the Effect of Temperature

In relation to temperature as a statistical parameter, regression analysis yielded the following: for the mass gain over the sixty (60) minute test, it can be stated with 99.99%

confidence that temperature was a significant parameter. For total mass gain (over the heating period **plus** the 60 minute test), temperature was found to be the only significant parameter, and was indisputably significant (99.99% confidence). Finally, temperature was found to be significant in the ratio of mass gained in the period prior to oxygen introduction to total mass gained during the heating period PLUS the 60 minutes exposure time.

Several interaction effects were also found, namely (i) between tin and temperature for average rate of mass gain (mg/cm^2hr) prior to oxygen introduction, (ii) between antimony and temperature on the fraction of mass gained prior to oxygen introduction, and (iii) between tin and temperature on the fraction of mass gained prior to oxygen introduction.

5.5.2 Discussion of Other Temperature-Related Behaviour

The effect of temperature is perhaps most easily appreciated, as its effect on the chemical kinetics of reaction is well-known and expressed by the Arrhenius equation:

$$k = A * \exp^{\left(\frac{-E_a}{RT}\right)} \tag{45}$$

where k is the rate coefficient (s^{-1}), A is a proportionality constant (s^{-1}), E_a (J mol^{-1}) is the activation energy, R is the universal gas constant, and T is the temperature (Kelvin). Using typical values[85] for reaction controlled systems (A = 2.1 x 10^{-9} s^{-1}, E_A = 500 kJ mol^{-1}), we find that k increases from 3.42 x 10^{-25} s^{-1} at 773 K (500 °C) to 2.54 x 10^{-21} sec^{-1} at 873 K (600 °C), a factor of roughly seven thousand.

The importance of E_a should not be underestimated. At higher temperatures, the translational velocity of atoms is higher; therefore, there is a higher probability that in a given medium of constant density two molecules will collide. A higher collision rate at higher velocities has the effect that more collisions are likely to have the activation energy required for the reaction[86]. From experimental observation, temperature seemed to "activate" more sluggish species such as the Pb-Sb-O liquid oxides. Whereas arsenic

"fluxing" was observed at 500 °C, antimony needed the additional energy to display accelerated oxidation behaviour.

In fact, temperature was the key suspect in the minds of the staff at Teck Cominco, who wondered what lay at the root of the observed "ignition point". Results have shown (especially where clean surfaces were exposed) that the chemical kinetics of this system in the 500 °C to 600 °C range are **very** sensitive to temperature and results from this study point to the existence of a softening reaction threshold temperature ("SRTT"). For Teck Cominco, thermodynamic predictions are therefore of limited use.

In addition to the effect of surface tension discussed in Section 5.2.2, several additional temperature-dependent factors may contribute to the "ignition point" phenomena observed in industry. Viscosity of liquid metals decreases with increasing temperature[87] and in this way viscosity could have an indirect effect on reaction kinetics during industrial O_2 gas injection into the lead bullion, because of resulting variations in bubble shape, rising velocity and residence time. As low-temperature systems are generally reaction rate controlled, the effects of viscosity are not expected to be significant in the temperature range considered in this study or in industrial application. At temperatures sufficiently above the reaction threshold temperature, the system will be mass transfer controlled, and the impact of viscosity would have to be considered.

The final factor considered is the exothermicity of oxidation reactions, since this would have the effect of locally increasing of temperature at the gas-liquid interface, the location of the chemical reaction (DVTGA44). The implication of this increase is that while the bulk temperature in industrial melts must reach 600 °C before the reaction is ignited, the effective ignition temperature at the local site of reaction activation might actually be significantly higher.

5.6 Teck Cominco Lead Softener Feed & Simulated Feed Samples

In examining the TGA curves for the Teck Cominco softener feed ((DVTGA 29 (500 °C), DVTGA 30 (550 °C) and DVTGA 28 (600 °C), Figure 111) the strong resemblance to

curves presented earlier for the Pb-As-Sb-O system (DVTGA 37 (500 °C) and DVTGA 21 (600 °C), Figure 88) is immediately noticeable. Moreover, similar 'surface cleaning' behaviour was observed on the 500, 550 and 600 °C samples, though the rate of mass gain on the 500 °C was remarkably low. This lends support to the idea that although a liquid phase complex oxide is an important factor in increasing the kinetics of mass transfer across the gas-liquid interface, temperature is the **most** significant factor.

Examining the Simulated Softener Feed captured images and TGA curves, Figure 122 and for example, Figure 127, differences can easily be seen between these and the actual industrial feed material. It is known that other impurities (e.g. Bi, Cu) are present in the industrial feed, and there is no way to predict the influence that these elements may have on oxidation behaviour and kinetics because as yet, since a model for the behaviour of arsenic, antimony and tin in lead solution has not yet been developed.

Parenthetically, a number of complex Pb-Sb-O oxide phases were detected on the Simulated 550 and 600 °C samples which were not detected on any other samples.

5.7 Overall Kinetics

Since the experimental procedure employed lacked the precision and rigour of studies designed to examine kinetics, relatively little space is devoted here to commenting on the overall kinetics of oxidation of the alloys investigated. In comparison to the values presented for previous work on oxidation rates of lead alloyed with known amounts of impurity elements (Table 6), almost all the trials presented herein had approximate oxidation rates in the order of 1 to 100 mg/cm^2hr, which would place them towards the upper end of the reported range. Values for rates at 300 seconds are presented below in Table 22.

5.8 Summary

A sizeable body of experimental data was collected in this study on the effect of the various parameters in lead softening, namely wt% As, wt% Sb, wt% Sn, and temperature. It has been shown that, with varying degrees of significance, each of these parameters contributes

to softening reaction mechanisms and mass gain kinetics. Tin, for example, though present in only small amounts (0.13 – 0.26 wt%) – and the values used in this study were comparatively high – appeared to be preferentially oxidized in all the trials, forming an impervious oxide layer, which was not possible to skim.

Arsenic appeared to be the most "active" of the impurity elements, able to react with lead and oxygen to form a complex liquid phase oxide, even at 500 °C, and yielding the highest initial oxidation rates of all the trials. This liquid oxide was able to "break through" the tin oxide layer mentioned above, creating an oxygen corridor to the liquid interface.

Table 22. Average oxidation rates at 300 seconds, mg/cm^{2}hr.

Trial	ED#	Date	Composition	Temp, °C	Average Rate Mass Gain (300 secs), mg/cm^{2}hr
DVTGA 17	ED1	13-Feb-03	Pure Pb	500°C	13.5
DVTGA 38	ED16	16-Mar-03	Pure Pb	600°C	23.0
DVTGA 35	ED13b	15-Mar-03	Pb0.26Sn	500°C	7.0
DVTGA 26	ED9	22-Feb-03	Pb0.26Sn	600°C	28.0
DVTGA 32	ED12	04-Mar-03	Pb2.00Sb	500°C	11.5
DVTGA 27	ED10	22-Feb-03	Pb2.00Sb	600°C	62.4
DVTGA 24	ED7	20-Feb-03	Pb2.00Sb0.26Sn	500°C	2.5
DVTGA 31	ED11	03-Mar-03	Pb2.00Sb0.26Sn	600°C	34.0
DVTGA 25	ED8	21-Feb-03	Pb0.90As	500°C	92.9
DVTGA 40	ED18	16-Mar-03	Pb0.90As	600°C	78.4
DVTGA 36	ED14	15-Mar-03	Pb0.90As0.26Sn	500°C	3.5
DVTGA 18	ED2	17-Feb-03	Pb0.90As0.26Sn	600°C	14.0
DVTGA 37	ED15	15-Mar-03	Pb0.90As2.00Sb	500°C	6.5
DVTGA 21	ED4	19-Feb-03	Pb0.90As2.00Sb	600°C	43.0
DVTGA 23	ED6	20-Feb-03	Pb0.90As2.00Sb0.26Sn	500°C	1.5
DVTGA 39	ED17	16-Mar-03	Pb0.90As2.00Sb0.26Sn	600°C	4.5
DVTGA 20	ED3b	18-Feb-03	Pb0.45As1.00Sb0.13Sn	550°C	5.0
DVTGA 22	ED5	19-Feb-03	Pb0.45As1.00Sb0.13Sn	550°C	8.0

Antimony, though apparently more sensitive to temperature than arsenic, had the greatest effect on oxidation through the full trial duration. Over the course of the sixty minute test, the overall mass gains with antimony samples were the greatest. The antimony-lead oxide appeared to wet the alumina crucible while the solid oxide grew laterally. This configuration was seen to promote mass transfer to the liquid interface.

Chapter 5: Discussion

Temperature was consistent in its effect on mass gains, when trials conducted at 500 °C were compared to those run at 600 °C. A significant increase in mass gain was demonstrated at the higher temperature. In the 600 °C tests, temperature had the effect of increasing kinetic energy, and increasing to a noticeable degree the activity of the impurity elements described above.

CHAPTER 6: CONCLUSIONS

1. Temperature was the **most** significant parameter of those evaluated, demonstrated by its effect on mass transfer and chemical reaction kinetics. The response of mass gain to temperature (parameter D) for the sixty minute test was shown to be significant with a t value of 5.46, and a P value of 8.5E-05 with an overall fit of F = 0.0004.

2. Arsenic appeared to be the most active of the impurity elements, and was the only one of the three to be statistically significant in increasing mass gain over the sixty (60) minute test; for initial wt% As (parameter A), t = 1.83, P = 8.8E-02 with an overall fit of F = 4.0E-04.

3. The effect of tin on the rate of mass gain was significant, even when present in very small amounts. This was attributed to the rapid formation of a passive layer of tin oxide that thereafter acted as a barrier to mass transfer. For example, a higher tin content, parameter C (t = 9.38, P = 8.4E-05), resulted in the majority of mass gain taking place during the heating period, with an overall fit of F = 3.8E-05.

4. The presence of antimony reduced the average rate of mass gain in the heating period, prior to purposeful oxygen exposure. During the heating period oxygen was present on the order of 200 ppm. The statistical significance of this observation for initial wt% Sb (parameter B) is demonstrated by a t value of -4.81 and a P value of 7.0E-04, with an overall fit F = 1.1E-3.

5. "Self-cleaning" liquid phase complex oxides were significant in increasing the kinetics of mass transfer across the gas-melt interface, as compared to the solid oxide phases which formed at the surface. These liquid phases were found in Pb-As and Pb-Sb alloy systems.

6. Some solid phase complex Pb-As-O and Pb-Sb-O oxide species appear to have crystal and defect structures that were less impeding of mass transfer than those of PbO. This feature is attributed to a "vacant place" mechanism in the oxide crystal structure or to the action of the slag as a "conveyor" of oxygen to the metal by the alternate oxidation and reduction of antimony and/or arsenic.

7. Observed behaviours in the As- and Sb- bearing Pb alloys were unanticipated, specifically (i) complex liquid oxides, e.g., the reddish droplets, (ii) elastic oxide films, e.g. PbO and (iii) unskimmable films, e.g. in Sn-bearing Pb alloys.

8. Some conclusions can be drawn regarding the industrial softening process, based on the experimental results presented herein: chemical kinetics are very sensitive to temperature in the 500 to 600 °C range, and results suggest the existence of a softening reaction threshold temperature (SRTT). It does not appear possible that efficient oxidation of impurities will take place at lower temperatures than those currently used at Teck Cominco.

CHAPTER 7: RECOMMENDATIONS FOR FUTURE WORK

It would be of interest to understand more fully the nature of the liquid oxide phases observed in the present study. In particular, it would be useful to design experiments to address the question of whether the temperature-dependent liquid oxide phases are in fact responsible for the improved mass transfer that is manifested as the apparent "ignition point" seen in the industrial softening operation.

A further question that remains is whether, in light of the findings of the present study, there is a way to improve the lead softening process. One possible area of investigation is the design of an optimal softener feed composition. For example, it has also been observed that in continuous processing, maintaining the lead bath at an antimony content near 0.02 wt% results in a very high oxidation rate.

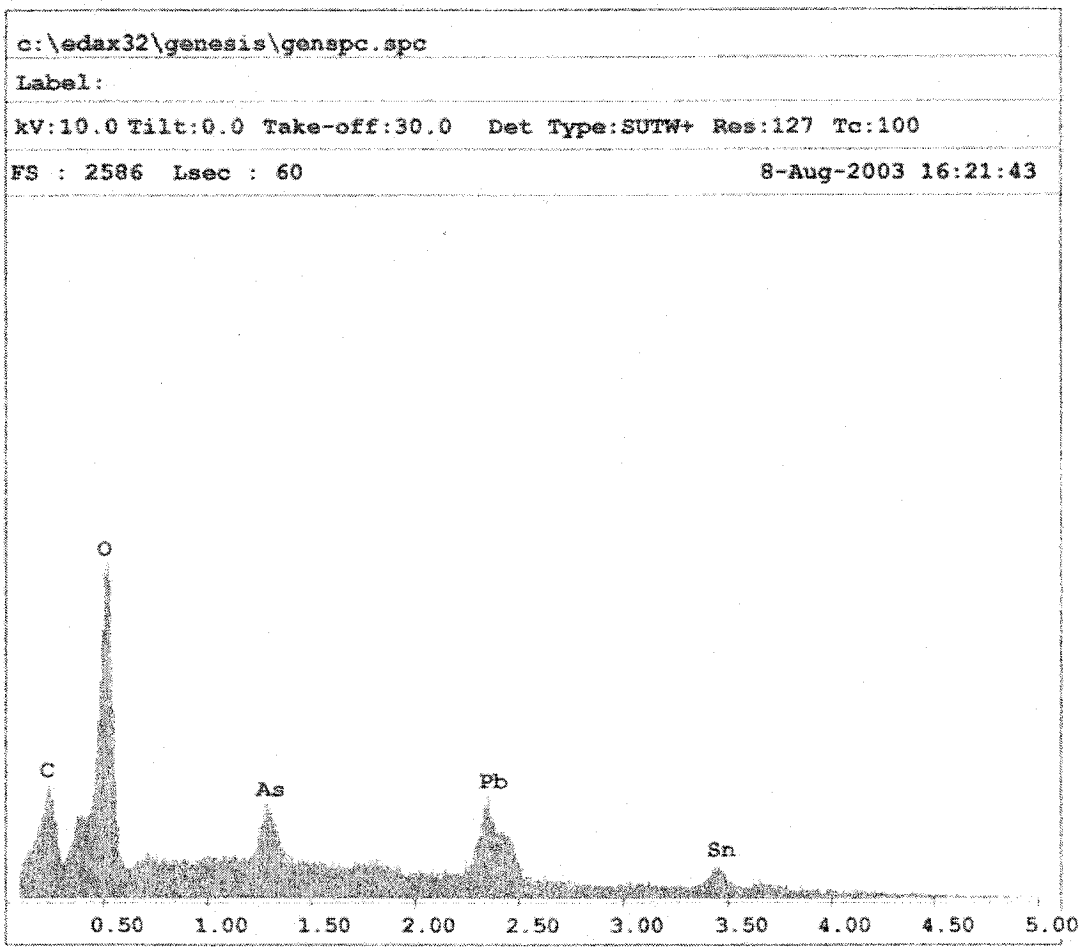

Figure A1. Sample EDX spectrum for DVTG36

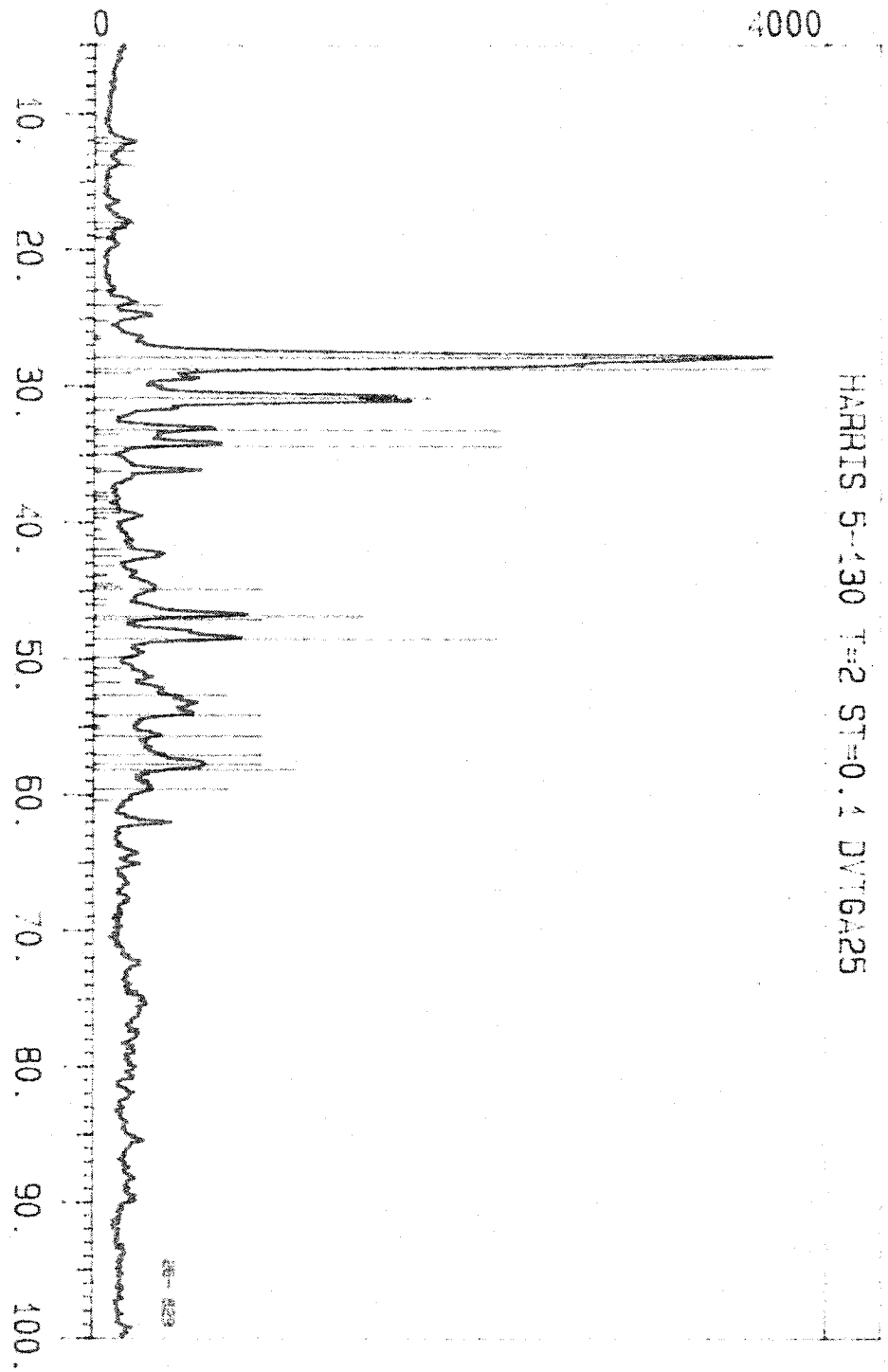

Figure A2. Sample XRD spectrum for DVTGA25

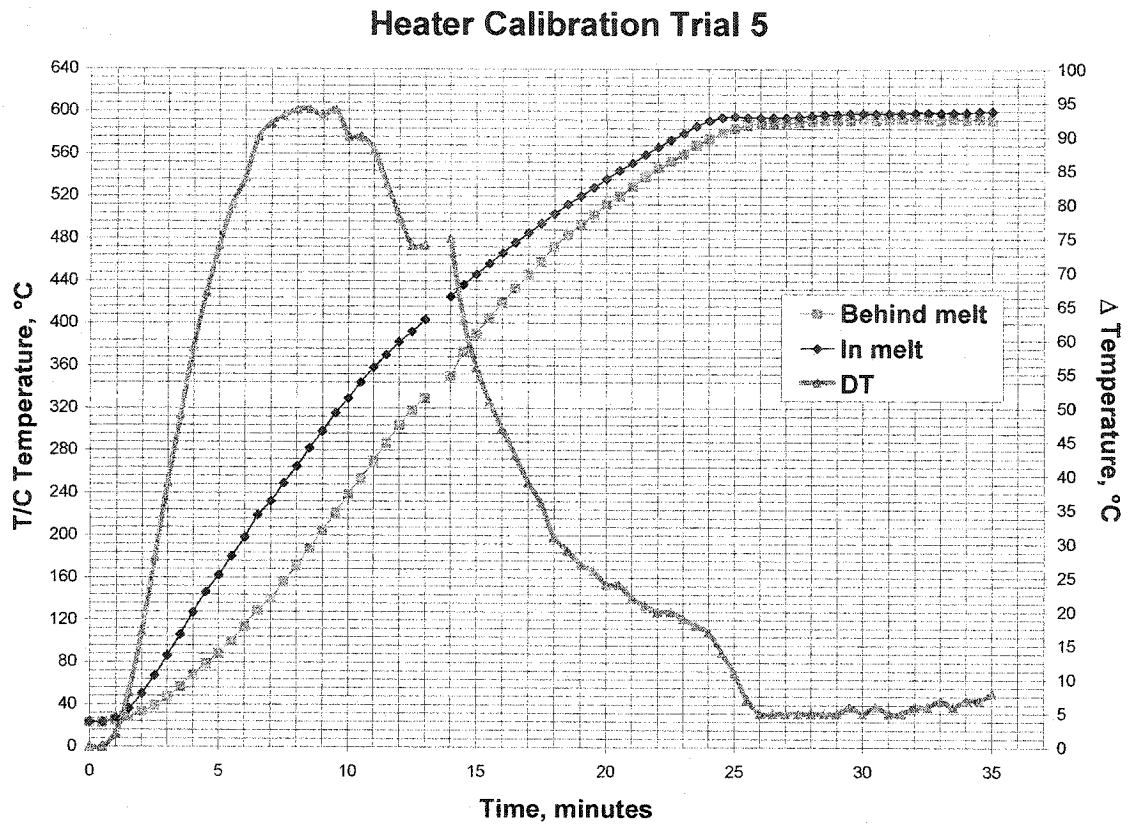

Figure A3. Heater and thermocouple calibration trial

Appendix I

Nominal Compositions

Description	Sample Date	Lot/Time	wt% Ag	wt% Al	wt% As	wt% Au	wt% B	wt% Bi
Alloy 425	20020601	9427			1.700			440 ppm
Alloy 414	20011003	9405	5 ppm		12.00			26 ppm
Alloy 422	20021204	9444			0.4300			110 ppm
Alloy 423	20020501	9421			0.6300			290 ppm
Pb5.0Sb		Q6641	0.96 ppm		0		0.025 ppm	0.24 ppm
HiFlo Solder	20000824	00323742	10 ppm	< 10 ppm	< 10 ppm	10 ppm		30 ppm
Refined Lead	20030123	0101	2 ppm		< 1 ppm			0.0086

Description	Sample Date	Lot/Time	wt% Ca	wt% Cd	wt% Cu	wt% Fe	wt% In	wt% Mg
Alloy 425	20020601	9427		5 ppm	20 ppm	1 ppm		
Alloy 414	20011003	9405			2 ppm	< 1 ppm		
Alloy 422	20021204	9444			50 ppm			
Alloy 423	20020501	9421		2 ppm	20 ppm	< 1 ppm		
Pb5.0Sb		Q6641	0.11 ppm	0.025 ppm	1 ppm	0.24 ppm		0.30 ppm
HiFlo Solder	20000824	00323742		10 ppm	40 ppm	10 ppm	30 ppm	
Refined Lead	20030123	0101		< 1 ppm	< 1 ppm	< 1 ppm		

Description	Sample Date	Lot/Time	wt% Na	wt% Ni	wt% P	wt% Pb	wt% S	wt% Sb
Alloy 425	20020601	9427		3 ppm		92.1	5 ppm	6.2
Alloy 414	20011003	9405				88	23 ppm	180 ppm
Alloy 422	20021204	9444				97.52	< 3 ppm	2.05
Alloy 423	20020501	9421		2 ppm		96.23	< 3 ppm	3.14
Pb5.0Sb		Q6641	0.05 ppm	0.05 ppm		95		5
HiFlo Solder	20000824	00323742		< 10 ppm	80 ppm	100	< 10 ppm	40 ppm
Refined Lead	20030123	0101		< 1 ppm		99.9914		10 ppm

Description	Sample Date	Lot/Time	wt% Si	wt% Sn	wt% Tl	wt% Zn
Alloy 425	20020601	9427		< 1 ppm		< 1 ppm
Alloy 414	20011003	9405		< 1 ppm		< 1 ppm
Alloy 422	20021204	9444		3 ppm		
Alloy 423	20020501	9421		3 ppm		< 1 ppm
Pb5.0Sb		Q6641	0.05 ppm	0.95 ppm	1.9 ppm	0.01 ppm
HiFlo Solder	20000824	00323742		63.43		< 10 ppm
Refined Lead	20030123	0101		< 1 ppm		< 1 ppm

Figure A4. Nominal compositions of commercial alloys used in study

Alloy Calculation

Pure Pb		Alloy 414		Pb5.0Sb		HiFlo Solder	
Element	**Wt%**	**Element**	**Wt%**	**Element**	**Wt%**	**Element**	**Wt%**
Pb	99.9895	Pb	87.9764	Pb	94.9994	Pb	36.5390
Sb	0.0010	Sb	0.0180	Sb	5.0000	Sb	0.0040
As	0.0001	As	12.0000	As	0.0000	As	0.0010
Sn	0.0001	Sn	0.0001	Sn	0.0001	Sn	63.4300

Required	
Element	**Wt%**
Pb	96.84
Sb	2.00
As	0.90
Sn	0.26

	Alloy 1	Alloy 2	Alloy 3	Alloy 4	Spec	Total
Pb	1.000	0.880	0.950	0.365	-0.968	0
Sb	0.000	0.000	0.050	0.000	-0.020	0
As	0.000	0.120	0.000	0.000	-0.009	0
Sn	0.000	0.000	0.000	0.634	-0.003	0
Spec	0	0	0	0	1	6.25
	1.0003	-19.0056	-7.3051	-0.5749	0.5213	
	0.0000	0.0002	8.3334	-0.0001	0.0750	
	-0.0002	20.0038	-0.0285	-0.0011	0.3996	
	0.0000	0.0000	0.0000	1.5765	0.0041	
	0	0	0	0	1	

Amount Needed	
6.25	g

Amount Required		
Pure Pb	3.258	g
Alloy 414	0.469	g
Pb5.0Sb	2.498	g
HiFlo Solder	0.026	g
Total	6.25	g

Figure A5. Sample alloy calculation using commercial alloys

Appendix I

Miscellaneous thermodynamics information:

$\frac{1}{2}\ O_{2\ (1\ atm)} \rightarrow O_{(1\ at.pct)}\ \vert_{Pb}$	$\Delta G°_{600C} = -105.9\ kJ\ mol^{-1}$	(46)
	from Otsuka et al.[88]:	
	$\Delta G° = -117170 + 12.90T\ (\pm 500)\ J \bullet mol^{-1}$	
$\frac{1}{2}\ O_{2\ (1\ atm)} \rightarrow \underline{O}_{(1\ at.pct)}\ \vert_{Pb}$	$\Delta G°_{(in\ Pb5wt\%Sb)} = -105.7\ kJ\ mol^{-1}$ (ref. 89)	(47)

Wang et al.[90]: The activity coefficients of the infinitely diluted oxygen in lead and antimony are ln $\gamma^{\circ}_{O\{Pb\}} = -6.20$ and ln $\gamma^{\circ}_{O\{Sb\}} = -7.66$ and the self-interaction parameter of are $\varepsilon^{O}_{O(Pb)} = -7.8$ and $\varepsilon^{O}_{O(Sb)} = -164.0$. The interaction parameters were found as ${}^{Pb}\varepsilon^{Sb}_{O} = -4.8$ and ${}^{Sb}\varepsilon^{Pb}_{O} = -0.6$.

Taskinen[91]: in lead and dilute lead-based alloys, the temperature dependence of the first order interaction coefficient ε^{Sb}_{O} can be expressed by equation $\varepsilon^{Sb}_{O} = 15.30 - 22.16 \times 10^{3} / T$. The temperature dependence of the activity coefficient of oxygen at infinite dilution in lead can be expressed as ln $f^{O}_{O} = 6.133 - 14.04 \times 10^{3} / T$, and the self-interaction coefficient of oxygen as $\varepsilon^{O}_{O} = 51.99 - 70.90 \times 10^{3} / T$.

Otsuka et al.[89]: Interaction parameter of antimony on oxygen in lead $\varepsilon^{(Sb)}_{o} = -4.80$ at 1103 K. Temp dependence expressed as $\varepsilon^{(Sb)}_{o} = 15.30\text{-}22.16 \times 10^{3} / T$

Taskinen and Jylhä[92] determined first order interaction coefficients of arsenic, antimony and tin on oxygen at 900°C:

ε_O^{As} = 1.228 – 2224.4 / T → so at 900°C, ε_O^{As} = -0.668. From other studies: ε_O^{Sb} = -3.6, ε_O^{Sn} = -34.6

From Agrawal et al[93]: free energy (ε_i^i), enthalpy (ρ_i^i) and entropy (σ_i^i) of self-interaction of binary lead-bearing substitutional solution component i in its dilute solution. For Pb-Sn alloy at 1050 K : ε_{Pb}^{Pb} = 8.5 kJ, ε_{Sn}^{Sn} = -51.5kJ, ρ_{Pb}^{Pb} = -8 kJ, ρ_{Sn}^{Sn} = -14 kJ, σ_{Pb}^{Pb} = -0.004 kJ, σ_{Sn}^{Sn} = 0.0552 kJ

Taskinen[94]: temperature dependence of the first order interaction coefficient ε_O^{Sn} can be expressed by equation $\varepsilon_O^{Sn} = 75.5 - 129.13 \times 10^3 / T$.

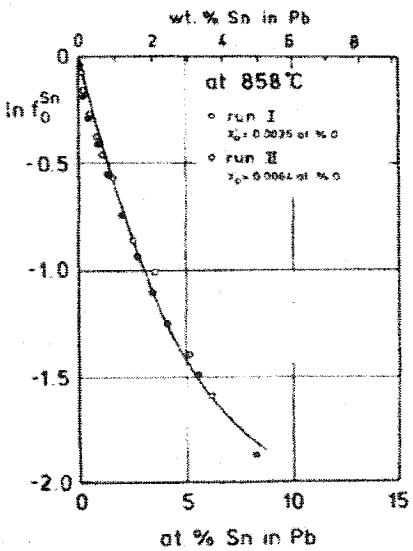

Figure A6. Effect of tin on the activity coefficient of oxygen in lead at 858°C (after Taskinen, 1981, ref. 94)

Prabhakar et al.[95]: thermo of oxygen in liquid lead – tin alloys

ε_O^{Sn} = -74.2 at 973K. Temp dependence: ε_O^{Sn} =139 – 206160/T

REFERENCES

1. D.R. Blaskett and D. Baxall. Lead and its Alloys. Ellis Horwood Limited, Chichester, England, 1990.
2. http://minerals.er.usgs.goc/minerals/pubs/commodity/lead. Site consulted April 2003.
3. http://www.epa.gov/history/topics/perspect/lead.htm. Site consulted June 2003.
4. Lead Material Safety Data Sheet (CAS#7439-92-1), ESPI Metals, Ashland, OR.
5. G.R. Smith, U.S. Geological Survey Minerals Yearbook 2001 – Lead. Link from http://minerals.er.usgs.goc/minerals/pubs/commodity/lead. Site consulted April 2003.
6. http://www.ilo.org/public/english/dialogue/sector/sectors/metal.htm. Site consulted April 2003.
7. G.R. Smith, U.S. Geological Survey Mineral Commodity Summaries, January 2003, 96-97. Link from http://minerals.er.usgs.goc/minerals/pubs/commodity/lead. Site consulted April 2003.
8. Teck Cominco Trail Operations Technical Overview booklet, 28 pp. Teck Cominco Trail Operations, P.O. Box 1000, Trail, British Columbia V1R 4L8.
9. T.R.A. Davey, "The physical chemistry of lead refining", Lead-Zinc-Tin '80, J.M. Cigan, T.S. Mackey and T.J. O'Keefe, Eds., The Metall. Soc. of AIME, New York, 1980, 477-507.
10. J.P. Kapusta, "Sensing and modeling for oxygen lead softening", PhD Thesis, University of British Columbia, Vancouver, British Columbia, Canada, 1995.
11. T.R.A. Davey, "Equilibrium versus kinetics in lead refining", Lead-Zinc 2000, J.E. Dutrizac, Ed., TMS, Warrendale, Pa, 2000, 617-636.
12. F. Ojebuoboh, S. Wang and M. Maccagni, "Refining Primary Lead by Granulation-Leaching-Electrowinning", JOM, 55(4), April 2003, 19-23.
13. Empresa Minera del Centro del Perú: Operaciones Metalurgicas de la Oroya – Año 1974. Departamento de Fundición y Refinerias, La Oroya, Peru, 1974.
14. H. Perez, R. Leclair, P. Hancock, and J.G. Lenz, "Recent process intensification efforts at the Brunswick lead smelter", International Symposium on Challenges in Process Intensification, C.A. Pickles, P.J. Hancock, and J.R Wynnyckyj, Eds., Met. Soc. CIM, Montreal, Quebec, Canada, 1996, 247-266.
15. E.T. de Groot, M.T. Martin and G.W. Toop, "Partial Softening of Lead Bullion with Oxygen", Non-ferrous Smelting Symposium, AusIMM/IE Aust Port Pirie Combined Group, Port Pirie, South Australia, September, 1989, 61-63.
16. E.F.G. Milner and E.T. de Groot, "Method for Softening Lead Bullion", Canadian Patent 1,333,664, 1994.
17. G.W. Toop, "Pyrometallurgy operations of the Cominco Lead-Zinc Smelter", CIM Bulletin, 87 (983), 1994, 89-92.

References

18. J.P. Kapusta, T.R. Meadowcroft and G.G. Richards, "Oxygen Softening of Lead: On-line Measurement of Bullion Quality", Can. Metall. Q., 41(4), 2002, 451-464.
19. S. Barclay, Teck Cominco Trail Operations, personal communication, April 2002.
20. Y. Oyediran, Teck Cominco Trail Operations, personal communication, March 2003.
21. G.K. Williams, "Continuous Lead Refining", Trans. AIME, 121, 1936, 226-263.
22. C.G. Maier, "Thermodynamic data on some metallurgically important compounds of lead and the antimony-group metals and their applications", Progress Reports. Met. Div. 9 Bureau of Mines Report of Investigations, 1934, 1-54.
23. E. Levin, R. Robbins and H. McMurdie, Eds., Phase Diagrams for Ceramists, Am. Ceram. Soc., Columbus, Ohio, USA, 1964.
24. FACT*Sage*™ 5.1 Thermochemical software and database package, especially F*A*C*T compound and solution databases. Copyright© Thermfact Ltd. 2002.
25. S. Otsuka and Z. Kozuka, "Further Study on the Activities of Oxygen in Liquid Pb and Sb by a Modified Coulometric Titration Method", Metall. Trans. B, 12B, Sept. 1981, 616-620
26. Ya.L. Kharif, S.I. Sin'kovskii, I.L. Nesterova, D.A. Tyurin, V.Yu. Brezhnev and P.V. Kovtunenko, "Fusibility Diagram and PO2 Diagram of PbO", Inorg. Mater (USSR) (English Translation), 17(9), 1981, 1213-1216.
27. A.E. McHale, Phase Diagrams for Ceramists – Annual '91, The Am. Ceram. Soc., Columbus, Ohio, USA, 1991.
28. C.B. Alcock and T.N. Belford, "Thermodynamics and Solubility of Oxygen in Liquid Metal from E.M.F. Measurements Involving Solid Electrolytes, Part I - Lead", Trans. Faraday Soc., 60, 1964, 822-835.
29. K.T. Jacobs and J.H.E. Jeffes, "Thermodynamics of Oxygen in Liquid Copper, Lead and Copper Lead Alloys", Trans. IMM, 10B, 1971, C32-C41.
30. N.A. Gokcen. "The As (Arsenic) system", Bull. Alloy Phase Diagrams, 10(1), 1989, 11-22.
31. T.B. Massalski, Ed.-in-chief, Binary Alloy Phase Diagrams, 2nd Edn., ASM, Metals Park, Ohio, USA, 1990.
32. N.A. Gokcen, "The As-Pb (Arsenic-Lead) System", Bull. Alloy Phase Diagrams, 11(2), 1990, 120-4.
33. K. Itagaki, T. Shimizu & M. Hino, "Thermodynamic studies of the liquid lead-arsenic system", Tohoku Daigaku Senko Seiren Kenkyusho Iho, 34(1), 1978, 45-52.
34. B. Onderka and J. Wypartowicz, "Thermodynamic Activities in the Liquid and the Liquidus Line in the Pb-As System", Zeitschrift fur metallkunde, 81(5), 1990, 345-348.
35. S. Sundström and P. Taskinen, "The Optimized Equilibrium Phase Diagram and Solution Thermodynamics of Arsenic-Lead Alloys", Helsinki University of Technology Report TKK-V-B50, 1989.
36. H. Rannikko, S. Sundstroem, and P. Taskinnen, "An Optimised Equilibrium Phase Diagram and Solution Thermodynamics of Arsenic-Lead Alloys", Thermochimica Acta, 216(1-2), 1993, 1-14.
37. A.D. Zunkel and A.H. Larson, "Slag-metal equilibria in the lead-litharge-arsenic trioxide system", Trans. Metall. Soc. AIME, 239(11), 1967, 1771-5.

References

38. B.K. Kasenov, R.B. Shashchanova, A.Z. Beilina, and V.B. Malyshev, "Phase equilibriums in the arsenic pentoxide/lead oxide (PbO) system", Neorganicheskie Materialy, 27(7), 1991, 1236-1240.

39. R.S. Roth, J.R. Dennis and H.F. McMurdle, Eds., Phase Diagrams for Ceramists, Vols. I, III, IV, VI, XI, XII, Am. Ceram. Soc., Westerville, Ohio, USA, 1996.

40. B.K. Kasenov, Chemical-Metallurgical Institute, Academy of Sciences of Kazakhstan, personal communication, May 2003.

41. R.J. McClincy and A.H. Larson, "Activity of Arsenic in Dilute Arsenic-Lead Alloys at 703°C", Trans. Metall. Soc. AIME, 245, January 1969, 173.

42. R.R. Hultgren, Ed.-in-chief, Selected Values of the Thermodynamic Properties of Binary Alloys, ASM, Metals Park, Ohio, USA, 1973.

43. Z. Moser, K.L. Komarek, and A. Mikula, "Thermodynamics and phase diagram of the lead-antimony system", Zeitschrift fur metallkunde, 67(5), 1976, 303-306.

44. P. Taskinen and O. Teppo, "Critical assessment of the thermodynamic properties of antimony-lead alloys", Scandinavian Journal of Metallurgy, 21(3), 1992, 98-103.

45. H. Seltz and B.J. DeWitt, "A thermodynamic study of the lead-antimony system", Am. Chem. Soc., 61, 1939, 2594-2597.

46. S. Itoh, K. Yamanishi and A. Kikuchi, "Phase equilibria and activities of components in liquid Pb-Sb-O", Shigen To Sozai, 117(2), 2001, 138-142.

47. P.M. Milyan, E.E. Semrad, S.V. Kun, and A.M. Solomon, "Study of complex oxides in the Pb-Sb-O system", Ukranian Chemistry Journal, 65(7), 1999, 8-9.

48. H. Hennig and E.J. Kohlmeyer, "The mutual behavior of lead-antimony oxides in the molten condition", Z. Erzbergbau u. Metallhuttenw, 10, 1957, 8-15, 64-71.

49. A.Bush, Yu.N. Venevtsev, "Phase diagram of the lead oxide-antimony oxide (PbO-Sb_2O_3) system in the presence of atmospheric oxygen and the preparation of single crystals of phases of this system", Russ. J. Inorg. Chem., 23(8), 1978, 1207- 1211.

50. C.G. Maier and W.B. Hincke, "The System PbO-Sb_2O_3 and Its Relation to Lead Softening", AIME Technical Publication No. 449, 1932, 12 pp.

51. D. Taloi, "A thermodynamic study of the reaction of antimony removal from lead", Scientific Bulletin - Polytechnical Institute of Bucharest, Chemistry and Materials Science, 54(1-2), 1992, 109-19.

52. R.J. McClincy and A.H. Larson, "Activity of Sb_2O_3 in PbO-Sb_2O_3 and PbO-SiO_2-Sb_2O_3 Slags", Trans. Metall. Soc. AIME, 245, January 1969, 23-27.

53. A.D. Zunkel and A.H. Larson, "Slag-metal equilibria in the Pb-PbO-Sb_2O_3 System", Trans. Metall. Soc. AIME, 239(4), 1967, 473-477.

54. S.K. Das and A. Ghosh, "Thermodynamic measurements in molten lead-tin alloys", Metall. Trans., 3(4), 1972, 803-806.

55. C.S. Sivaramakrishnan and M.L. Kapoor, "Thermodynamic properties of liquid lead-tin system by EMF method", NML Technical Journal, 20(1-2), 1978, 20-23.

56. I.A. Kurzina, S.I. Galanov and L.N. Kurina, "Phase composition of the lead-tin oxide system", Russ. J. Appl. Chem., 75(1), 2002, 5-8.

57. T.F. Archbold and R.E. Grace, "The Oxidation of Liquid Lead", Trans. Metall. Soc. AIME, 212, 1958, 658-659.

References

58. L.L. Bircumshaw and G.D. Preston, "Studies on the Oxidation of Metals", Philosophical Magazine, 25, 1938, 769-782.

59. U. Heubner, F. Nilmen, M. Reinert, and A. Ueberschaer, Metallgesellschaft AG Lead Handbook, 1983, 60-79.

60. W. Gruhl, "Uber Die Oxydation Ruhender Bleischmelzen", Zeitschrift für Metallkunde, 40, 1949, 225-240.

61. T.E. Weyand, "The Oxidation of Liquid Lead and Lead Alloys", PhD Thesis, University of Missouri-Rolla, Rolla, Missouri, USA, 1970.

62. E. Weber and W.M. Baldwin, Jr. "Scaling of Lead in Air", Trans. AIME J. Metals, August 1952, 854-859.

63. J.R. Anderson and V.B. Tare, "Reactions of Oxygen with Evaporated Films of Lead", J. Phys. Chem., 68(6), June 1964, 1482-1489.

64. G. Shimaoka, "Electron Diffraction Study of Oxide Films Formed on Molten Alloys", Erzmetall, 1, 1959, 1-17.

65. R.A. Konetzki, Y.A Chang and V.C. Marcotte, Oxidation Kinetics of Lead-Tin Alloys, J. Mater. Res., 4(6), 1989, 1421-1426.

66. W.W. Krysko, "Oxidation of Molten Lead", Lead 68: Proceedings 3rd Int'l Conference on Lead, Venice. R.H. Dunlop, Ed., Pergamon Press, Oxford, England, 1969, 353-361

67. W. Hoffman and K.H. Malich, "Die Verkrätzung von Bleischmelzen an ruhender Luft", Werkstoffe u. Korrosion, 2, 1951, 55-68.

68. W. Hoffman, Lead and Lead Alloys: Properties and Technology (English translation of Blei und Bleilegierungen). Springer-Verlag, Berlin/Heidelberg, 1970.

69. G. Ross and S.A. Peabody, "Monterrey refinery uses continuous lead softening and desilverizing process", JOM, 4, 1952, 915-18.

70. J. Blanderer, "The Refining of Lead by Oxygen", JOM, December, 1984, 53-54.

71. J.G. Peacey, J.G. Lenz and R. Firlotte, "High temperature softening of lead bullion". Canadian Patent 1 225 242 (1987), 26 pp.

72. J. Kapusta and G.G. Richards, "A process control system for oxygen lead softening". Quality in Non-Ferrous Pyrometallurgy, Proceedings of 2nd International Symposium M. Kozlowski, R.W. McBean and S. Argyropoulos, Eds., CIM, Vancouver, Canada, 1995, 173-83.

73. J.O. Betterton and C.W. Hanson, "Slag formation and reduction in lead softening". US Patent 1950387 (1934)

74. G.C. Hancock, D.H. Hart and L.A.H. Pelton, "Lead Smelting and Refining and Slag Fuming at the Broken Hill Associated Smelters Pty. Ltd". AIME World Symposium on Mining and Metallurgy of Lead & Zinc : Volume II :Extractive Metallurgy of Lead & Zinc, C.H. Cotterill and J.M Cigan, Eds., AIME, Inc., New York, 1970, 790-823.

75. F.A. Green, "The Refining of Lead and Associated Metals at Port Pirie, South Australia", The Refining of Non-Ferrous Metals, IMM London, 1950, 297-325.

76. P. Kofstad, High Temperature Oxidation of Metals, John Wiley and Sons, New York, U.S.A., 1966.

77. http://www.matter.org.uk/matter_glossary/ficks_first_law_of_diffusion.html. Site consulted August 2003.

References

78. D. Vineberg, KW. Ng and R. Harris, "Cominco NSERC CRD Progress Report", unpublished document, 2002.

79. G.R. Belton and E.S. Tankins, "The Thermodynamic Behavior of Oxygen in Liquid Binary-Metallic Solvents – A Simple Solution Model", Trans. Metall. Soc. AIME, 233, 1965, 1892-1898.

80. I. Egry, M. Langen and G. Lohofer, "Measurements of thermophysical properties of liquid metals relevant to Marangoni effects", Philosophical Transactions of the Royal Society of London, Series A: Mathematical, Physical and Engineering Sciences, 356 (1739), 1998, 845-856.

81. S. Sun, L. Zhang and S. Jahanshahi, "From Viscosity and Surface Tension to Marangoni Flow in Melts", Mills Symposium Proceedings, IOM, London, UK, August 2002, 141-143.

82. T. Emi and H. Yin, "Marangoni Flow at the Solid/Melt Interface of Steel", Mills Symposium Proceedings, IOM, London, UK, August 2002, 53-69.

83. T.Li and P. Hager, "New Chemistry for the Recovery and Separation of Arsenic and Antimony", The Reinhardt Schuhmann Int'l Symp. On Innovative Techn. And Reactor Design in Extraction Met., 1986, 845-868.

84. R.A. Konetzki and Y.A.Chang, "Oxidation of Pb-2.9 at.% Sn alloys", J. Mater. Res., 3(3), 1988, 466-70.

85. T. Rosenqvist, Principles of Extractive Metallurgy, 2nd Edn., McGraw Hill, Tokyo, Japan, 1983.

86. http://www.shodor.org/unchem/advanced/kin/arrhenius.html. Site consulted August 2003.

87. D.R. Gaskell, An Introduction to Transport Phenomena in Materials Engineering, Macmillan Publishing Company, New York, U.S.A., 1992.

88. S. Otsuka and Z. Kozuka, "Further Study on the Activities of Oxygen in Liquid Pb and Sb by a Modified Coulometric Titration Method", Metall. Trans. B, 12B, 1981, 616-620

89. S. Otsuka, Y. Kurose and Z. Kozuka, "Activity of Oxygen in Liquid Pb-Sb Alloys Determined by a Modified Coulometric Titration Method", Zeitschrift fur metallkunde, 75(1), 1984, 46-52.

90. M. Wang, S. Anik and M.G. Frohberg, "Thermodynamics of oxygen in the lead-antimony system at 1173K", Erzmetall, 40(6), 1987, 316-319.

91. A. Taskinen, "Activity coefficient of oxygen in lead-bismuth and lead-antimony melts", Zeitschrift fur Metallkunde, 73(3), 1982, 163-168.

92. A. Taskinen and K. Jylhä, "Influence of arsenic on the activity coefficient of oxygen in liquid lead", Scand. J. of Metall., 11(3), 1982, 158-160.

93. R.D. Agrawal, V.N.S. Mathur and M.L. Kapoor, "Thermodynamics of binary lead-bearing substitutional solutions", Trans. Indian Inst. Met., 33(3), 1980, 237-240.

94. A. Taskinen, "Oxygen Metal (Ag, Au, Bi, In, Ni, Sb, Sn, Te) Interaction in Dilute Molten Lead", Acta Polytechnica Scandinavica, Series 146, 1981, 44 pp.

95. S.R. Prabhakar and M.L. Kapoor, "Thermodynamic behavior of oxygen in liquid lead-tin alloys", Zeitschrift fur Metallkunde, 84(5), 1993, 358-364.